The Roll Motion of Trimaran Ships

By

Thomas James Grafton

A Thesis Submitted for a Doctor of Philosophy

Department of Mechanical Engineering

University College London

2007

Volume 2

Chapter (5) Why doesn't the Standard Monohull Analysis Procedure work for Trimarans?

Chapter (5) Why doesn't the Standard Monohull Analysis Procedure work for Trimarans? 275
5.1 Introduction 277
5.2 Assumptions in the Analysis of Free Roll Decay Experiments 279
5.3 Appropriateness of Chosen Roll Damping Model 281
5.3.1 Analysis Method 281
5.3.2 Data Manipulation Prior to Analysis 282
5.3.3 The Quadratic Damping Model 288
5.3.4 The Cubic Damping Model 295
5.4 Repeatability of the Roll Decay and Stability of the Roll Damping Coefficients 302
5.4.1 The Repeatability of the Roll Decay 304
5.4.2 The Stability of Measured Damping Results 310
5.5 Variations in the Coefficients of an Uncoupled Equation of Roll Motion .. 313
5.5.1 Roll Decay with Time Variation of the Roll Stiffness 313
5.5.2 Comparisons with Monohull Roll Decay 320
5.5.3 A More Complete Simulation of Trimaran Roll Decay in the Time Domain 322
5.5.4 Summary 334
5.6 Coupling of Roll With Other Motions in Free Decay 335
5.6.1 Heave Motion 335
5.6.2 Pitch Motion 341
5.6.3 Further Studies 342
5.7 Assumptions in the Analysis of Seakeeping Experiments in Regular Waves 346
5.8 The Applicability of Linear Theory to a Trimaran in Beam Regular Waves 347
5.8.1 Rolling in Regular Beam Waves 348
5.8.2 Heaving in Regular Beam Waves 353

5.8.3 Pitching in Regular Beam Waves 362
5.8.4 Summary 366
5.9 Conclusions 367

5.1 Introduction

The purpose of this chapter is to document additional research carried out to determine why the hypothesis tested in Chapter 4, which has been successfully applied to monohulls over a long period of time, is not suitable for trimarans. The hypothesis put forward in Chapter 4 was underpinned by three major assumptions:-

1. Linear seakeeping theory could be applied to a trimaran,
2. The linear equation of motion could be solved using Potential Flow Theory in the frequency domain, and
3. The roll damping term in the equation of motion could be accurately predicted using either:-
    a. The results of roll decay experiments, where a quadratic damping model was assumed and therefore linear and quadratic damping coefficients were obtained from the measured decay, or
    b. From a suitable selection of semi-empirically derived theoretical roll damping components developed for monohulls.

In the conclusion to Chapter 4 it was suggested that solution of the equation of motion in the frequency domain was inappropriate for a trimaran (assumption 2). This assertion was made because in the model experiments, at large angles of roll, one side hull often emerged completely from the water, with the opposing side hull becoming deeply immersed. The shape of the side hulls, with pronounced flare above the waterline (due to the haunches), means that when a side hull is deeply immersed or completely emerges from the water there will be changes in the hydrodynamic properties of the trimaran hull and these changes will vary with time over the course of a roll cycle. The significance of these changes is unknown; however, if appendages of the types proposed in Chapter 4 are fitted below the side hulls it has been shown that the variations in the lift that they generate as they are pulled towards the water surface are significant. The research showed that the lift that these appendages develop will increase the roll damping and these increases occur at relatively low forward speeds. Therefore, it is

considered that accurate roll motion predictions will only be achieved for trimarans with such appendages if the equation of motion is solved in the time domain where the time varying lift of the appendages is properly accounted for. As no time domain seakeeping computer codes were available to the author and, as time for further research was limited, no further work on this assumption is carried out in this chapter. However, this topic is revisited in Chapter 6 where proposals for further work to improve the understanding of the physics of trimaran roll motion are developed.

The issue of the prediction of trimaran roll damping by empirically derived empirical components was also considered in Chapter 4 (assumption 3b above). This work showed that logical extensions to existing components derived and validated for monohulls, as well as some new components specific to trimarans, did not yield accurate roll motion predictions. Thus, no further investigations into this assumption are carried out in this chapter. A series of model experiments using simplified trimaran midship sections is proposed in Chapter 6, aimed at aiding the development of new roll damping components suitable for trimarans.

Therefore, the focus for this chapter is to investigate whether the remaining assumptions, numbers 1 and 3a, are valid for trimarans. Investigations will focus on further in-depth analysis of the existing model experiment results for trimaran DVZ and simple mathematical simulations of roll decay. As all the analysis work in this thesis has been performed on a single trimaran, the purpose of the new work in this chapter is to understand which of the main or underlying assumptions are likely to have contributed to the inaccurate estimates of roll motion for trimaran DVZ in Chapter 4, not to make definitive conclusions for all trimarans. This work is left for other researchers.

This chapter starts with further analysis of the roll decay experimental data collected for trimaran DVZ to question the assumptions supporting roll decay analysis (assumption 3a). After this, the assumption of linear seakeeping theory is scrutinised (assumption 1) by further examination of the results of seakeeping experiments in regular waves with trimaran DVZ.

5.2 Assumptions in the Analysis of Free Roll Decay Experiments

In this section the assumptions that support the analysis of free roll decay are set out. Research is then conducted in order to understand which of the assumptions that have been traditionally used in the analysis of monohulls are not appropriate for a trimaran. The assumptions which are traditionally used in roll decay analysis for monohulls were given in Section 2.6 of Chapter 2 and are repeated below, the first two assumptions are general and apply to seakeeping analysis in all degrees of freedom, whereas the rest relate to roll decay:-

1. The motions of the ship in any single degree of freedom are adequately modelled by a forced spring-mass-damper system. Thus, motions in each degree of freedom are represented by a second order differential equation. The complete motion of the ship is determined by coupling the six equations representing surge, sway, heave, roll, pitch and yaw in a suitable manner.
2. Motions in each degree of freedom are represented by a second order linear differential equation *with constant coefficients.*
3. In a free or forced rolling experiment the roll motion can be modelled by an uncoupled equation of roll motion.
4. The output roll motion in the experiment is pure roll, unaffected by motions in the other degrees of freedom.
5. Unless a Parameter Identification Technique is used, see Section 2.4.2.2 in Chapter 2, it is generally assumed that the inertia and added inertia term, $(I_4 + A_{44})$, and the roll stiffness term, C_{44}, are constant. This implies that over the range of roll angles tested the $\overline{GZ}$ curve is linear.
6. The roll damping coefficients derived from the model experiments are constant.
7. The chosen roll damping model, e,g, quadratic with linear and quadratic damping coefficients, adequately models the recorded roll motion.

The scrutiny of these assumptions will begin by looking at those which are easiest to investigate. Therefore, a good start point is to assume that roll decay can be modelled by an uncoupled equation of motion with constant coefficients and to begin investigations by looking at the appropriateness of a quadratic damping model. This is the topic for the next section.

5.3 Appropriateness of Chosen Roll Damping Model

In this section the 2002 roll decay experiment results for trimaran model DVZ are re-analysed to investigate the effect of changing the damping model. For these investigations it is assumed that the roll decay can be modelled using an uncoupled equation of roll motion with constant coefficients. We recall from Chapter 3 that Zhang and Andrews (8) predicted trimaran roll motion using a quadratic damping model, with linear and quadratic damping coefficients. This was used for the research undertaken by the author described in Chapter 4 because Zhang and Andrews showed adequate correlation between roll motions measured from seakeeping experiments and theoretical roll predictions using linear Potential Flow Theory, with linear and quadratic damping coefficients measured from roll decay experiments. Zhang and Andrews theoretical predictions were acceptable at high speeds, however at zero speed they were poor.

The literature review contained in Section 2.2.3.1 of Chapter 2 showed that there was no consensus amongst researchers as to which was the best damping model to use. Of the research reviewed, most authors preferred either the quadratic or cubic models (with linear and either quadratic or cubic damping coefficients). The appropriateness of these two damping models for predicting trimaran roll motion will be investigated in the next few sub-sections.

5.3.1 Analysis Method

The focus of this analysis is to look at the difference between roll damping predictions using either a quadratic or cubic damping model. To determine the accuracy of the chosen damping model, it is best to compare the theoretical fit (quadratic or cubic) to the spread of roll damping throughout the decay. The easiest way to do this is to consider the variation of the equivalent linear damping term, b_e, over each half roll cycle in the measured decay. This point of view is

supported by Haddara, Bass and Wang (177) with their analysis of large amplitude rolling.

The equivalent linear damping term, b_e, can be easily obtained using the quasi-linear method described in Section 2.4.2.1 of Chapter 2. Using this method the nature of the damping can be investigated by calculating the equivalent linear damping over half a roll cycle and comparing this with values for subsequent half cycles until the motion has decayed away completely. This approach has been used recently by Cotton and Spyrou (94) to investigate the nature of roll damping for a ship undergoing large amplitude motions. This method will be used to re-analyse the roll decay experiment results in the subsequent sections.

It is difficult to determine the equivalent linear damping for every half cycle using the energy method implemented in the decay analysis documented in Section 4.2.4.2 of Chapter 4. This is because, with this method, the equivalent linear damping cannot be measured directly, rather the damping coefficients have to be determined after performing the analysis over each half cycle and then these can be used to obtain the equivalent linear damping. Performing the energy method over only half a roll cycle rather than using the complete decay time history means it is very difficult to get stable roll damping coefficients. If roll damping coefficients obtained from an analysis of half a roll cycle are used to simulate the roll decay the simulated decay will in general provide a poor match to the measured data. The energy method works much better when a large number of roll cycles are used. For this reason, the quasi-linear method is preferred for the re-analysis of the roll decay results in this Chapter.

5.3.2 Data Manipulation Prior to Analysis

The roll decay analysis reported on in Section 4.2.4.2 of Chapter 4 utilised the energy method which uses the roll velocity time history obtained by differentiation of the roll displacement time history. Any noise in the roll displacement time history is greatly amplified in the differentiation process, therefore a mathematical expression was fitted to the measured data to eliminate

the noise prior to the energy method analysis. The expression used is given below:-

$$x_4(t) = a_1 e^{-k_a t}\cos(\omega t + \theta_1) + a_2 e^{-k_b t}\cos(\omega t + \theta_2) \qquad \text{5-3- 1}$$

Where a_1, a_2, k_a, k_b, θ_1 and θ_2 are coefficients determined using a least squares fit to the measured decay history. If linear theory were valid, an exponentially decaying cosine term should adequately model the decay. However, considering that, in the conclusions to Chapter 4 the assumption of an uncoupled single degree of freedom roll equation has been questioned, forcing a mathematical fit to the data may remove any non-linear effects or the influence of any coupling with motions in the other 5 degrees of freedom. To avoid this, a more accurate method of fitting a smooth line through the experimental data was sought.

The fitting method chosen was to apply a Savitzky-Golay smoothing filter, see (107) for further information. Savitzky-Golay filters are normally used to smooth out a noisy signal which comprises a large range of frequency components (without the noise). The method works by fitting a polynomial to a small part of the signal of a chosen window size using the least squares method. It then moves on, stepping through the signal in steps equal in size to the chosen window. The complete signal is then the summation of these individual least squares fits. For the results of the decay experiment a fourth order polynomial was fitted to a length of the decay containing 31 data points, equating to a time span of 0.62 seconds. This was found by trial and error to give the best fit to the data. The method was implemented in the MATLAB computer language using the predefined routine **sgolayfilt**, see www.mathworks.com.

The difference between using the Savitzky-Golay fitting method and the mathematical function in equation 5-3-1 can be seen by contrasting Figure 5-3- 1 with Figure 5-3- 2. Both figures represent the roll decay for trimaran DVZ with initial roll to starboard (without any roll damping appendages fitted). The Savitzky-Golay fit is much better, especially over the first few cycles of the

decay. The Savitzky-Golay method is even better at higher speeds, see Figure 5-3- 3 and Figure 5-3- 4, which show the roll decay at 25 knots (ship speed) with a pair of roll damping fins fitted to the side hulls.

A better comparison can be seen by comparing the decrement of the peaks of the decay. The absolute value of the decay history is taken so that all troughs at negative roll angles are reflected and become peaks. Taking the absolute values and reflecting the peaks implies that the decay is symmetrical about zero degrees, i.e. there is no initial heel angle that would induce bias into the signal or any drift that would cause the "zero position" to move. A comparison between the two methods is given in Figure 5-3- 5 and Figure 5-3- 6. This shows that the function in equation 5-3-1 smoothes out some of the fluctuations in the decay. These fluctuations could occur as a result of inadequacies in the original assumptions and may therefore be important. For this reason, they are included in the re-analysis. If one was entirely satisfied with the underpinning assumptions, then these fluctuations could be considered to be entirely due to an accumulation of experimental errors, it would then be appropriate to fit a smooth curve through the decrement prior to any further analysis.

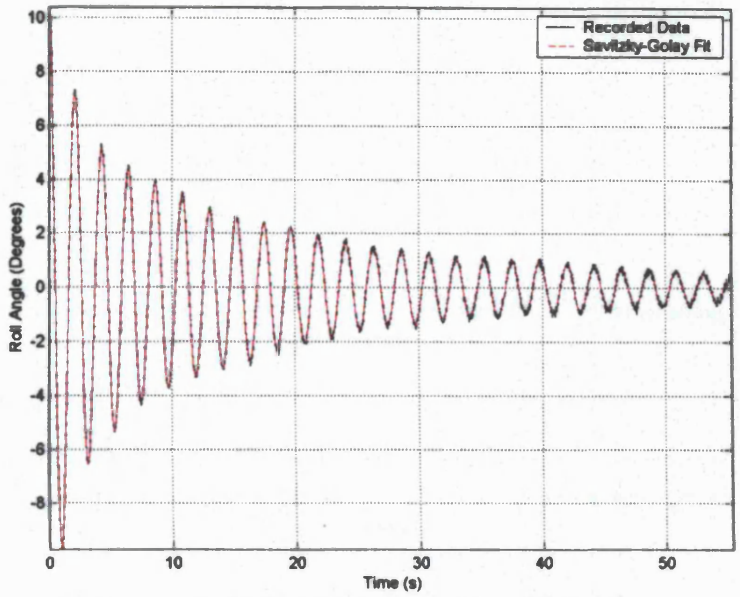

Figure 5-3- 1: Roll decay of Trimaran model DVZ without roll damping appendages at zero speed, initial roll to starboard, compared with a mathematical fit using the Savitzky-Golay method

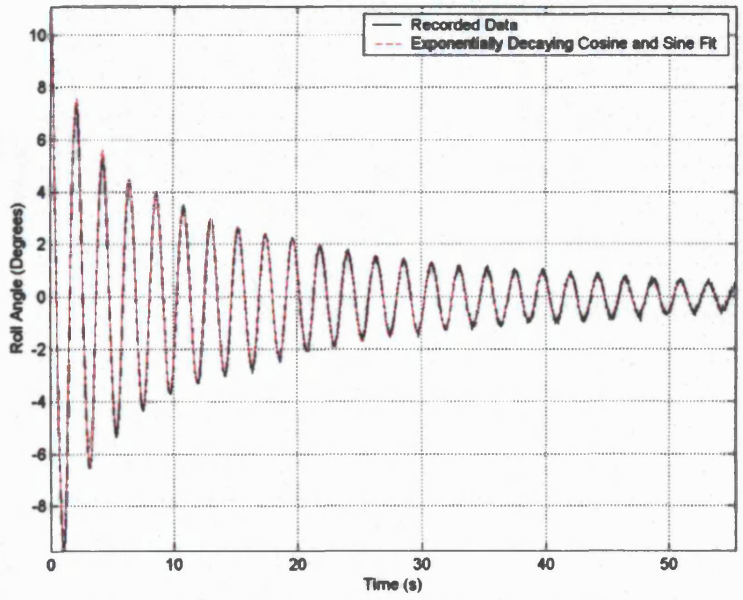

Figure 5-3- 2: Roll decay of Trimaran model DVZ without roll damping appendages at zero speed, initial roll to starboard, compared with a mathematical fit using equation 5-3-1

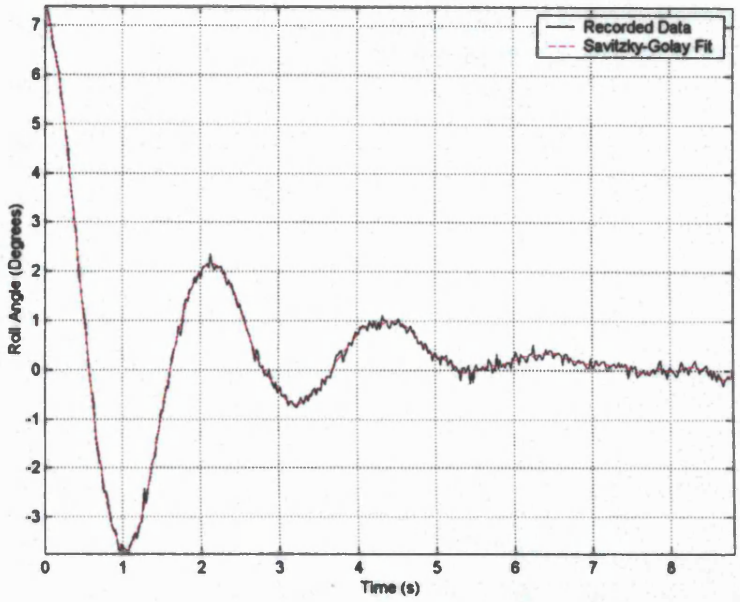

Figure 5-3- 3: Roll decay of Trimaran model DVZ fitted with roll damping appendages on the side hulls at a speed equivalent to 25 knots compared with a mathematical fit using the Savitzky-Golay method

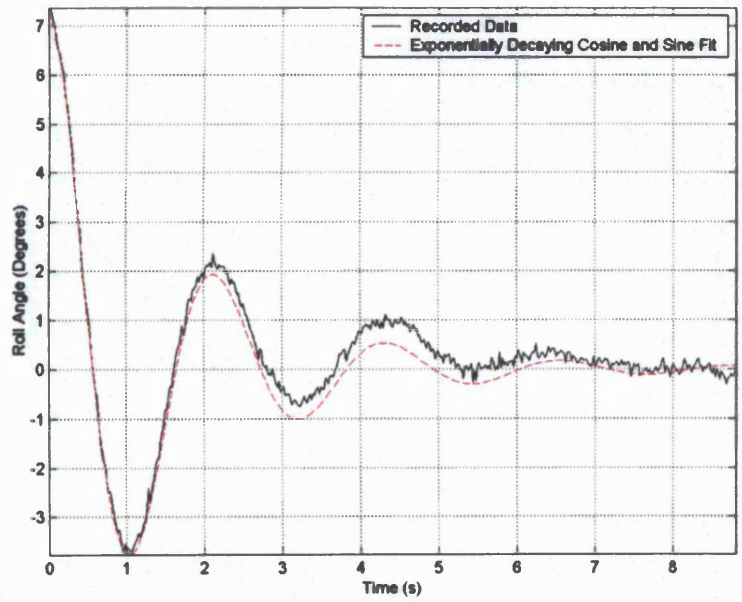

Figure 5-3- 4: Roll decay of Trimaran model DVZ fitted with roll damping appendages on the side hulls at a speed equivalent to 25 knots compared with compared with a mathematical fit using equation 5-3-1

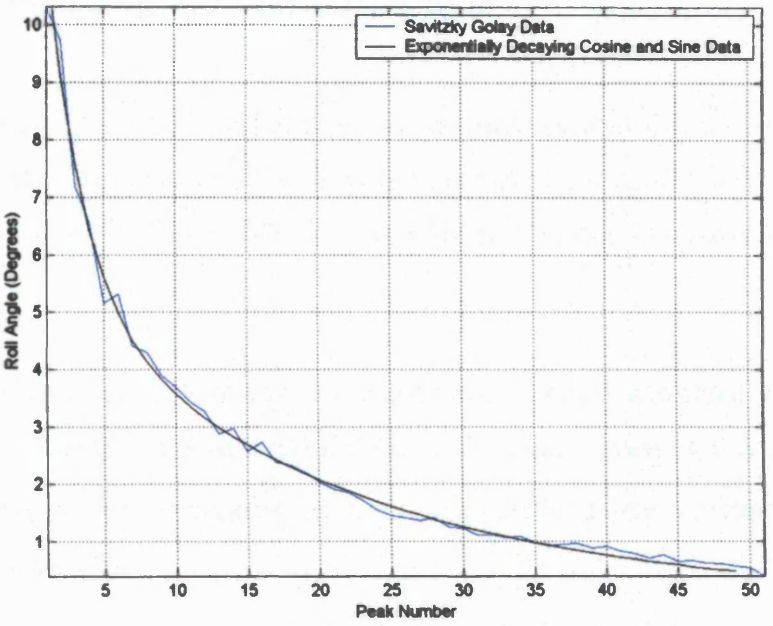

Figure 5-3- 5: Decay of peak roll amplitudes (absolute values taken so both positive and negative roll angles are included) using the Savitzky-Golay method and equation 5-3-1 to fit the recorded data for trimaran model DVZ at zero speed without roll damping appendages

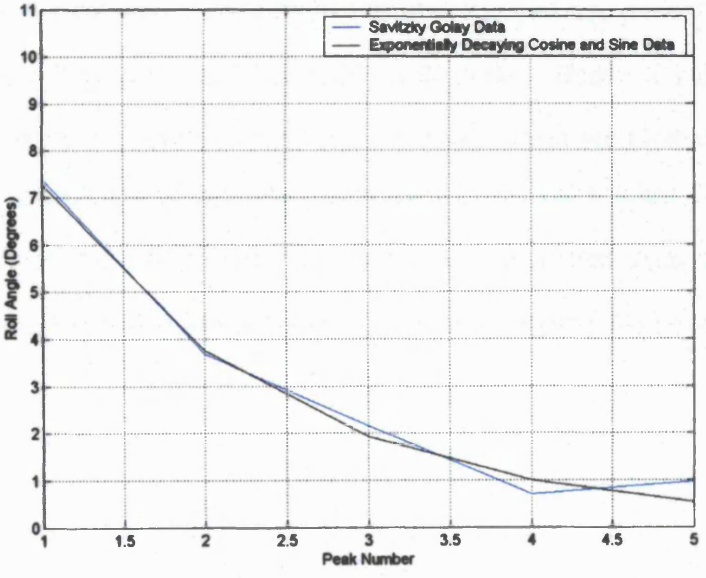

Figure 5-3- 6: Decay of peak roll amplitudes (absolute values taken so both positive and negative roll angles are included) for data fitted to the measured roll decay data using the Savitzky-Golay method and equation 5-3-1 for trimaran model DVZ fitted with roll damping appendages on the side hulls at a speed equivalent to 25 knots

5.3.3 The Quadratic Damping Model

This model will be considered at three speeds, equivalent to ship speeds of 0, 12 and 25 knots. At zero speed the fitted roll decrement (using the Savitzky-Golay method) is given in Figure 5-3- 7 for the trimaran model without roll damping appendages.

Using the peak decrement and the quasi-linear method described in Section 2.4.2.1 of Chapter 2 the equivalent linear roll damping term, b_e, is calculated between two successive peaks in the decay using the following equation (equation 2-4-1 in Chapter 2):-

$$b_e = \frac{2\omega_d}{\pi} \ln\left[\frac{x_{4p}}{x_{4p+1}}\right] \qquad \text{5-3- 2}$$

Where b_e is the equivalent linear roll damping term per unit roll inertia and added inertia, ω_d, is the damped natural frequency and x_{4p} and x_{4p+1} are the amplitude of successive roll peaks describing half a roll cycle. Hence a value of b_e is obtained for every half cycle of the decay. These values are plotted against the mean of the amplitudes of the two peaks used in the calculation for b_e as red circles in Figure 5-3- 8. These b_e values are calculated assuming the roll stiffness, inertia and added inertia remain constant throughout the decay.

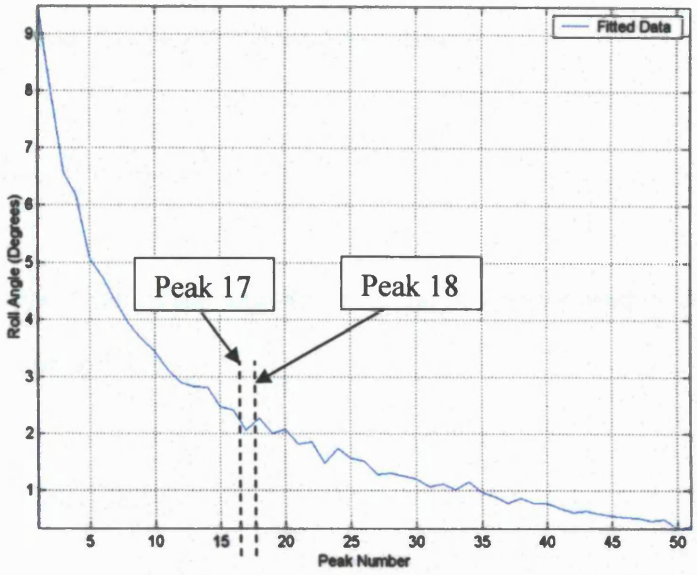

Figure 5-3- 7: Decay of peaks (absolute values taken so includes both positive and negative angles) in the fitted decay data for trimaran model DVZ without roll damping appendages at zero speed

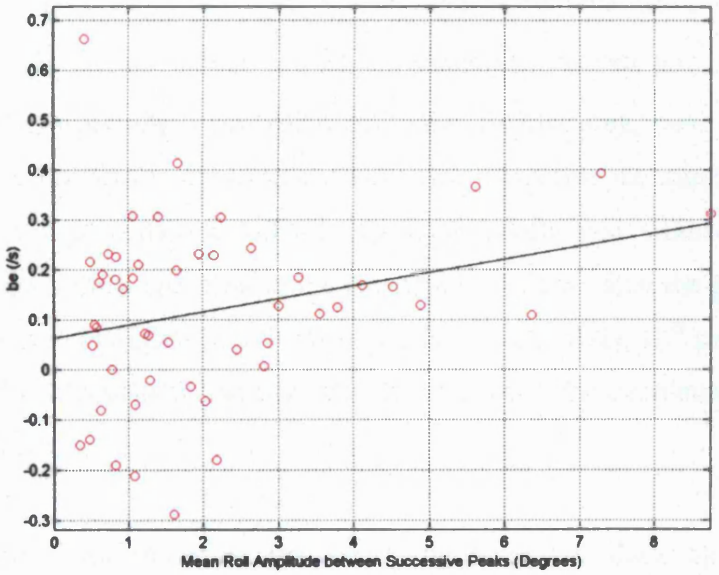

Figure 5-3- 8: Equivalent linear roll damping (be) plotted against mean roll angle between two successive peaks (red spots) for trimaran model DVZ without roll damping appendages at zero speed. The black line is a least square's fit to the data used to obtain linear and quadratic damping coefficients (b_1 and b_2).

If a quadratic damping model is assumed then the variation in b_e is described by equation 2-4-2 from Chapter 2, reproduced below:-

$$b_e = b_1 + \frac{8}{3\pi} b_2 \omega_d x_{4m} \qquad \textbf{5-3- 3}$$

Where x_{4m} is the mean of the amplitudes of the two peaks used in the calculation for b_e in equation 5-3-2:-

$$x_{4m} = \frac{x_{4p} + x_{4p+1}}{2} \qquad \textbf{5-3- 4}$$

Hence if this quadratic model of the damping is correct a least squares fit of equation 5-3-3 to the equivalent linear damping calculated between successive peaks in the decrement (red circles) should adequately represent the damping. This is plotted as a solid black line in Figure 5-3- 8. The gradient of this line gives the quadratic damping coefficient, b_2, whilst the intercept gives the linear damping coefficient, b_1. There is a large variation of the data points around this line of best fit, especially at low roll amplitudes. Furthermore, *some of the values of the equivalent linear damping are negative*. Negative damping, that is roll amplification in proportion to roll velocity, is physically most unlikely. Negative damping occurs when one peak in the decrement is higher than the previous one. This can be seen in Figure 5-3- 7 where the magnitude of the 18th peak is greater than the 17th. If a smooth line had been fitted through the decrement this would not have occurred.

The equation of motion can be simulated using the derived damping coefficients, b_1 and b_2, and the damped natural frequency, ω_d, measured from the decrement. A Runge-Kutta numerical method is used to simulate the equation of motion using the MATLAB function **ode45**. This simulation of the roll decay is shown in Figure 5-3- 9 along with the original fitted data (using the Savitzky-Golay method). It can be seen that, generally speaking, the fit is good. However, the simulated data slightly under predicts the roll at low amplitudes and over predicts

it at the higher amplitudes. An imperfect fit is to be expected because of the large spread of equivalent linear damping values around the fitted line in Figure 5-3- 8.

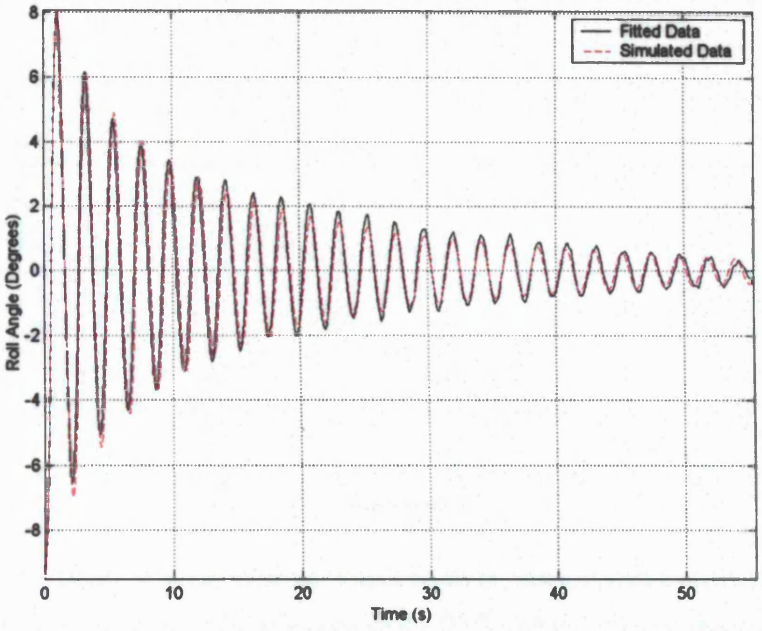

Figure 5-3- 9: Simulated roll decay history (calculated using linear and quadratic damping coefficients derived from the least squares fit to the equivalent linear damping values calculated between subsequent peaks) compared with the fitted decay data (using the Savitzky-Golay method) for trimaran model DVZ without roll damping appendages at zero speed

The same analysis was performed on decay data for trimaran DVZ without roll damping appendages at a speed equivalent to 12 knots. The decrement of the peaks is given in Figure 5-3- 10, with the plots of the equivalent linear damping between successive peaks and the comparison between the simulated and fitted decay histories in Figure 5-3- 11 and Figure 5-3- 12. Once again, there is a considerable spread of equivalent linear damping terms around the fitted line, although this time there are no negative damping values. Once again, generally speaking the fit of the simulated decay to the fitted data history (using the Savitzky-Golay method) is good. However, the damped natural frequency of the simulated fit does not match that of the fitted data causing a small phase difference between the fitted and simulated roll decays.

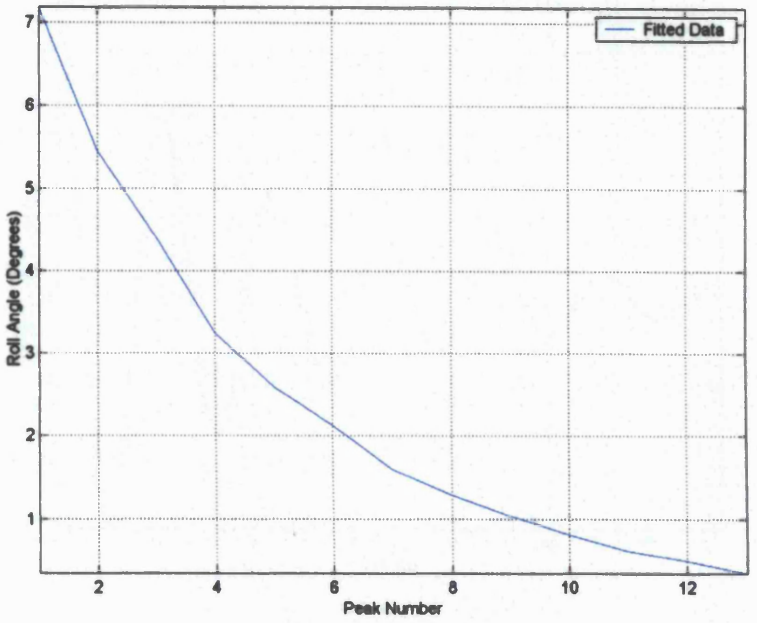

Figure 5-3- 10: Decay of peaks (absolute values taken so includes both positive and negative angles) in the fitted decay data for trimaran model DVZ without roll damping appendages at full scale speed equivalent to 12 knots

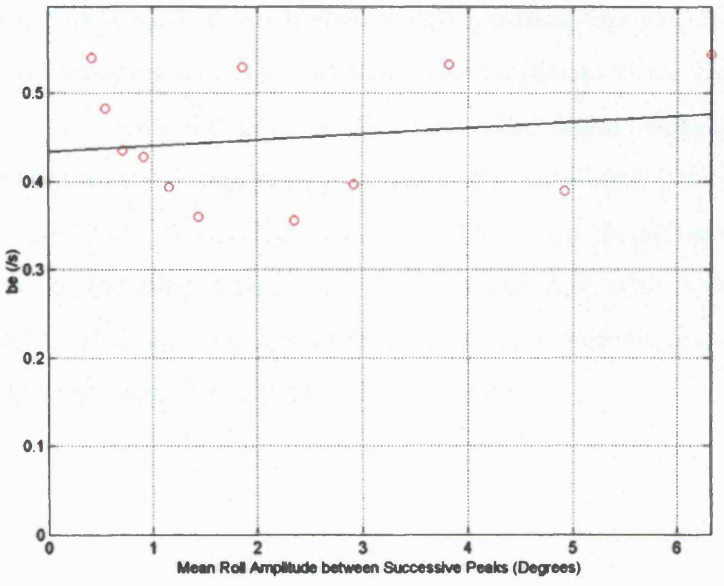

Figure 5-3- 11: Equivalent linear roll damping (be) plotted against mean roll angle between two successive peaks (red spots) for trimaran model DVZ without roll damping appendages at a speed equivalent to 12 knots at full scale. The black line is a least squares fit to the data used to obtain linear and quadratic damping coefficients (b_1 and b_2).

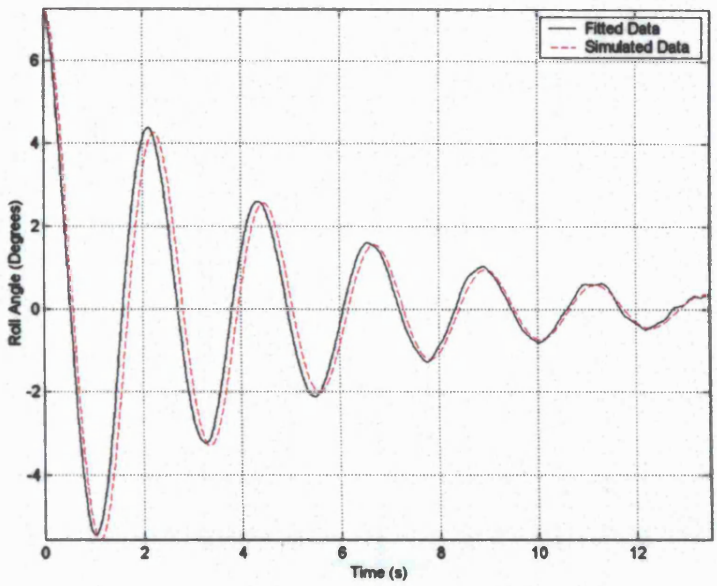

Figure 5-3- 12: Simulated roll decay history (calculated using linear and quadratic damping coefficients derived from the least squares fit to the equivalent linear damping values calculated between subsequent peaks) compared with the fitted decay data (using the Savitzky-Golay method) for trimaran model DVZ without roll damping appendages at a speed equivalent to 12 knots at full scale

A final comparison is made at the highest speed recorded, equivalent to 25 knots, without any roll damping appendages fitted. The decrement of the peaks is given in Figure 5-3- 13, with the plots of the equivalent linear damping between successive peaks and the comparison between the simulated and fitted decay histories in Figure 5-3- 14 and Figure 5-3- 15. There is a considerable spread of equivalent linear damping terms around the fitted line with some negative damping values. This time the simulated decay history provides a poor fit to the fitted decay history (using the Savitzky-Golay method).

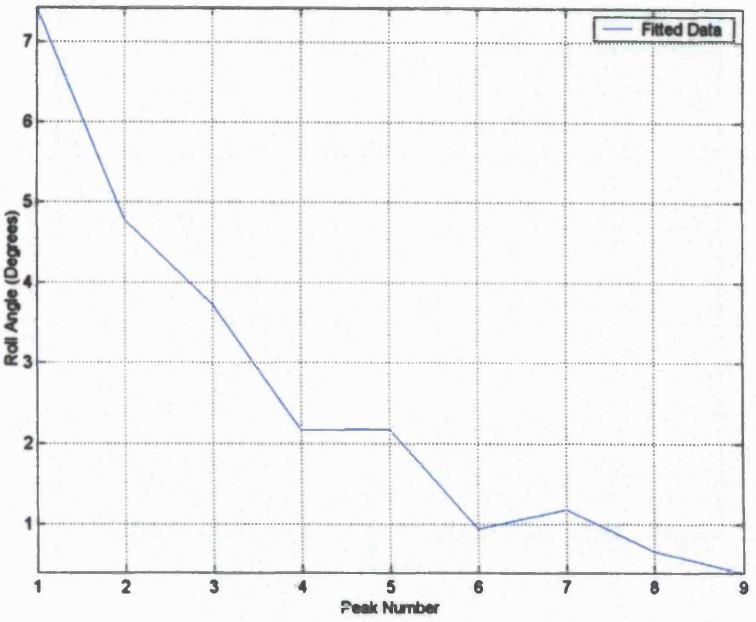

Figure 5-3- 13: Decay of peaks (absolute values taken so includes both positive and negative angles) in the fitted decay data for trimaran model DVZ without roll damping appendages at full scale speed equivalent to 25 knots

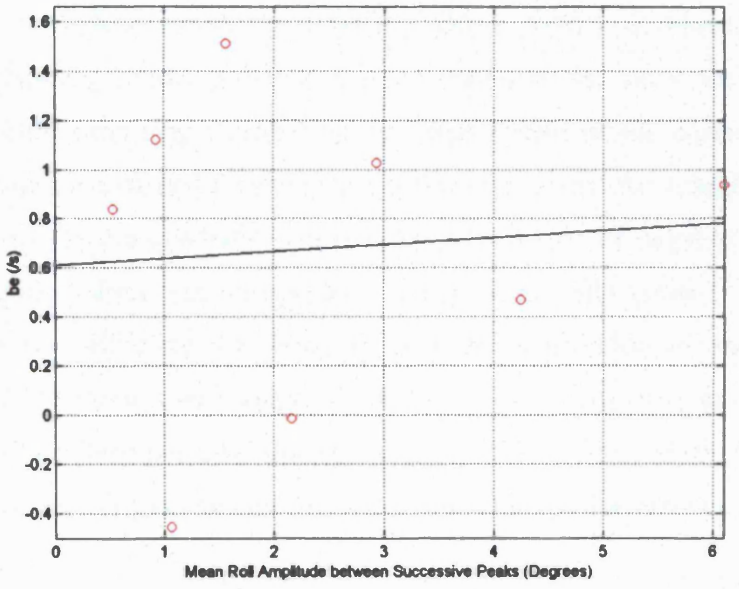

Figure 5-3- 14: Equivalent linear roll damping (be) plotted against mean roll angle between two successive peaks (red spots) for trimaran model DVZ without roll damping appendages at a speed equivalent to 25 knots at full scale. The black line is a least squares fit to the data used to obtain linear and quadratic damping coefficients (b_1 and b_2).

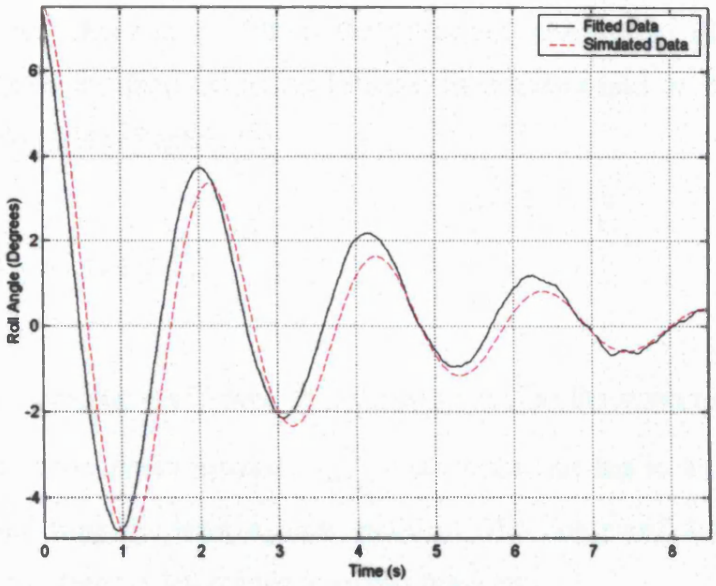

Figure 5-3- 15: Simulated roll decay history (calculated using linear and quadratic damping coefficients derived from the least squares fit to the equivalent linear damping values calculated between subsequent peaks) compared with the fitted decay data (using the Savitzky-Golay method)for trimaran model DVZ without roll damping appendages at a speed equivalent to 25 knots at full scale

Except at the highest speed, the simulated decay history developed using the quadratic damping model provides a good match to the fitted data. This is perhaps a little surprising considering the large spread of the equivalent linear damping values (calculated for every half roll cycle) around the straight line fitted through them for the quadratic model. The occurrence of negative equivalent linear damping values was unexpected. These could only occur if some other mechanism was affecting the decay so that the assumption of an uncoupled equation of roll motion with constant coefficients was incorrect, or if there has been drift of the "zero position" during the decay (the method reflects the negative peaks around zero degrees so that they are included in the decrement).

5.3.4 The Cubic Damping Model

The cubic damping model will now be considered over the same three conditions considered in Section 5.3.3, namely the model without roll damping appendages

at speeds equivalent to 0, 12 and 25 knots. The linear and cubic damping coefficients are obtained by fitting the following equation to the values of equivalent linear damping calculated between successive peaks in the roll decay (equation 2-4-3 from Chapter 2):-

$$b_e = b_1 + \frac{3}{4} b_3 \omega_d{}^2 x_{4m}{}^2 \qquad \text{5-3- 5}$$

As the cubic damping coefficient, b_3, is proportional to the mean roll amplitude between successive peaks squared, $x_{4m}{}^2$, a quadratic line has to be fitted to the damping data using the least squares method. The linear and cubic damping coefficients can then be determined from this fitted curve.

For the model at zero speed, the plots of the equivalent linear damping between successive peaks and the comparison between the simulated and fitted decay histories are given in Figure 5-3- 16 and Figure 5-3- 17. Once again, there is a considerable spread of equivalent linear damping terms around the fitted line with many negative damping values at low roll amplitudes. It can be seen that the simulated data does not match the fitted data quite so well at low roll amplitudes. This was also the case with the quadratic damping model.

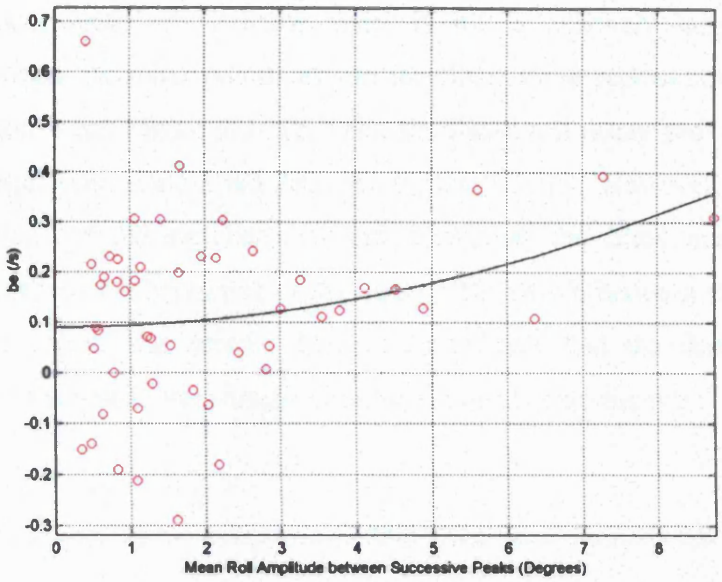

Figure 5-3- 16: Equivalent linear roll damping (be) plotted against mean roll angle between two successive peaks (red spots) for trimaran model DVZ without roll damping appendages at zero speed. The black line is a least square's fit to the data used to obtain linear and cubic damping coefficients (b_1 and b_3).

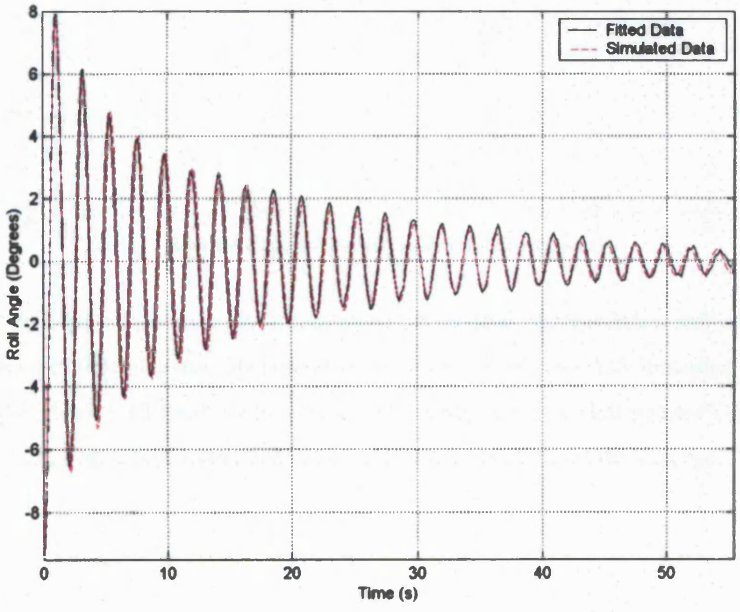

Figure 5-3- 17: Simulated roll decay history (calculated using linear and cubic damping coefficients derived from the least squares fit to the equivalent linearised damping values calculated between subsequent peaks) compared with a mathematical fit to the measured roll decay data using the Savitzky-Golay method for trimaran model DVZ without roll damping appendages at zero speed

With a model speed of 12 knots, there is still a relatively large spread of equivalent linear damping points around the fitted curve representing the cubic damping model, see Figure 5-3- 18. The simulated roll decay provides a pretty good representation of the fitted data, see Figure 5-3- 19. However, the damped natural period for the simulation is not correct as the fitted curve lags the simulated curve at the beginning of the decay. The match between them is better towards the end of the decay. This could indicate that the damped natural frequency of the model was changing during the decay experiment.

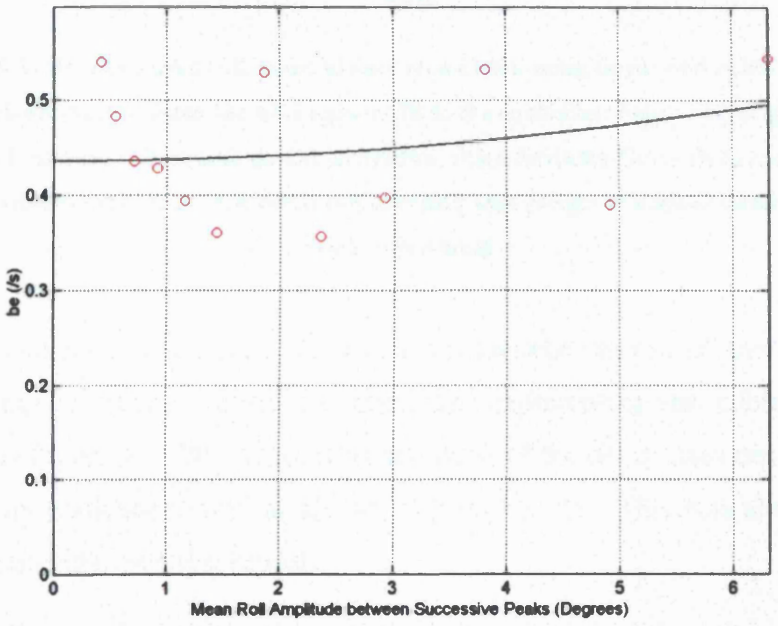

Figure 5-3- 18: Equivalent linear roll damping (be) plotted against mean roll angle between two successive peaks (red spots) for trimaran model DVZ without roll damping appendages at a speed equivalent to 12 knots at full scale. The black line is a least square's fit to the data used to obtain linear and cubic damping coefficients (b_1 and b_3).

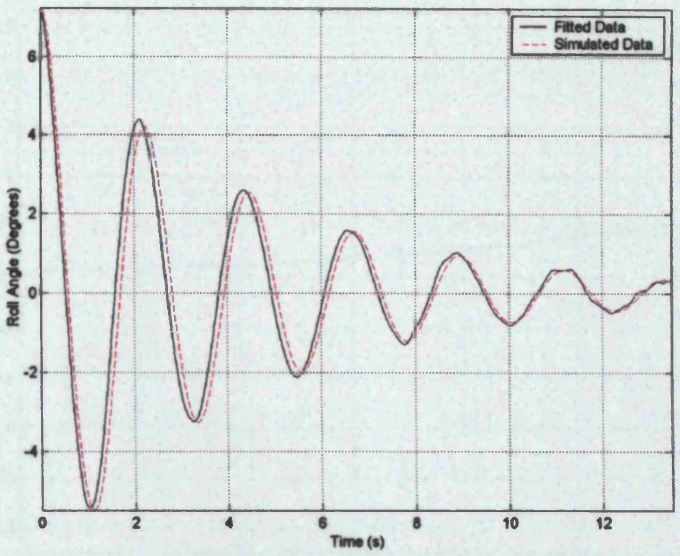

Figure 5-3- 19: Simulated roll decay history (calculated using linear and cubic damping coefficients derived from the least squares fit to the equivalent linear damping values calculated between subsequent peaks) compared with a Savitzky-Golay fit to the recorded data for trimaran model DVZ without roll damping appendages at a speed equivalent to 12 knots at full scale

For the final high speed case, there is a considerable spread of the equivalent linear damping values around the fitted line representing the cubic damping model, see Figure 5-3- 20. Thus, the simulation of the decay does not match the fitted decay particularly well at all, see Figure 5-3- 21. This was also the case with the quadratic damping model.

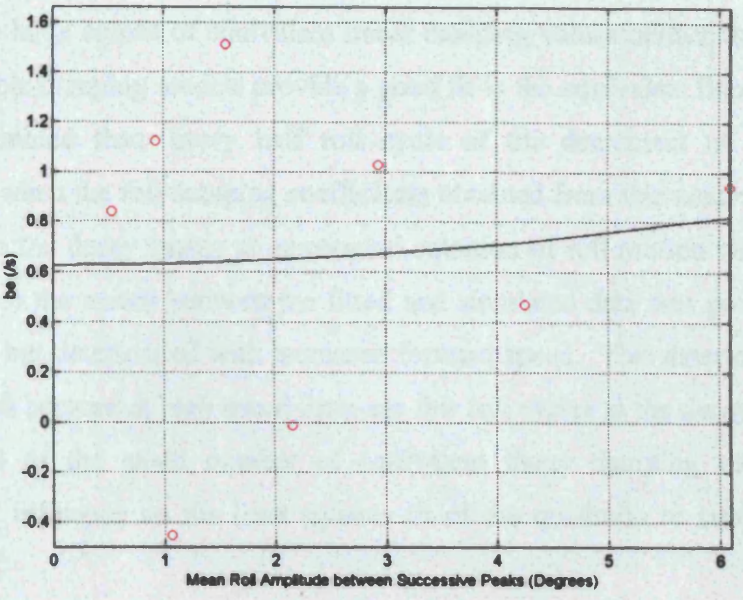

Figure 5-3- 20: Equivalent linear roll damping (be) plotted against mean roll angle between two successive peaks (red spots) for trimaran model DVZ without roll damping appendages at a speed equivalent to 25 knots at full scale. The black line is a least squares fit to the data used to obtain linear and cubic damping coefficients (b_1 and b_3).

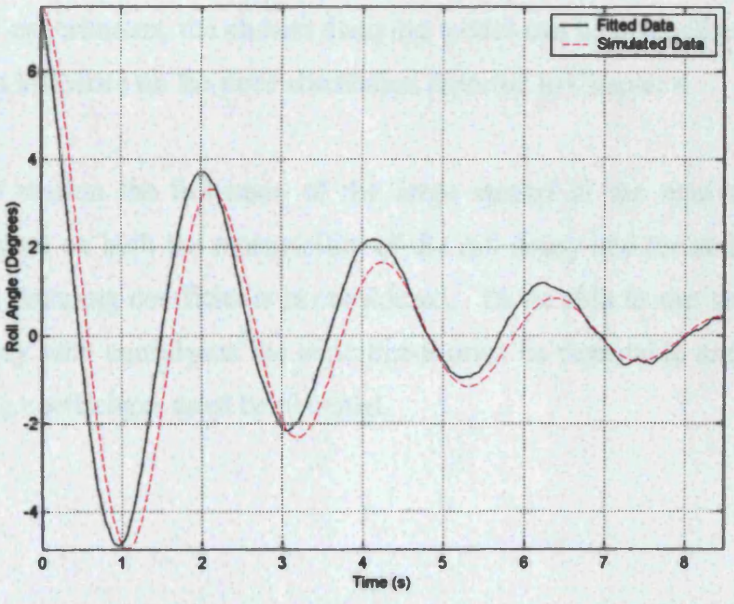

Figure 5-3- 21: Simulated roll decay history (calculated using linear and cubic damping coefficients derived from the least squares fit to the equivalent linear damping values calculated between subsequent peaks) compared with a Savitzky-Golay fit to the measured data for trimaran model DVZ without roll damping appendages at a speed equivalent to 25 knots at full scale

Due to the large spread of equivalent linear damping values neither the quadratic nor the cubic damping models provide a good fit to the equivalent linear damping data determined from every half roll cycle of the decrement of the decay. However, when the roll damping coefficients obtained from this analysis are used to simulate the decay (using an uncoupled equation of roll motion with constant coefficients) the match between the fitted and simulated data was pretty good at low speed but deteriorated with increased forward speed. This deterioration is to be expected because at high speed there are few roll cycles in the decay and hence the spread of the small number of equivalent linear damping values has a significant influence on the least squares fit of the quadratic or cubic damping model.

In Chapter 4, roll motion predictions obtained using linear Potential Flow Theory and roll damping coefficients measured in roll decay experiments did not correlate very well at all to roll RAO's obtained from model experiments in regular waves at low speeds in the region of roll resonance. Given that either the quadratic or cubic damping model provide a reasonably good fit to the roll decay measured from model experiments, the chosen damping model can be discounted as having a significant influence on the poor correlation reported in Chapter 4.

In the next section the influence of the large spread in the equivalent linear damping values on both the repeatability of the roll decay and the stability of the derived roll damping coefficients is considered. To be able to use the results of the roll decay with confidence the experiment must be repeatable and consistent roll damping coefficients must be obtained.

5.4 Repeatability of the Roll Decay and Stability of the Roll Damping Coefficients

A useful start point for investigations in this section is the variation of the linear and quadratic damping coefficients measured from the original analysis of the 2002 roll decay data (using the energy method). These results are shown in Figure 5-4- 1 and Figure 5-4- 2 where variations in the linear and quadratic damping coefficients are plotted separately against speed. In these figures the linear damping coefficient, b_1, has been made non-dimensional by dividing by $2\omega_n$ to get k_1, and the quadratic damping coefficient has been divided by 2 to give a non-dimensional coefficient k_2, see Spouge (95). The natural frequency, ω_n, has been determined from the measured (damped) roll period, therefore it has been assumed that $\omega_n \approx \omega_d$. Results are shown for the link-fins and T-foils discussed in Chapter 4 as well as for a pair of bilge keels and a pair of horizontal fins attached to the inboard face of the side hulls for comparison.

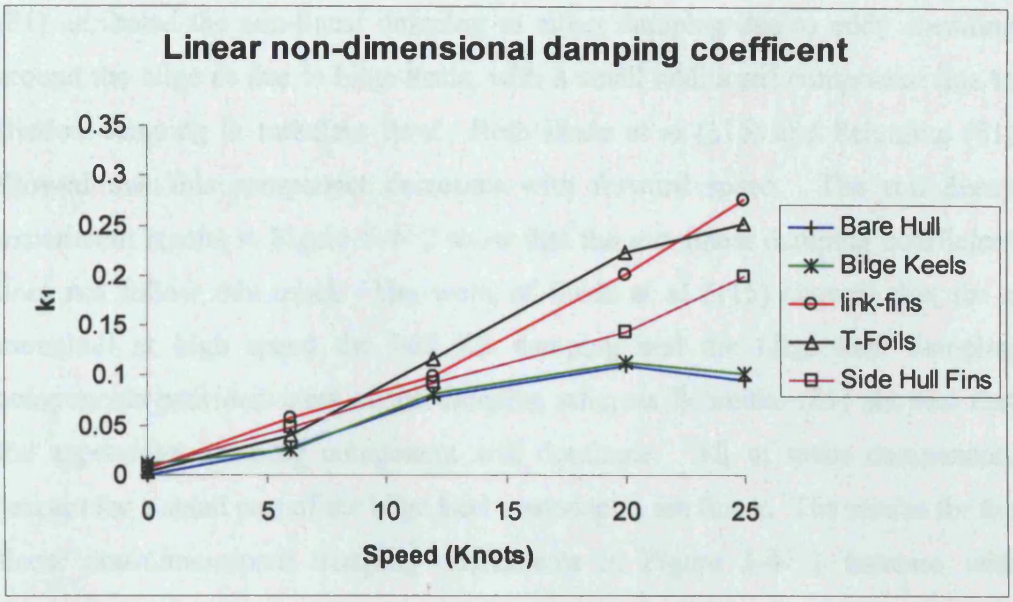

Figure 5-4- 1: Variation in the linear non-dimensional linear roll damping coefficient (k_1) with speed for a range of appendages tested in the 2002 model experiments on trimaran DVZ

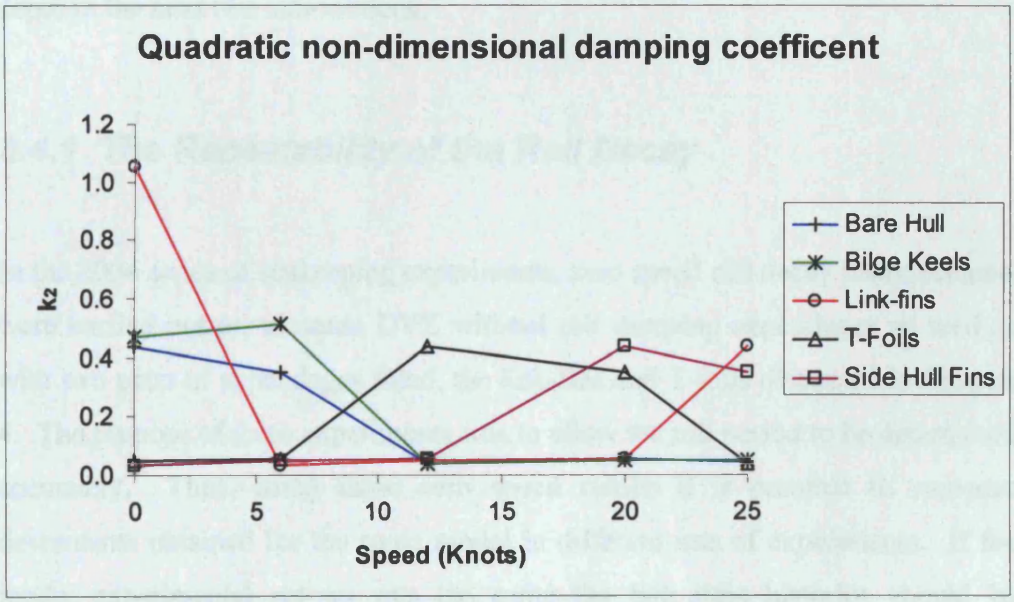

Figure 5-4- 2: Variation in the linear non-dimensional non-linear roll damping coefficient (k_2) with speed for a range of appendages tested in the 2002 model experiments on trimaran DVZ

In Chapter 2 it was shown that, for a monohull, Ikeda et al (114) and Schmitke (81) attributed the non-linear damping to either damping due to eddy shedding around the bilge or due to bilge keels, with a small additional component due to friction damping in turbulent flow. Both Ikeda et al (115) and Schmitke (81) showed that this component decreases with forward speed. The roll decay experiment results in Figure 5-4- 2 show that the non-linear damping coefficient does not follow this trend. The work of Ikeda et al (115) showed that for a monohull at high speed the hull lift damping and the bilge keel damping components provided most of the damping whereas Schmitke (81) showed that the appendage damping component will dominate. All of these components (except for a small part of the bilge keel component) are linear. The results for the linear non-dimensional damping coefficients in Figure 5-4- 1 increase with forward speed following the trends reported by Ikeda et al and Schmitke for monohulls. So, why are the results for the non-dimensional non-linear damping coefficient so variable? To try to understand this, free decay results measured from both the 2002 and 2004 series of model experiments are investigated in more depth in the next two sub-sections.

5.4.1 The Repeatability of the Roll Decay

In the 2004 series of seakeeping experiments, zero speed roll decay measurements were carried out on trimaran DVZ without roll damping appendages as well as with two pairs of appendages fitted, the link-fins and T-foils discussed in Chapter 4. The purpose of these experiments was to allow the roll period to be determined accurately. Thus, using these zero speed results it is possible to compare decrements obtained for the same model in different sets of experiments. If the model experimental set up was the same the two time histories should be identical. This would show that the results are repeatable.

The analysis of the 2004 roll decay results showed that there appeared to be bias in the model set up for the 2004 experiments. Figure 5-4- 3 shows the decrement of the peaks of the decay at zero speed from 2004. There is a noticeable "saw tooth" effect from peak number 5 onwards. This could occur if the decay was not

symmetrical around zero degrees, i.e. if there was a static heel angle, as taking the absolute values of the peaks will reflect them about zero degrees. This is not uncommon in roll decay analysis; Spouge (88) presents a decrement exhibiting this behaviour for the monohull Fishery Protection Vessel Sulisker. Mathisen and Price (85) and Renyuan (89) also show this on their analysis of the same Sulisker roll decay data. Spouge removed the bias by fitting a mean line through the peak decrement data. The problem with smoothing the data in this way is that other effects such as variations in roll stiffness or inertia during the decay could be removed. For this reason this approach is not adopted here.

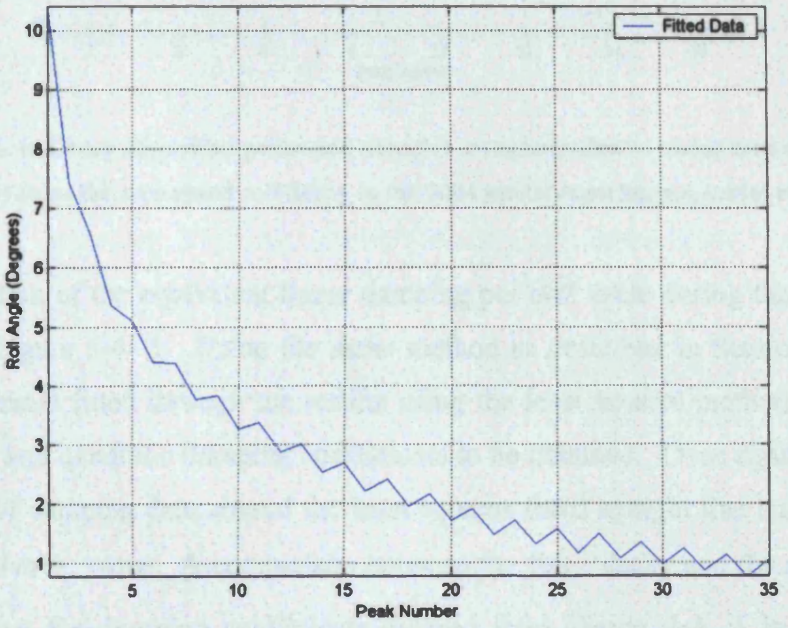

Figure 5-4- 3: Peak decrement of trimaran DVZ without roll damping appendages fitted. Results at zero speed from the 2004 model experiments. Absolute values are shown so that both positive maxima and negative minima are included

An indication of the magnitude of the bias can be obtained by comparing the decrement of the positive and negative portions of the complete decay. This is shown in Figure 5-4- 4. The difference between the two decrements is almost constant. The decay history was adjusted by trial and error until the two decrements were as near coincident as possible.

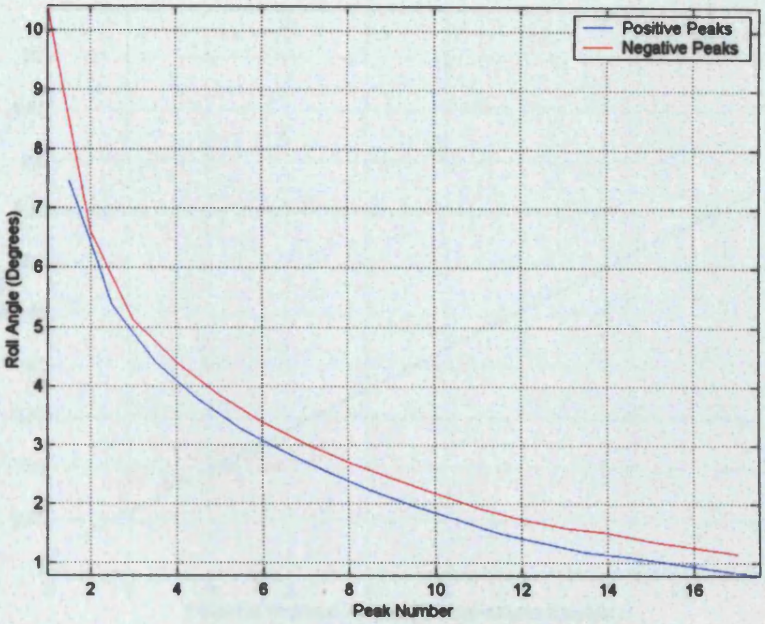

Figure 5-4- 4: Decay of positive peaks and negative troughs (reflected about zero degrees to be positive) from the zero speed roll decay in the 2004 model experiments, initial roll to port

The variation of the equivalent linear damping per half cycle during the decay is given in Figure 5-4- 5. Using the same method as described in Section 5.3.3 a straight line is fitted through the results using the least squares method to allow the linear and quadratic damping coefficients to be obtained. Once again there is a spread of damping data around the least squares fitted straight line and there is one negative b_e value. A comparison between the fitted decay and the simulated decay using the damping coefficients derived from Figure 5-4- 5 is given in Figure 5-4- 6. The correlation between the simulation of the decay using the quadratic damping model and the fitted data obtained using the Savitzky-Golay method is generally pretty good, being poorest at the larger roll amplitudes. The graph is truncated at 35 seconds as this was the point at which the data logger was switched off. In hindsight it would have been preferable to record a longer history, as most of the negative values of b_e from the analysis of the 2002 roll decay experiments occurred at the lowest roll amplitudes, see Figure 5-3- 16 and Figure 5-3- 17.

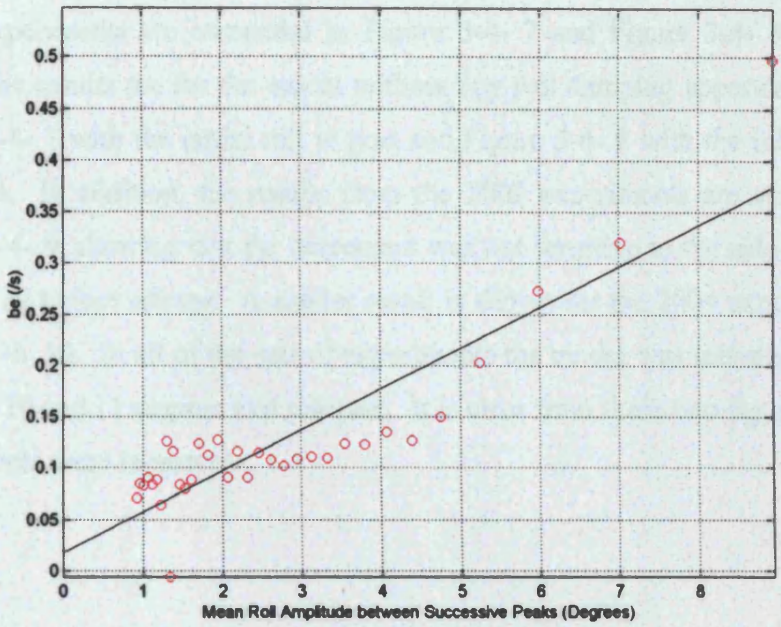

Figure 5-4- 5: Equivalent linear roll damping (be) plotted against mean roll angle between two successive peaks (red spots) for trimaran model DVZ without roll damping appendages at zero speed from the adjusted 2004 model experiment results

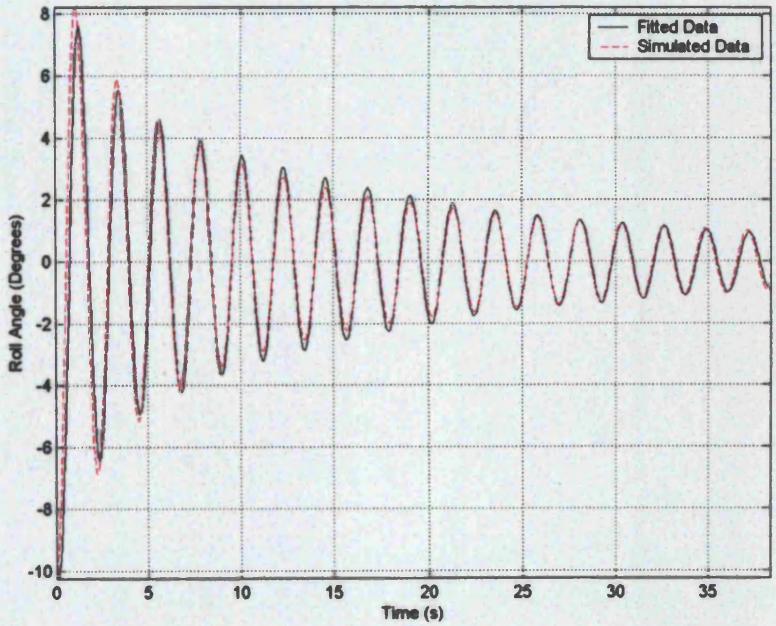

Figure 5-4- 6: Comparison between the simulated decay and the fitted decay for trimaran model DVZ without roll damping appendages at zero speed taken from the adjusted 2004 model experiment results

The decrement of the peaks from both the 2002 and 2004 series of zero speed roll decay experiments are compared in Figure 5-4- 7 and Figure 5-4- 8. In both figures the results are for the model without any roll damping appendages fitted, Figure 5-4- 7 with the initial roll to port and Figure 5-4- 8 with the initial roll to starboard. In addition, the results from the 2002 experiments are compared in Figure 5-4- 9, showing that the decrement was not sensitive to the side the model was heeled before release. A similar result is shown for the 2004 experiments in Figure 5-4- 10. In all of the sets of experiments the model was initially heeled to between 10 and 11 degrees and released. It is clear from these two figures that the experiments were repeatable.

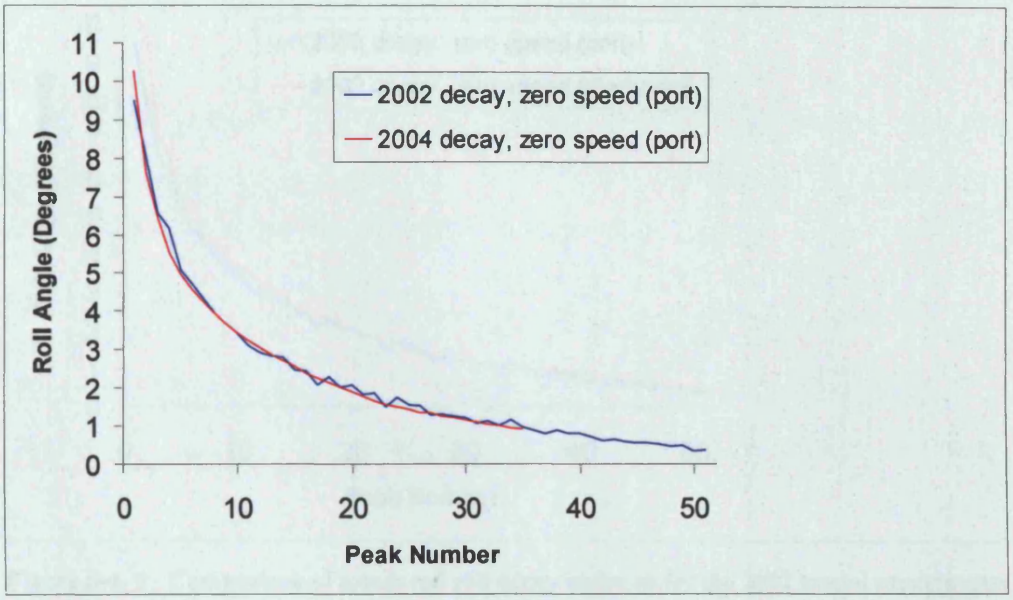

Figure 5-4- 7: Comparison of measured roll decay histories with initial heel to port for both the 2002 and 2004 model experiments for trimaran DVZ without roll damping appendages at zero speed. The 2004 results were adjusted to remove a bias

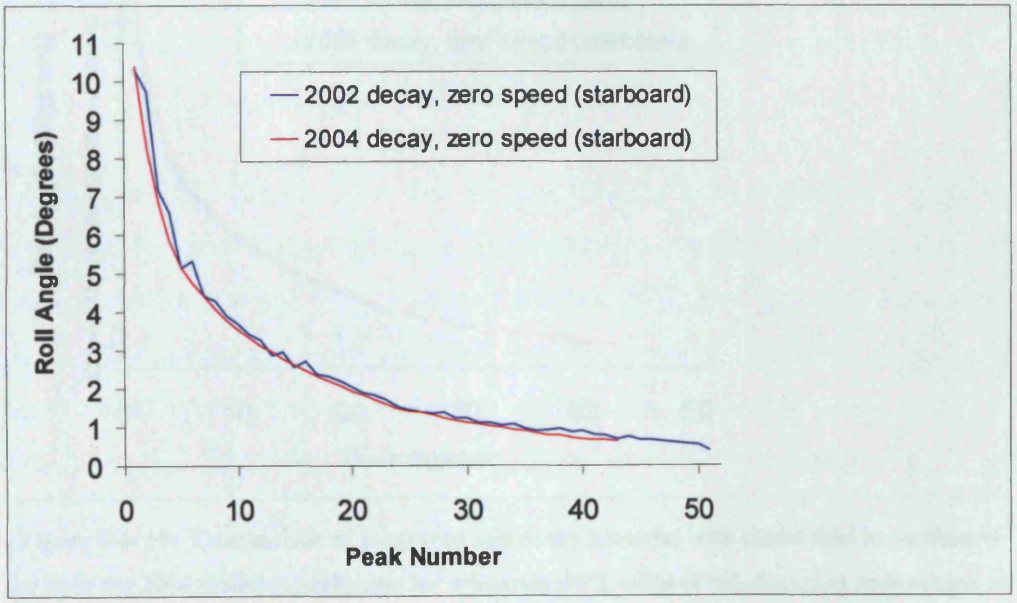

Figure 5-4- 8: Comparison of measured roll decay histories with initial heel to starboard for both the 2002 and 2004 model experiments for trimaran DVZ without roll damping appendages at zero speed. The 2004 results were adjusted to remove a bias

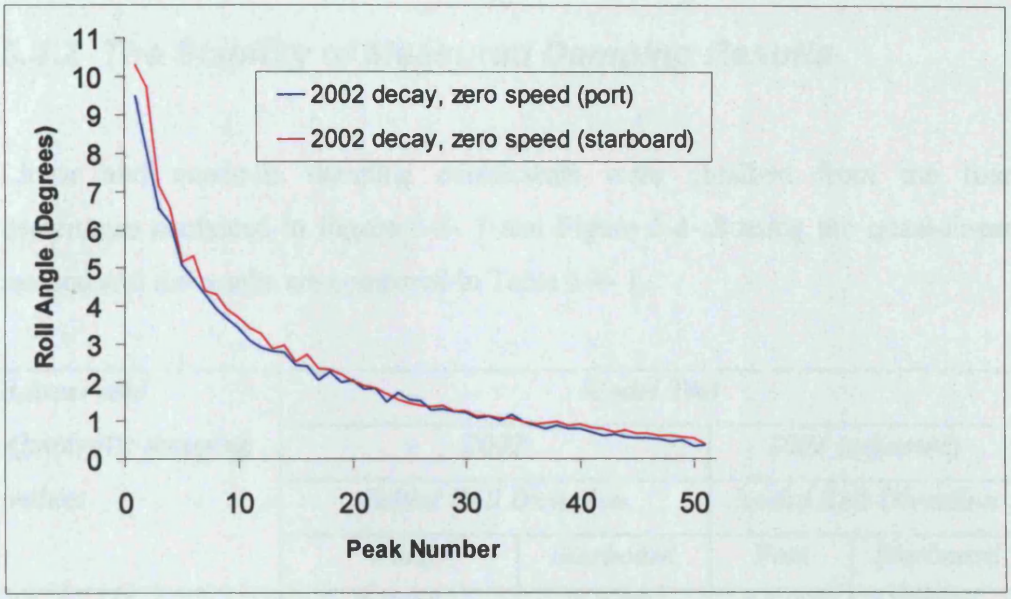

Figure 5-4- 9: Comparison of measured roll decay histories for the 2002 model experiments for trimaran DVZ without roll damping appendages at zero speed

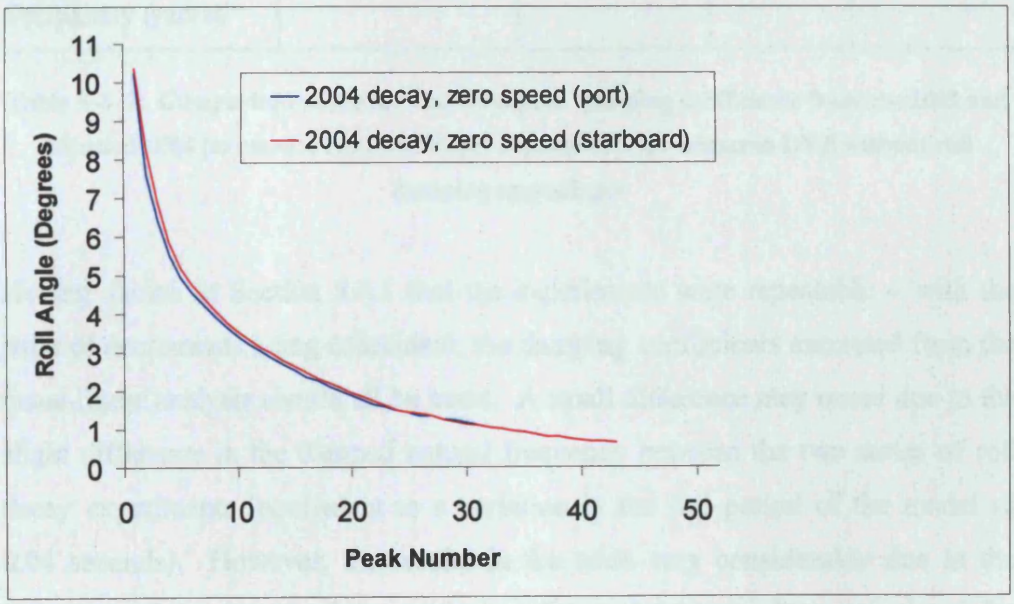

Figure 5-4- 10: Comparison of measured roll decay histories with initial heel to starboard for both the 2004 model experiments for trimaran DVZ without roll damping appendages at zero speed. The presented results were adjusted to remove a bias

5.4.2 The Stability of Measured Damping Results

Linear and quadratic damping coefficients were obtained from the four decrements contained in Figure 5-4- 7 and Figure 5-4- 8 using the quasi-linear method and the results are compared in Table 5-4- 1.

Linear and Quadratic damping values	*Model Test*			
	2002		*2004 (adjusted)*	
	Initial Roll Direction		*Initial Roll Direction*	
	Port	*Starboard*	*Port*	*Starboard*
Linear (/s)	0.0632	0.0663	0.0415	0.0174
Quadratic (/s)	0.6220	0.5246	0.7658	0.9625
Damped Natural Frequency (rad/s)	2.85	2.85	2.80	2.80

Table 5-4- 1: Comparison of Linear and Quadratic damping coefficients from the 2002 and adjusted 2004 (to remove bias) roll decay experiments for trimaran DVZ without roll damping appendages

Having shown in Section 5.4.1 that the experiments were repeatable – with the pairs of decrements being coincident, the damping coefficients extracted from the quasi-linear analysis should all be same. A small difference may occur due to the slight difference in the damped natural frequency between the two series of roll decay experiments (equivalent to a variation in the roll period of the model of 0.04 seconds). However, the results in the table vary considerably due to the influence of the spread of the equivalent linear damping values, calculated for each half period, on the fit of the straight line representing the chosen damping model (quadratic in this case). For this reason it is not possible to obtain stable damping coefficients from one decrement to the next using the quasi-linear method.

Whether this conclusion is specific to trimarans or also occurs when monohull roll decay is analysed using the same method is not known. However, the work in this

section has shown that there can be a considerable variation in roll decay coefficients derived from roll decay data using either of two different analysis methods, the energy method and the quasi-linear method.

The reason for the large spread of equivalent linear damping values must be understood. Due to this spread, damping coefficients cannot be determined from either set of the decay experiments with any degree of certainty. Differences even occur when the side the initial heel moment is applied is changed (from port to starboard). This would only be the case if the model was not symmetrical; trimaran DVZ is symmetrical about the x-z plane so this result is unexpected.

So, we have now answered the question about why the damping results can be so variable, the next question is what has caused this variation? If we stay with the assumption that roll decay can be modelled by an uncoupled equation of roll motion, the next assumption to consider is whether the coefficients of the equation are constant or not. This is the topic for the next section.

5.5 Variations in the Coefficients of an Uncoupled Equation of Roll Motion

In the previous section it was shown that stable roll decay coefficients could not be extracted from measured roll decay data using the quasi-linear method as there was a considerable spread in the measured values of equivalent linear damping calculated for every half roll cycle. The reason for this spread of equivalent linear damping data is unclear and it is also unclear whether it is caused by the trimaran hull shape or whether such a spread would occur in any roll decay experiment.

The aim of the research reported in this section was to see if a similar spread of equivalent linear damping data could be achieved using a simulation of the roll equation. The expectation being that a similar result, with a large spread of equivalent linear damping values, could be achieved by making parameters in the equation of motion time variant.

5.5.1 Roll Decay with Time Variation of the Roll Stiffness

The equation of motion for roll decay assumed so far in this thesis is the equation of uncoupled rolling:-

$$(I_4 + A_{44})\ddot{x}_4 + B_{44}\dot{x}_4 + C_{44}x_4 = 0 \qquad \text{5-5- 1}$$

If the whole equation is divided through by the sum of the roll inertia and the added inertia this becomes:-

$$\ddot{x}_4 + \frac{B_{44}}{(I_4 + A_{44})}\dot{x}_4 + \frac{C_{44}}{(I_4 + A_{44})}x_4 = 0$$

$$\Rightarrow \qquad \text{5-5- 2}$$

$$\ddot{x}_4 + b_{44}\dot{x}_4 + \omega_n{}^2 x_4 = 0$$

If a quadratic damping model is assumed and, for convenience, the natural roll frequency is considered approximately equal to the damped natural frequency (under the assumption of light damping) then the equation of motion becomes:-

$$\ddot{x}_4 + b_1\dot{x}_4 + b_2\dot{x}_4|\dot{x}_4| + \omega_d{}^2 x_4 = 0 \qquad \text{5-5-3}$$

In the conclusions to Chapter 4 it was postulated that for a trimaran the roll stiffness, roll inertia and roll added inertia could vary with time during roll motion due to changes in the hydrodynamic properties of the hull as the side hulls are immersed or emerge during one roll cycle. One way to account for such changes is to make the damped natural frequency in equation 5-5-3, ω_d, time variant. Strictly speaking, if the damped natural frequency is time variant then, because it is derived from the roll inertia and added inertia, it follows that both of the damping coefficients would be time variant also. However, to allow simulation of the roll decay to be compared with results from Section 5.4 the two damping coefficients, b_1 and b_2 shall be kept constant.

Equation 5-5-3 was simulated using the Runge-Kutta technique as implemented in the MATLAB software using the following damping coefficients and damped natural frequency consistent with the values in Table 5-4- 1 for zero speed roll decay:-

b_1 (/s)	0.04
b_2 (/s)	0.75
ω_d (rad/s)	2.85

The simulation of the decay was then analysed using the quasi-linear method and the results are shown in Figure 5-5- 1. The red circles are the values for the equivalent linear damping for each half roll period and the black straight line represents the assumed quadratic damping model. As this is a simulation, the red circles representing the equivalent linear damping all sit on the black line representing the quadratic damping model. Contrast this figure with Figure 5-3- 8

and Figure 5-4- 5 which both show a considerable spread of the equivalent linear damping results around the straight line representing the quadratic damping model.

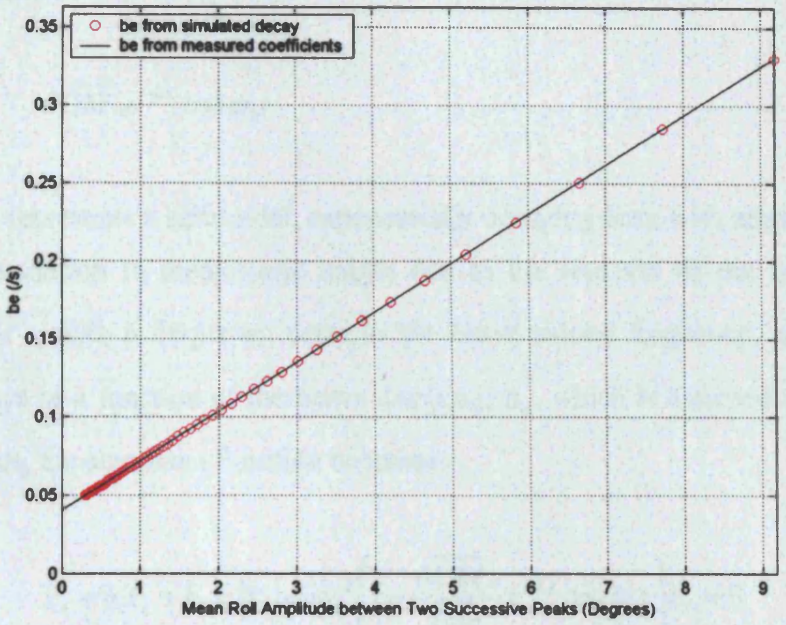

Figure 5-5- 1: Variation of equivalent linear roll damping (be) plotted against mean roll angle between two successive peaks (red spots) for a simulation of roll equation without stiffness variations

Next, the damped natural frequency is made time variant. There was some evidence of changes in the frequency of the roll decay history in Section 5.3, see the discussion regarding Figure 5-3- 19. In order for the simulation to be representative of the actual roll decay recorded in the model experiments a realistic variation of the damped natural frequency needed to be applied. The damped natural frequency varies in proportion with the roll stiffness, C_{44}, which is dependent on the product of the displacement and $\overline{GM}$:-

$$C_{44} = \rho \nabla g \overline{GM} \qquad \text{5-5- 4}$$

To instigate a roll decay experiment a force must be applied to the model on one side and then released. This force will heave the model downwards changing the

draught. At this new draught the displacement and $\overline{GM}$ will change which will in turn modify the roll stiffness. The model will heave up and down (whilst rolling) until the heave motion has decayed. To simulate this behaviour the following expression was added to the stiffness term (ω_d^2) in the equation of motion:-

$$\delta\overline{GM}_a e^{-b_h t}\cos\omega_h t \qquad \text{5-5-5}$$

This represents a sinusoidal, exponentially decaying term with amplitude equal to the variation in metacentric height due to the removal of the inclining force, $\delta\overline{GM}_a$, with a frequency equal to the heave natural frequency, ω_h. This term decays as a function of the heave damping, b_h, which is assumed to be constant. Hence, the equation of motion becomes:-

$$\ddot{x}_4 + b_1\dot{x}_4 + b_2\dot{x}_4|\dot{x}_4| + \omega_d^2\left(1+\frac{\delta\overline{GM}_a}{\overline{GM}}e^{-b_h t}\cos\omega_h t\right)x_4 = 0 \qquad \text{5-5-6}$$

To perform simulations using this equation of motion the unknowns need to be determined. For all of the zero speed roll decay experiments, in both 2002 and 2004, the model was heeled by hand to 10 degrees and released. The hydrostatic properties of the trimaran model were obtained using the Paramarine software (www.grc-ltd.co.uk). Thus, $\delta\overline{GM}_a$ was deduced by finding the weight required at the edge of the upper deck of the model to give 10 degrees of heel. This weight was then placed at the longitudinal centre of floatation (LCF) and the change of metacentric height assessed to give $\delta\overline{GM}_a$. The heave natural frequency was obtained by examination of the roll and heave time histories from the 2004 roll decay experiment results (see Section 5.6). It was not possible to determine the heave damping and so a number of different values were tried. The final values used for the simulation are given below:-

b_1 (/s)	0.04
b_2 (/s)	0.75
ω_d (rad/s)	2.85
ω_h (rad/s)	Approx 2.0
$\delta\overline{GM}_a$ (mm)	4.29
$\overline{GM}$ (mm)	142.10
b_h	Varies

A simulation was conducted with the heave damping term set to zero. The results are shown in Figure 5-5- 2 which contains four graphs: the top graph is the simulated roll decay; the second graph is the variation in metacentric height during the decay; the third graph is the decrement, where negative troughs have been reflected about zero degrees to give positive values; and the final graph is the change in equivalent linear damping during the decay. Compared to the previous graphs of equivalent linear damping, the final graph has had the scale on the x-axis reversed so that it starts with the high roll amplitudes which occur at the beginning of the decay on the left end, and finishes with the smaller amplitudes which occur at the end of the decay on the right hand side, hence following the same logic as the three graphs above it. The black line in the last graph joins together the equivalent linear damping points.

The results of this simulation are significant as the equivalent linear damping results exhibit a spread similar to that observed in the 2002 series of model experiments analysed in Section 5.3.

Looking at the plots of the metacentric height variation (the second graph in the series), if the heave damping, b_h, increases the metacentric height variation will reduce and so the spread of the equivalent linear damping results will reduce also. This is not what was observed in the model experiment results discussed in Section 5.3 where a large variation occurred at low roll amplitudes. To demonstrate this point, the simulation was repeated with the heave damping term,

b_h, set to 0.08. The results are shown in Figure 5-5- 3 where it can be seen that the increase in heave damping significantly reduces the spread in the equivalent linear damping values at low roll amplitudes.

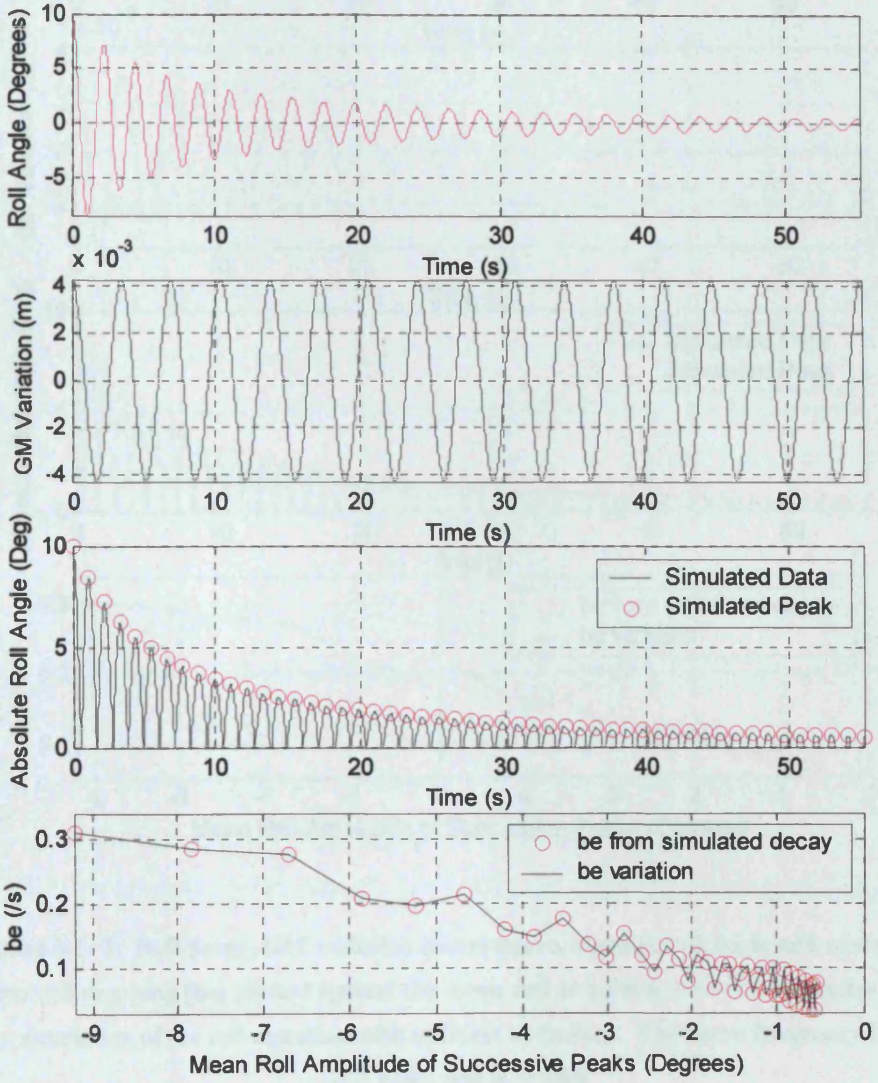

Figure 5-5- 2: Roll decay, GM variation due to heave, absolute roll angle and equivalent linear roll damping (be) plotted against the mean roll amplitude between successive peaks for a simulation of the roll equation with stiffness variations. The heave frequency is equal to 2 rad/s and there is no heave damping

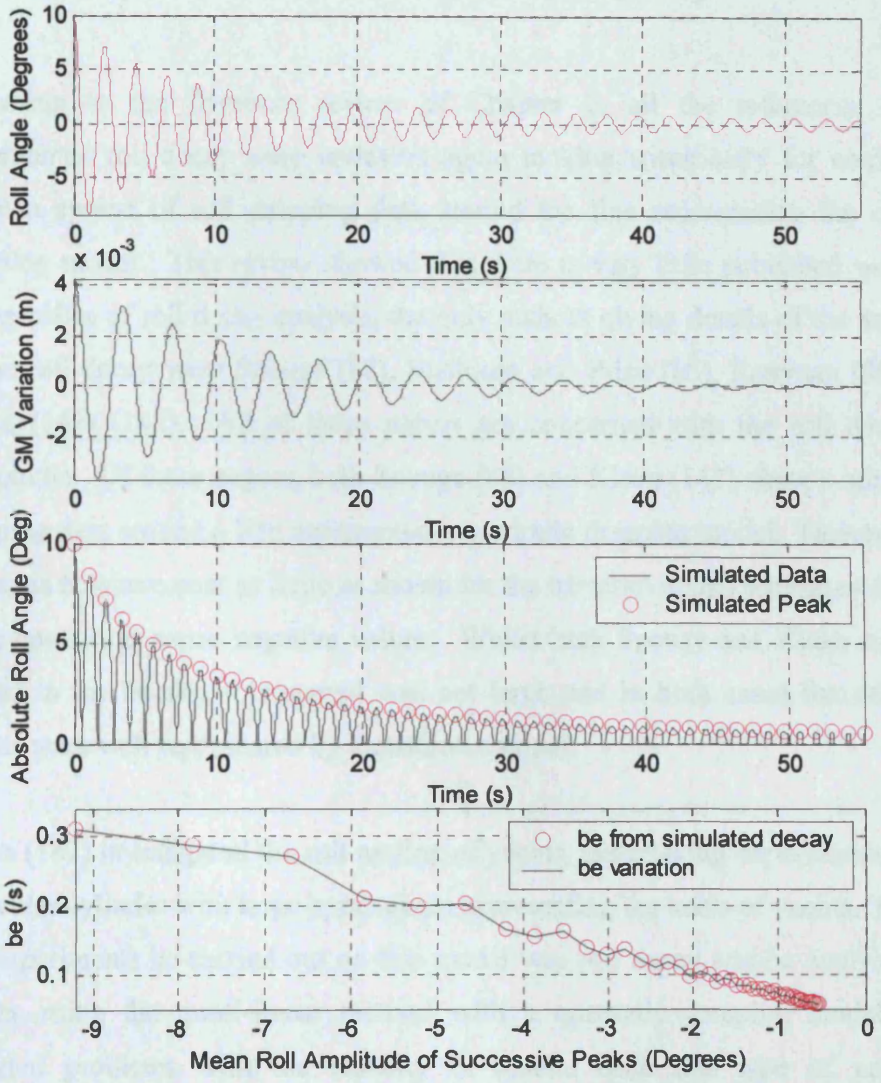

Figure 5-5- 3: Roll decay, GM variation due to heave, absolute roll angle and equivalent linear roll damping (be) plotted against the mean roll amplitude between successive peaks for a simulation of the roll equation with stiffness variations. The heave frequency is equal to 2 rad/s and $b_h = 0.08$

This result is significant as it shows that, when analysed using the quasi-linear method, a spread of equivalent linear damping values should occur in *any* roll decay experiment. However, to get a large spread at low roll amplitudes there must be little or no heave damping. Before moving on it is important to look back through the literature and see if any similar results have been reported for monohulls.

5.5.2 Comparisons with Monohull Roll Decay

Returning to the literature review of Chapter 2, all the references which documented roll decay were reviewed again looking specifically for comments about a spread of roll damping data around the line representing the chosen damping model. This review showed that there is very little published work on the specifics of roll decay analysis, the only authors giving details of the analysis of the roll decay were Spouge (88), Mathisen and Price (85), Renyuan (89) and Klaka (141) (142). All of these papers are concerned with the roll decay of monohulls. Of these papers, both Spouge (88) and Klaka (141) show a spread of damping data around a line represented a quadratic damping model. However the spread is nowhere near as large as shown for the trimaran in this section and never large enough to cause negative values. Whilst both Spouge and Klaka report a spread in the results, this spread was not large and in both cases the damping results were well represented by a quadratic model.

Klaka (142) investigated the roll motion of yachts, undertaking experiments using a circular cylinder with large appendages representing the keels of yachts. One of the experiments he carried out on this model was roll decay and he analysed the results using the quasi-linear method with a quadratic damping model. He reported problems with the stability of results from this type of analysis. However, he attributed the variation in linear and quadratic damping coefficients to different initial heel angles at the beginning of each experimental run. In the trimaran results presented in this chapter the initial heel angle was constant.

A further document was brought to the attention of the author written by Thompson, Cotton, Spyrou, de Souza and Bishop (178) about the Nonlinear Dynamics of Ship Roll and Capsize. In this report, two series of zero speed roll decay experiments are documented: the first were undertaken at DERA Haslar (now QinetiQ) using a 25^{th} scale model of a frigate and a second, less comprehensive series, were undertaken at University College London using a simple model based on the low freeboard model used by Wright and Marshfield (179) in their work on ship roll response and capsize. Both sets of results were

analysed using the quasi-linear method with a quadratic roll damping model fitting the frigate data best and a cubic model fitting the UCL model results best. In both cases there was a spread of damping data around the line representing the chosen damping model. However, for both sets of experiments, the line representing the chosen damping model provided a good fit to the equivalent linear damping data. The purpose of both of these experiments was to investigate the roll characteristics of ships at large angles and so the experiments started at large roll angles, between 25 and 40 degrees.

The results for the frigate were obtained in the same experimental facility as the trimaran results documented in this chapter using a model of similar size. The model represented a monohull frigate of approximately 5000 tonnes. The spread of equivalent linear damping data occurred at all roll amplitudes and, in general, appeared to decrease somewhat at low roll amplitudes. This result provides a useful comparison with the trimaran data, having been performed at the same experimental facility. The difference between the two sets of data is that, for zero speed roll decay, whilst there is a spread in equivalent linear damping data in both cases, for the trimaran the spread is such that a line representing either a quadratic or cubic damping model does not provide a good fit to the experimental data. Whereas for the monohull, the spread of data is not so great and a line representing a quadratic damping model provides a good fit to the data.

So, it would appear that a spread in the equivalent linear damping data obtained using the quasi linear method is not uncommon, however this spread is not generally large enough to influence the stability of the results, with most authors obtaining adequate results by fitting either a quadratic or cubic roll damping model to the experimental data. Therefore, many engineers make the decision to smooth the data by fitting a line through the decrement of the peaks (and reflected troughs) which would remove this spread. This approach was adopted by Spouge (88) when analysing roll decay data for a model of the monohull Fishery Protection Vessel Sulisker.

It would thus seem that the principal difference between the roll decay of the trimaran and the monohull is the spread of the damping data at low roll

amplitudes. On the trimaran, this spread is large enough to influence the fitting of a line representing the chosen damping model to the extent where stable results cannot be obtained.

The simulations of roll decay, using a single degree of freedom uncoupled roll equation with a time varying stiffness term to allow for the change in $\overline{GM}$ as the model heaves after the inclining force instigating the decay is removed, show that the only way to get such a spread in damping data is if the heave damping is very small indeed. Crossland, Wilson and Bradburn (173) performed free heave decay experiments on monohulls and in these experiments the heave motion was highly damped, decaying away completely within two or three cycles.

This indicates that for a trimaran any heave motion induced during the roll decay experiment may not decay away. In the next section a more complete simulation of the roll decay of trimaran DVZ is undertaken to see if any further light can be shed on the subject.

5.5.3 A More Complete Simulation of Trimaran Roll Decay in the Time Domain

In Section 5.5.1 roll decay was simulated in the time domain with a sinusoidal, exponentially decaying variation in the roll stiffness. This was thought to occur due to the heave motion applied to the model to obtain the initial heel angle at the start of roll decay. The logical extension to this would be to model the roll decay with a coupled roll and heave equation of motion. However, this has the disadvantage that there are a larger number of unknowns and the cross coupled terms in particular cannot be easily measured in model experiments. In any case, further experimentation was not possible therefore the only solution would be to determine these cross coupled terms using a seakeeping computer code. This makes the analysis much more complicated and it is then reliant on the accuracy of the seakeeping code. These added complexities are not desirable at this initial investigative stage. The aim of this section is to investigate the assumption of

constant coefficients in the equation of motion. The issue of motion coupling is dealt with in the next section (Section 5.6).

The focus of this sub section is examine the effect of heave motion on the roll stiffness in roll decay in greater detail to see if the large spread in the equivalent linear damping values obtained earlier in the chapter can be replicated. To allow comparison with the decay analysis of trimaran DVZ, simulations shall be performed using a modified single degree of freedom equation of motion.

First the problem must be broken down into parts. Coupled heave and roll can be considered as the sum of three effects:-

- Heave motion induced by removal of the inclining force *without roll motion* decaying at the heave natural frequency
- Roll motion *without heave* induced by removal of the inclining force decaying at the roll natural frequency, i.e. rolling around a fixed waterplane
- Heave motion induced by the additional buoyancy of the haunches as they are immersed during roll motion. This decays at the roll natural frequency

This is shown pictorially in Figure 5-5- 4 over the page. To maintain a single degree of freedom equation of motion, *the heave motion is modelled only by the effect it has on the roll stiffness.* If the model heaves the waterplane area will change which will in turn cause $\overline{GM}$ to change. For monohull ships the effect heave motion has on $\overline{GM}$ is small as flare is moderate and heave amplitudes are small. However, for a trimaran, small heave motions change the waterplane area of the side hulls due to the haunches and, because of the parallel axis theorem, this can cause significant changes in $\overline{GM}$ (through changes in $\overline{BM}$). These heave induced changes in $\overline{GM}$ will change the roll stiffness and thus coupled heave and roll can be modelled in a simplistic way by modifying the roll stiffness term.

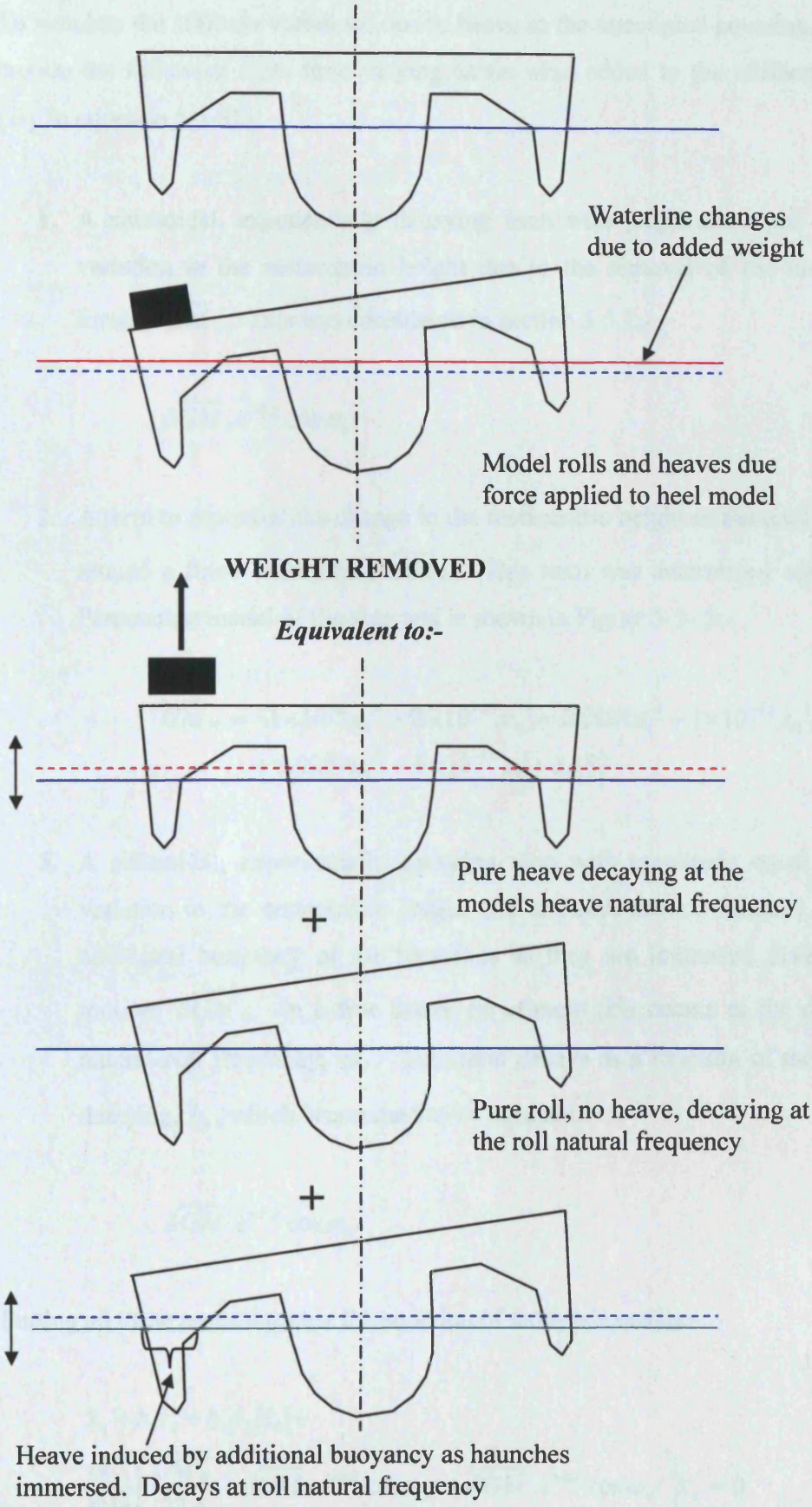

Figure 5-5- 4:- Movement of the trimaran model after removal of the inclining weight

To simulate the stiffness variations due to heave in the uncoupled equation of roll motion the following three time varying terms were added to the stiffness term (ω_d in equation 5-5-3):-

1. A sinusoidal, exponentially decaying term with amplitude equal to the variation in the metacentric height due to the removal of the inclining force, $\delta\overline{GM}_a$. This was considered in section 5.5.1:-

$$\delta\overline{GM}_a e^{-b_h t}\cos\omega_h t \qquad \textbf{5-5-7}$$

2. A term to represent the change in the metacentric height as the model rolls around a fixed waterplane, $\overline{GM}_w$. This term was determined using the Paramarine model of the ship and is shown in Figure 5-5- 5:-

$$\begin{aligned}\overline{GM}_w = &-1\times10^{-6}x_4^{\,6} - 2\times10^{-15}x_4^{\,5} - 0.0001x_4^{\,4} - 1\times10^{-12}x_4^{\,3} \\ &+ 0.0294x_4^{\,2} + 4\times10^{-10}x_4 + 3.183\end{aligned} \qquad \textbf{5-5-8}$$

3. A sinusoidal, exponentially decaying term with amplitude equal to the variation in the metacentric height due to heave motion induced by the additional buoyancy of the haunches as they are immersed during roll motion, $\delta\overline{GM}_v$. In a free decay experiment this occurs at the damped natural **roll** frequency, ω_d. This term decays as a function of the heave damping, b_h, which is assumed to be constant:-

$$\delta\overline{GM}_v e^{-b_h t}\cos\omega_d t \qquad \textbf{5-5-9}$$

Putting all these terms together the equation of motion becomes:-

$$\begin{aligned}&\ddot{x}_4 + b_1\dot{x}_4 + b_2\dot{x}_4|\dot{x}_4| + \\ &\frac{\omega_d^{\,2}}{\overline{GM}}\left(\frac{\overline{GM}_w}{22.4} + \delta\overline{GM}_a e^{-b_h t}\cos\omega_h t + \delta\overline{GM}_v e^{-b_h t}\cos\omega_d t\right)x_4 = 0\end{aligned} \qquad \textbf{5-5-10}$$

The 22.4 in the term for $\overline{GM}_w$ is to convert equation 5-5-8 from ship to model scale (the Paramarine solid model of the hull was produced at ship scale).

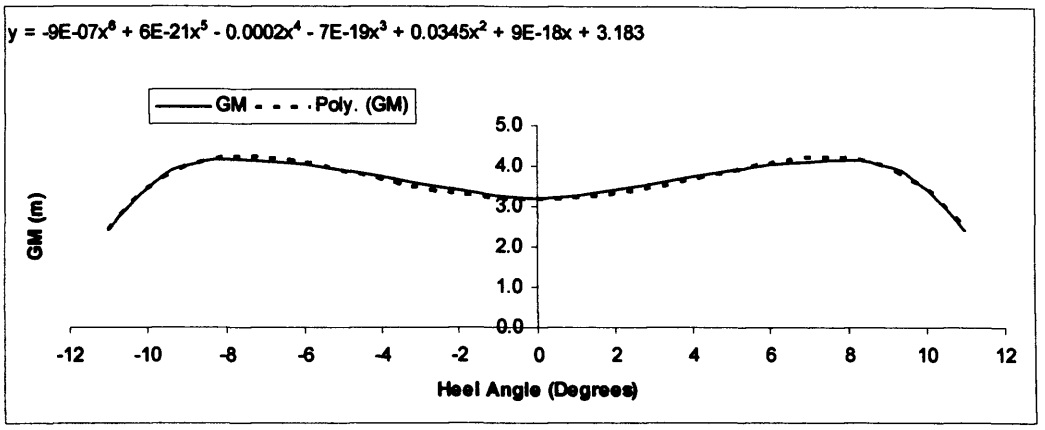

Figure 5-5- 5:- Change in GM due to heel about a fixed waterline (note that the displacement changes as haunches are immersed)

To perform the simulations the remaining unknowns in equation 5-5-10 need be determined. For all the zero speed roll decay experiments the model was initially heeled by hand to 10 degrees and released. Therefore, using Paramarine, the terms $\delta\overline{GM}_a$ and $\delta\overline{GM}_v$ could be determined. $\delta\overline{GM}_a$ was calculated in section 5.5.1 by finding the weight required at the edge of the upper deck to give 10 degrees of heel. This weight was then placed at the LCF and the change in metacentric height assessed to give $\delta\overline{GM}_a$. Similarly $\delta\overline{GM}_v$ was found by heeling the model to 10 degrees (about a fixed waterplane), accounting for the extra displacement due to the immersion of the haunches the change in metacentric height was assessed. The parameters used in simulation of the decay using 5-5-10 are as follows:-

b_1 (/s)	0.04
b_2 (/s)	0.75
ω_d (rad/s)	2.85
ω_h (rad/s)	Approx 2.0
$\delta\overline{GM}_a$ (mm)	4.29
$\delta\overline{GM}_v$ (mm)	6.25
$\overline{GM}$ (mm)	142.10
b_h	Varies

First of all, the effect of stiffness variations due to the ship rolling around a fixed waterplane will be considered (the $\overline{GM}_w$ term). For these simulations $\delta\overline{GM}_a$ and $\delta\overline{GM}_v$ are set to zero. The change in roll stiffness can be assessed by calculating the instantaneous value of $\overline{GZ}$ by multiplying the instantaneous value of $\overline{GM}$ (modified by the $\overline{GM}_w$ term as shown in Figure 5-5- 5) by the roll angle at each and every time step. This is shown in Figure 5-5- 6 where the blue circles are the values of $\overline{GZ}$ at each time step and the solid black line represents the case when $\overline{GZ}$ is obtained from the static value of $\overline{GM}$ (142.10 mm) multiplied by the instantaneous roll angle.

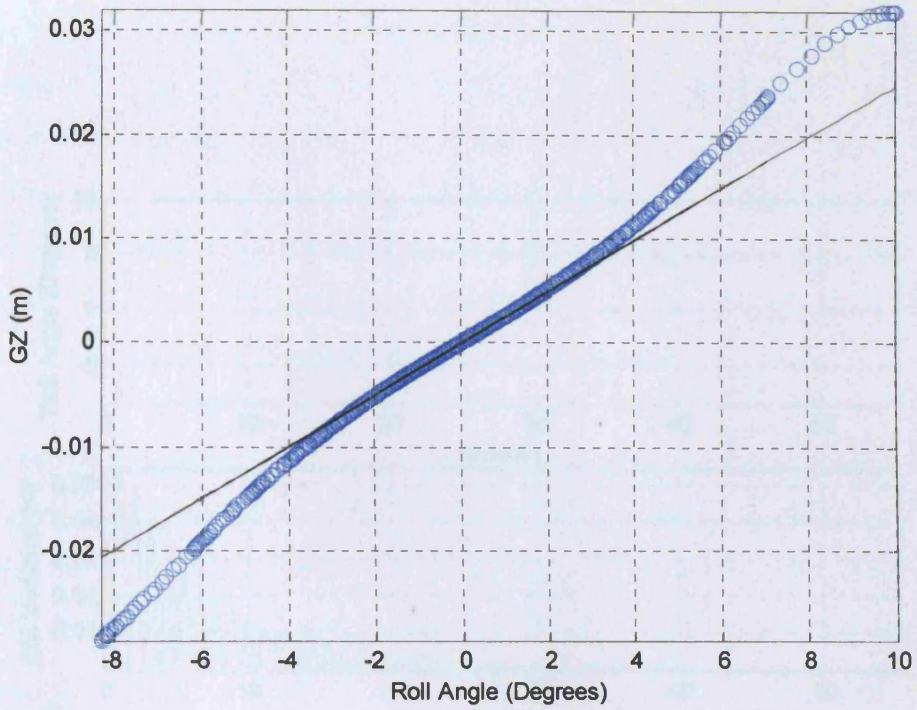

Figure 5-5- 6: Variation in GZ due to the time varying term GM_w. The blue circles are the time values of GZ at each time step in the simulation. The solid black line represents the value of GZ if a constant value of GM is used (142.10 mm)

From the figure, it can be seen that the $\overline{GM}_w$ term in equation 5-5-10 has the effect of increasing the roll stiffness for roll angles greater than 4 degrees. The resulting simulated decay and associated equivalent linear damping values are given in Figure 5-5- 7. This shows that there are no noticeable changes to the equivalent linear damping values, b_e, with all the red circles appearing to lie on a straight line as would be expected for a quadratic damping model (the solid black line joining the red circles in the figure is almost completely straight). The large variation of $\overline{GM}$ at the beginning of the decay does not cause the equivalent linear damping results to spread away from this straight line.

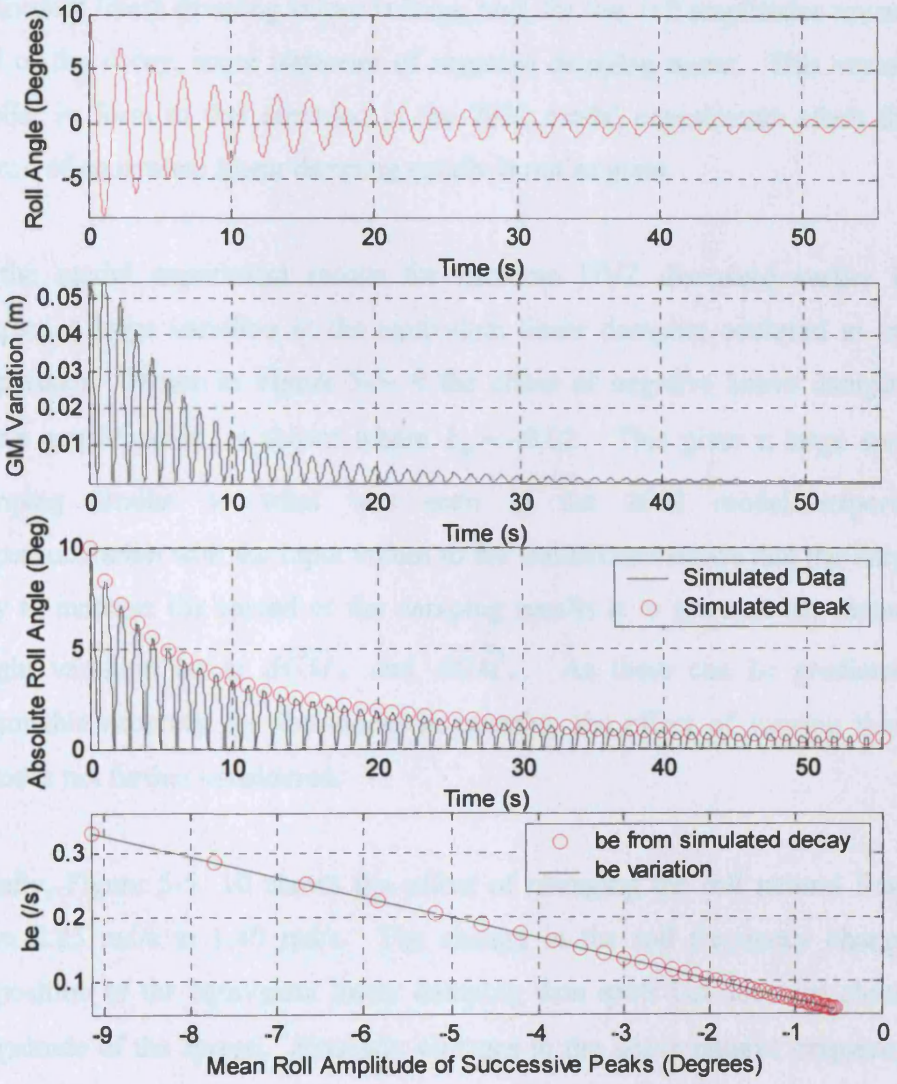

Figure 5-5- 7: Roll decay, GM variation due to heave, absolute roll angle and equivalent linear roll damping (be) plotted against the mean roll amplitude between successive peaks for a simulation of the roll equation with stiffness variations due to rolling around a fixed waterline only.

The next three figures look at simulations of the complete equation of motion, equation 5-5-10. In Figure 5-5- 8, the values for the coefficients are as given in the table above but with no heave damping. In this case the spread of the equivalent linear damping values is large, and, for low roll amplitudes towards the end of the decay, some instances of negative damping occur. This variation is similar in form to that recorded in the 2002 model experiments albeit that the spread of equivalent linear damping results is not as great.

In the model experiment results for trimaran DVZ discussed earlier in this chapter, a large variation in the equivalent linear damping occurred at low roll amplitudes. Hence in Figure 5-5- 9 the effect of negative heave damping, i.e. heave amplification, is shown where $b_h = -0.02$. This gives a large spread of damping similar to what was seen in the 2002 model experiments. Experimentation with the input values to the simulations shows that the only other way to increase the spread of the damping results is to increase the metacentric height variation terms $\delta\overline{GM}_a$ and $\delta\overline{GM}_v$. As these can be predicted with reasonable accuracy for the model in question the effect of varying these two terms is not further considered.

Finally, Figure 5-5- 10 shows the effect of changing the roll natural frequency from 2.85 rad/s to 1.40 rad/s. The change in the roll frequency changes the disposition of the equivalent linear damping data spots but does not change the magnitude of the spread. Similarly changes to the heave natural frequency, ω_h, leads to changes only in the distribution of the equivalent linear damping values not the maximum and minimum values.

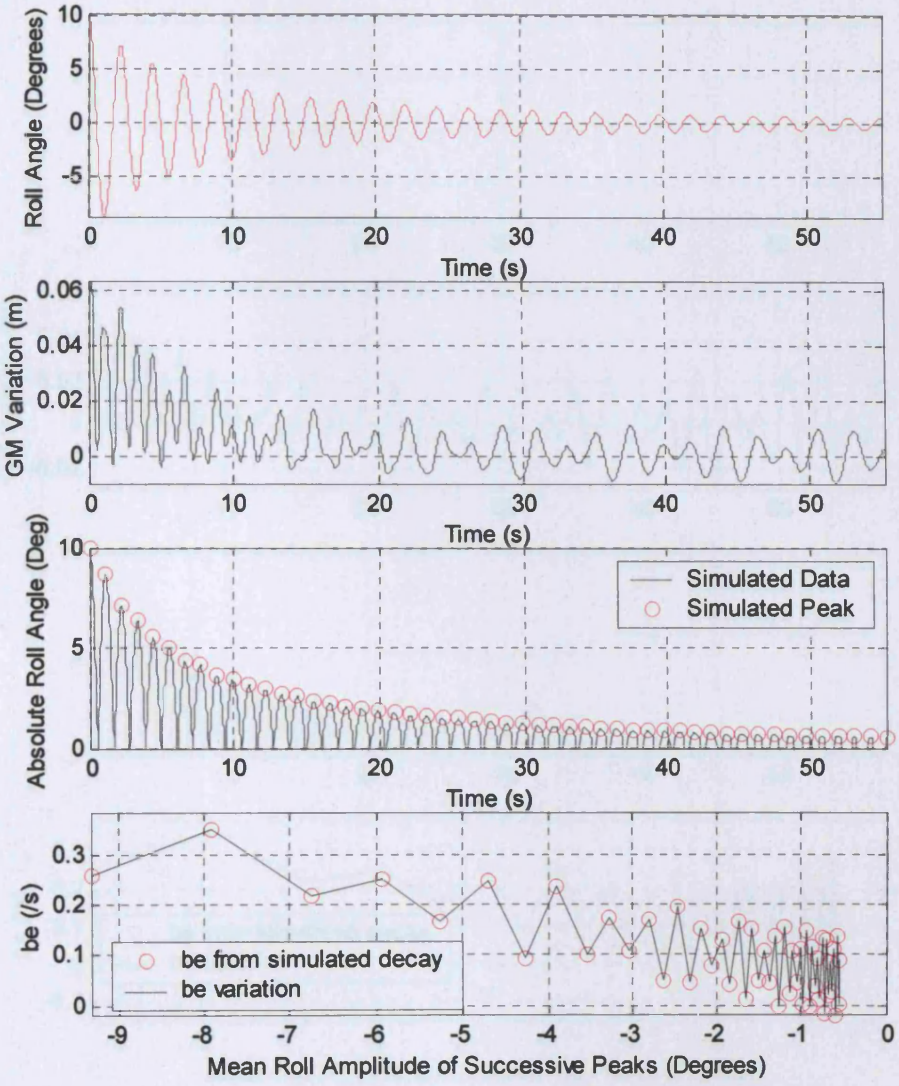

Figure 5-5- 8:- Roll decay, GM variation due to heave, absolute roll angle and equivalent linear roll damping (be) plotted against the mean roll amplitude between successive peaks for a simulation of the roll equation with stiffness variations. The heave frequency is equal to 2 rad/s and there is no heave damping

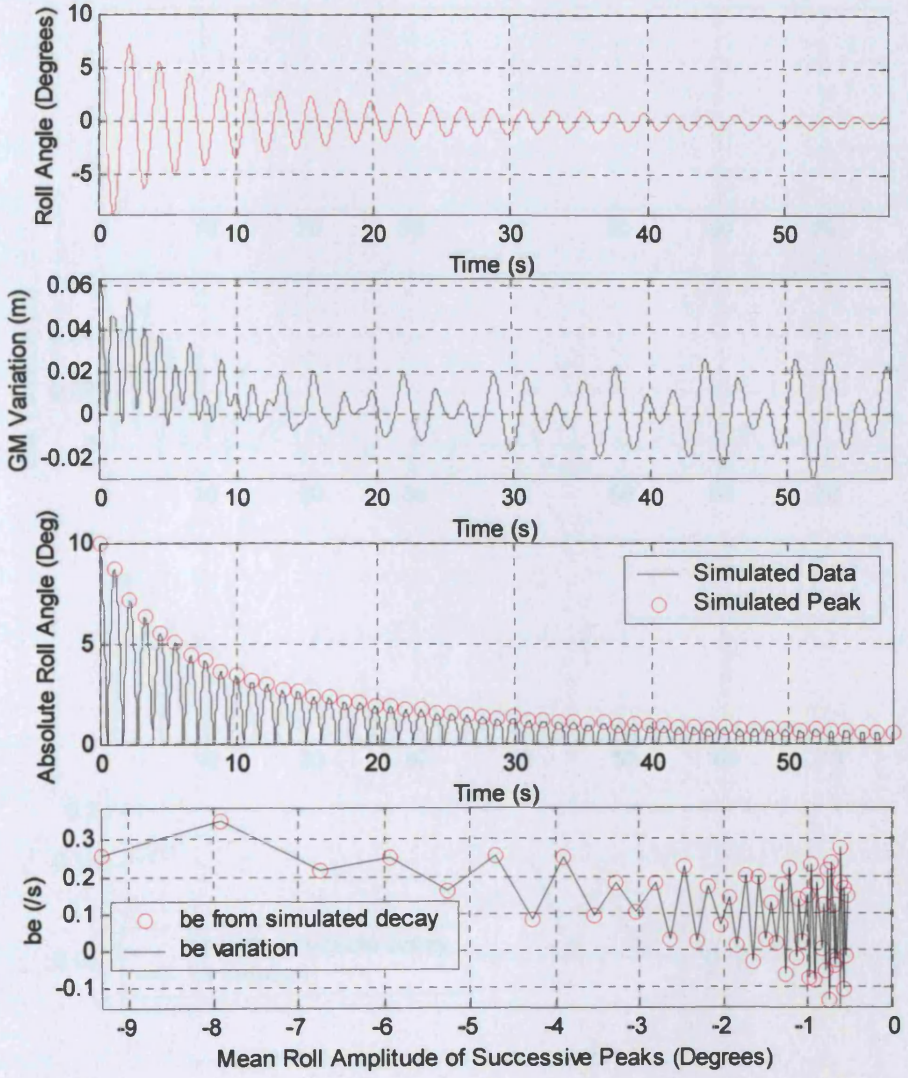

Figure 5-5- 9:- Roll decay, GM variation due to heave, absolute roll angle and equivalent linear roll damping (be) plotted against the mean roll amplitude between successive peaks for a simulation of the roll equation with stiffness variations. The heave frequency is equal to 2 rad/s and b_h=-0.02

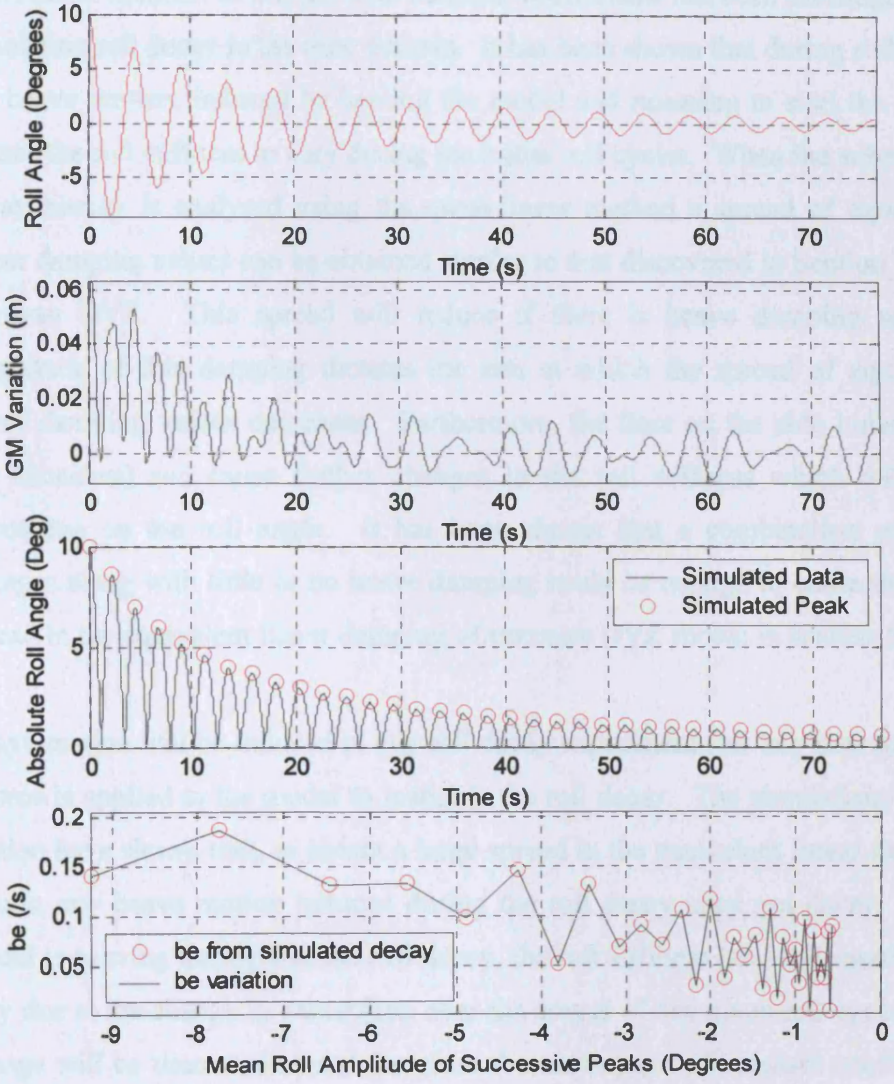

Figure 5-5- 10:- Roll decay, GM variation due to heave, absolute roll angle and equivalent linear roll damping (be) plotted against the mean roll amplitude between successive peaks for a simulation of the roll equation with stiffness variations. The heave frequency is equal to 2 rad/s, the roll frequency is equal to 1.40 rad/s and there is no heave damping

5.5.4 Summary

In this section the assumption that roll decay can be modelled by a single degree of freedom equation of motion with constant coefficients has been investigated by simulating roll decay in the time domain. It has been shown that during roll decay the heave motion, induced by heeling the model and releasing to start the decay, causes the roll stiffness to vary during the initial roll cycles. When the subsequent decay history is analysed using the quasi-linear method a spread of equivalent linear damping values can be obtained similar to that discovered in Section 5.3 for trimaran DVZ. This spread will reduce if there is heave damping and the magnitude of this damping dictates the rate at which the spread of equivalent linear damping values decreases. Furthermore, the flare on the side hulls (from the haunches) can cause further changes in the roll stiffness which will vary depending on the roll angle. It has been shown that a combination of these changes along with little or no heave damping could be enough to cause the large spread in the equivalent linear damping of trimaran DVZ shown in section 5.3.

Heave motion will be induced in any roll decay experiment (for any hull shape) if a force is applied to the model to instigate the roll decay. The simulations in this section have shown that, to obtain a large spread in the equivalent linear damping results, any heave motion induced during the roll decay must not decay. If the model is heaving throughout the roll decay, the roll stiffness (and roll inertia) will vary due to the change in waterplane over the course of any given roll cycle. This change will be time variant and therefore the assumption of constant coefficients is deemed inappropriate for trimarans fitted with haunches.

5.6 Coupling of Roll With Other Motions in Free Decay

5.6.1 Heave Motion

The next of the assumptions listed in Section 5.2 to consider is that roll decay can be modelled adequately using an uncoupled equation of roll motion. Having shown in the last section that it is most likely that roll couples with heave, roll and heave coupling will be investigated in this section.

In the 2004 series of model experiments with trimaran DVZ, roll decay experiments were performed at zero speed to allow the model roll period to be accurately determined. In these experiments, motion in all six degrees of freedom was recorded by the onboard data logger. An older system had been used for the 2002 experiments from which only roll motion and rudder angle were available.

In Section 5.5, it was postulated that roll and heave motion couple in roll decay. Therefore, the opportunity was taken to look at the heave motion during the 2004 roll decay experiments. This analysis was performed for roll decay without any roll damping appendages. In Section 5.5 the coupling was thought to be due to the haunches causing heave motion during rolling and so it was decided to look at a case without roll damping appendages as including them would shorten the length of the decay.

The onboard data logger recorded heave accelerations at the location of the data logger. These need to be adjusted to remove the pitch effect as the data logger was not located at the centre of gravity. Once again the data was analysed using MATLAB (www.mathworks.com). The following procedure was followed to obtain heave displacement:-

- Adjust the acceleration data so that it is relative to the acceleration due to gravity.
- Calculate the Discrete Fourier Transform (DFT) of the acceleration-time history and plot the absolute value of this against frequency using the appropriate scale. This particular analysis was conducted following the methodology set out in Newland (180) using the MATLAB **fft** command to calculate the DFT.
- Filter low frequencies from the DFT. This removes long period waves which would not be present in the experimental results. After some investigation 1.26 rad/s was found to be an appropriate cut off point and all data occurring at frequencies below this were removed.
- Divide the DFT by the square of the frequency matrix to obtain the heave displacement and convert back to the time domain using the inverse Fourier Transform. Only the real part of the signal needs to be inverted as the imaginary part will be zero. This was performed using the MATLAB **ifft** command.
- For the Fourier analysis to work, the signal must be truncated to represent an integer number of cycles. Accordingly, the roll history was chopped after 40 seconds.

The resulting heave displacement time history is shown in Figure 5-6- 1 along with the heave acceleration and roll decay. The heave acceleration appears to be dominated by a single frequency component until around 5 seconds, after which a number of frequency components are evident. The heave displacement decays during this period (0 to 5 seconds) after which there is no evidence of any decay. This supports the analysis of Section 5.5, where heave decay had to be zero if a large spread of the equivalent linear damping was to be achieved at low roll amplitudes towards the end of the simulation of the decay.

The peak heave motion is 9.37mm. In section 3.2, the heave displacement due to the removal of the inclining weight (giving a $\overline{GM}$ variation of 4.29 mm) was calculated as 6.61 mm. The heave displacement due to the immersion of one haunch during roll motion (giving a $\overline{GM}$ variation of 6.25 mm) was 3.35 mm.

Hence, the maximum possible heave displacement calculated from the vessel geometry was 9.96 mm which is very close to the maximum recorded value of 9.37 mm. This is an error of 6%.

To learn anything further, the breakdown of the frequency components must be investigated. The frequency breakdown from the absolute DFT of the heave displacement is given in Figure 5-6- 2 which exhibits four distinct peaks. These peaks represent the dominant frequency components of the heave – time history. In Figure 5-6- 2 there are peaks at 1.4173, 2.0472, 2.8345 and 5.669 rad/s. The heave natural frequency of trimaran DVZ was calculated using the Tonnes Per Centimetre Immersion (TPC) at the design draught taken from the Paramarine geometry model. The TPC is a measure of the heave stiffness. Using this approach the heave natural frequency was estimated as 1.825 rad/s.

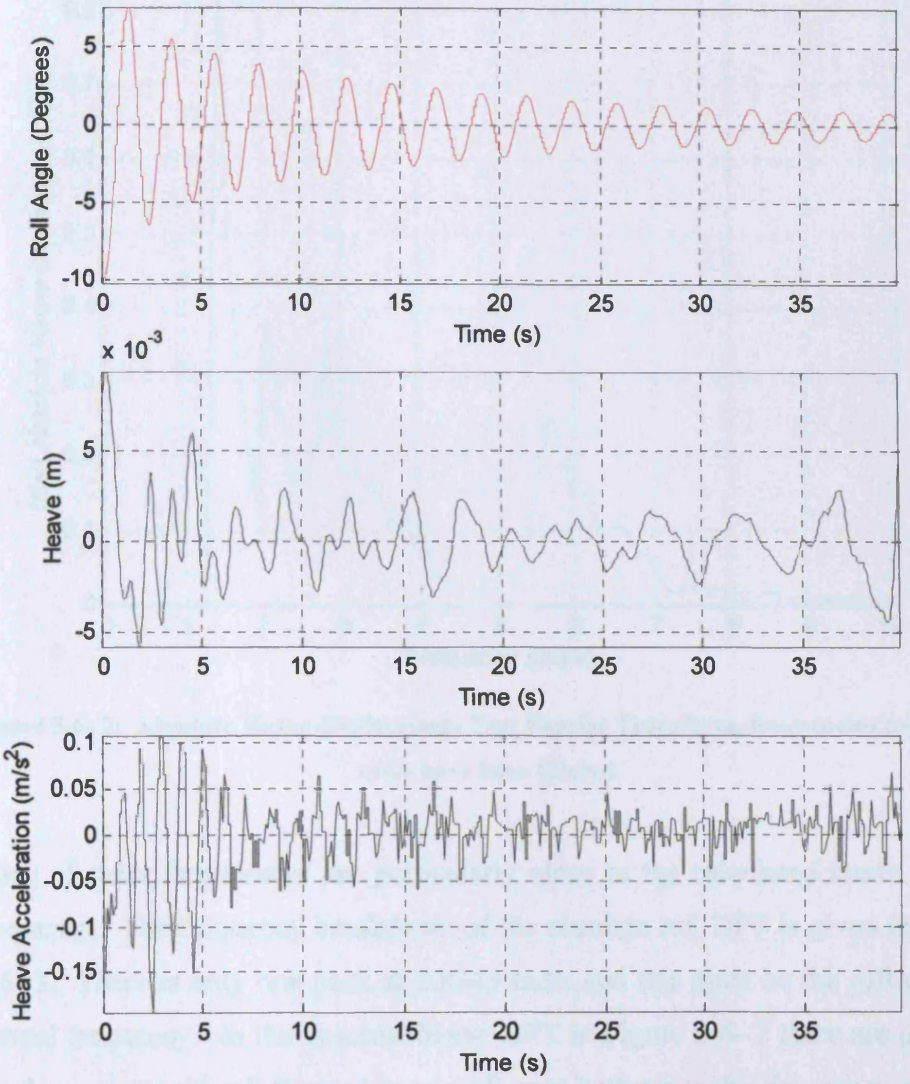

Figure 5-6- 1: Heave displacement and acceleration during roll decay taken from the 2004 zero speed roll decay experiments on trimaran DVZ with initial roll to port

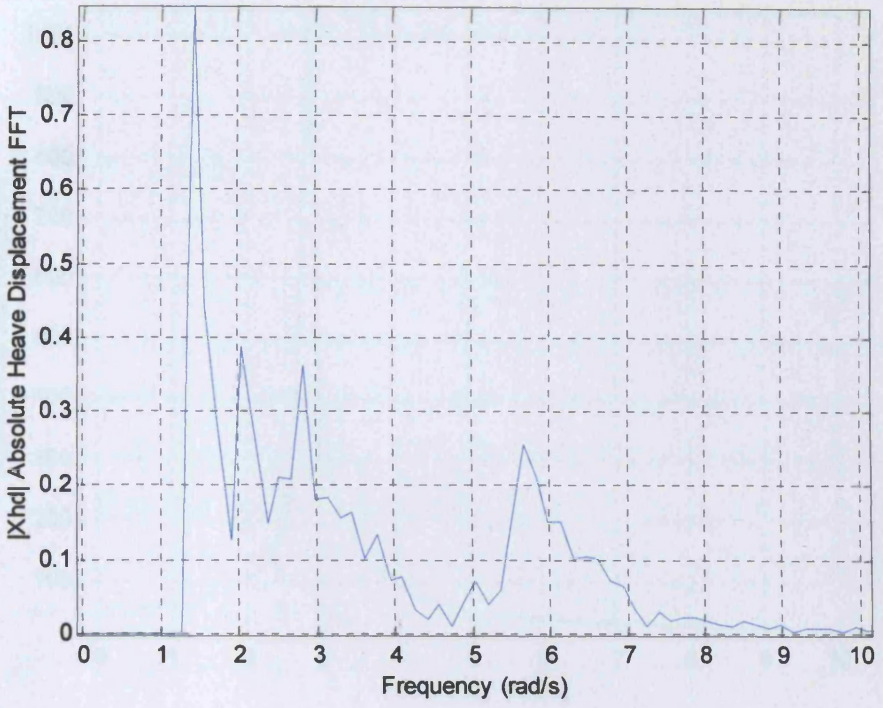

Figure 5-6- 2: Absolute Heave displacement Fast Fourier Transform, frequencies below 1.26 rad/s have been filtered

None of these frequencies are particularly close to the calculated heave natural frequency. The frequency breakdown of the absolute roll DFT is given in Figure 5-6- 3. There is only one peak at 2.8345 rad/s and this must be the roll damped natural frequency. In the absolute heave DFT in Figure 5-6- 2 there are peaks at the damped natural roll frequency, as well as at both twice this frequency and half this frequency. The remaining peak frequency at 2.0472 rad/s is most likely to be the heave frequency. Whilst this is not the same as the calculated heave frequency, if the draught of the model is greater than the design draught then the Tonnes Per Centimetre Immersion (TPC) will increase as the waterplane area increases leading to an increase in the heave natural frequency. The difference between this peak frequency at 2.0472 rad/s and the calculated heave natural frequency of 1.825 rad/s is 10.85%. For this reason, the simulations in Section 5.5 took the heave natural frequency to be 2.0 rad/s.

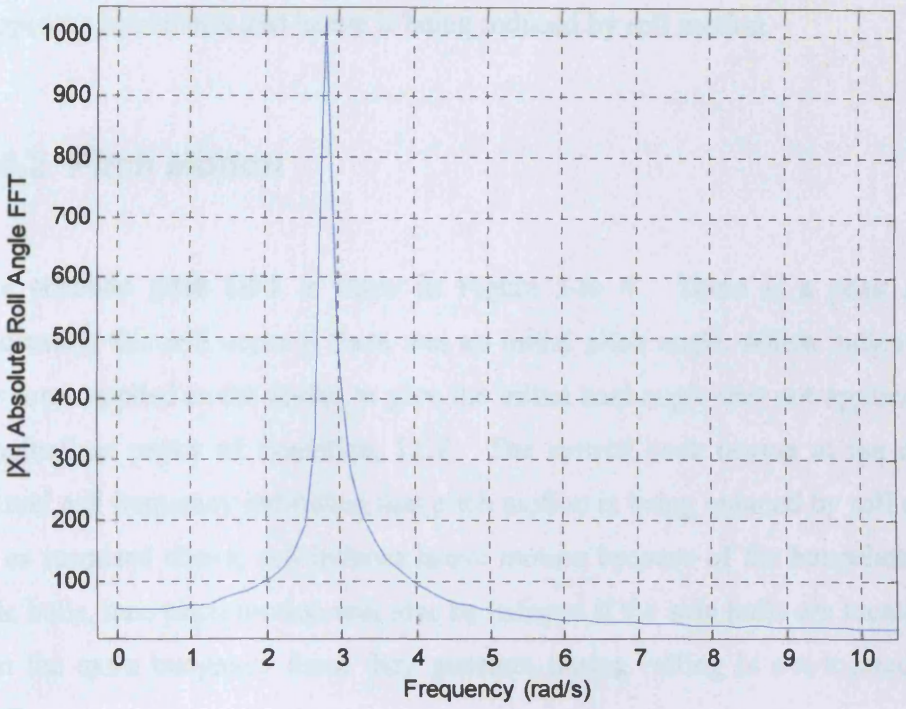

Figure 5-6- 3: Absolute roll Fast Fourier Transform

During one roll cycle, heave upward is induced as the haunches are immersed further and further as the model rolls to one side. As the model returns to the upright condition it heaves downwards to obtain the same initial condition. This is one heave cycle and occurs for every half a roll cycle. Hence, in a complete roll cycle there will be two heave cycles:-

1) Roll from upright position to port	One heave cycle	Heave upwards
(Start of roll cycle)		
2) Roll back to upright position		Heave downwards
3) Roll from upright position to starboard	One heave cycle	Heave upwards
4) Roll back to upright position		Heave downwards
(End of roll cycle)		

So, if heave motion is being induced by roll motion at the roll frequency, heave motion will be occurring at twice the roll frequency (half the period). Hence a peak in the absolute value of the DFT of the heave decay, which is a measure of

the power at a given frequency, at twice the damped natural roll frequency supports a hypothesis that heave is being induced by roll motion.

5.6.2 Pitch Motion

The absolute pitch DFT is show in Figure 5-6- 4. There is a peak at zero frequency; this will occur if there was an initial pitch angle, which indicates that the force applied to the model to give the initial heel angle was not applied at the longitudinal centre of floatation, LCF. The second peak occurs at the damped natural roll frequency indicating that pitch motion is being induced by roll motion. If, as surmised above, roll induces heave motion because of the haunches on the side hulls, then pitch motion will also be induced if the side hulls are located such that the extra buoyancy force they generate during rolling is not located at the LCF.

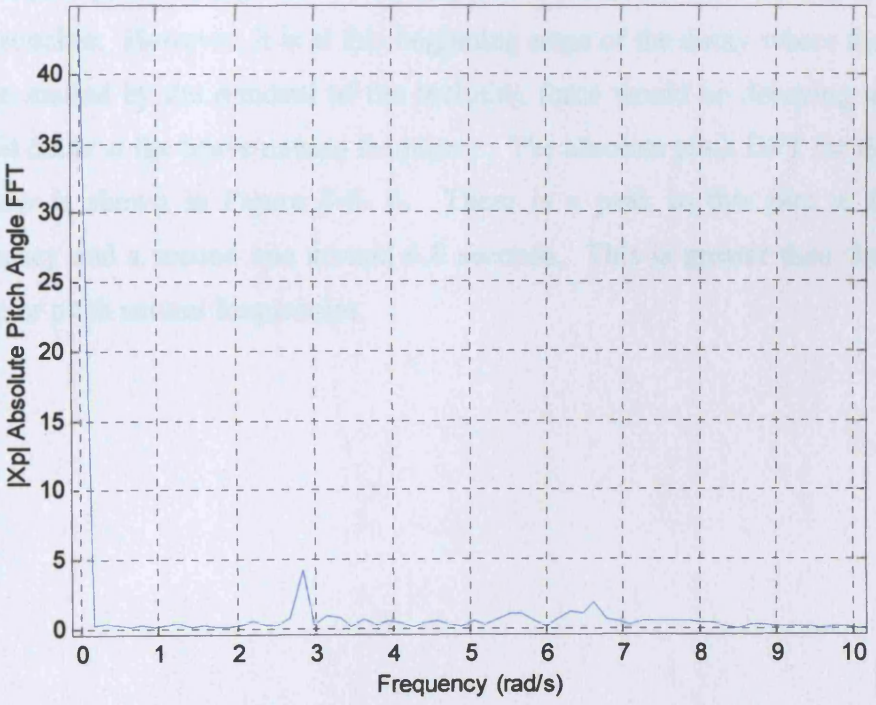

Figure 5-6- 4: Absolute pitch Fast Fourier Transform

5.6.3 Further Studies

To try and gain further understanding the decay is broken down into windows to see if it is possible to isolate parts of the decay where the heave motion is dominant at just one frequency.

As the heave acceleration appears to be driven by one dominant frequency for the first 5 seconds of the decay, a small snapshot of the decay (of integer roll cycles) was analysed to see if the heave displacement was occurring at one frequency. A window from 0 to 4.6 seconds was chosen. The absolute heave DFT for this window is shown in Figure 5-6- 5. The damped roll frequency for this window was calculated from the peak of the absolute roll DFT as 2.732 rad/s. There are peaks in the absolute heave displacement DFT at half and twice this frequency. The bandwidth of the first peak is large and encompasses the roll frequency as well as the assumed heave frequency (2.0472 rad/s). It is tempting to draw the conclusion that during this part of the decay the heave motion occurs only at the roll frequency, indicating heave is entirely due to the immersion and emergence of the haunches. However, it is at this beginning stage of the decay where the initial heave, caused by the removal of the inclining force would be decaying and this should occur at the heave natural frequency. The absolute pitch DFT for this time window is shown in Figure 5-6- 6. There is a peak in this plot at the roll frequency and a second one around 6.8 seconds. This is greater than the likely heave or pitch natural frequencies.

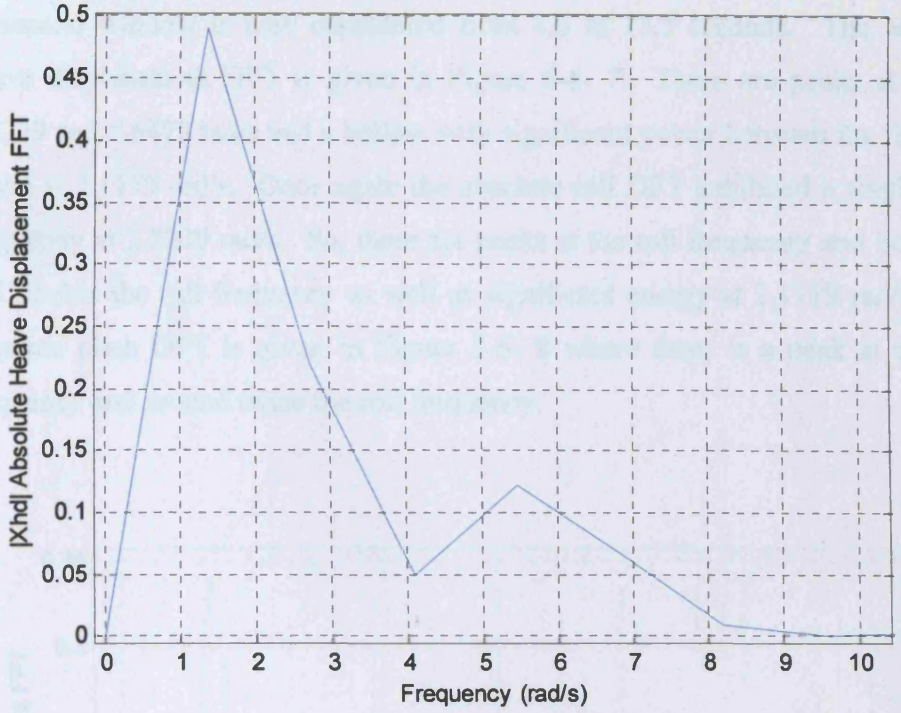

Figure 5-6- 5: Absolute Heave displacement Fast Fourier Transform for signal from 0 – 4.6 seconds, frequencies below 1.26 rad/s have been filtered

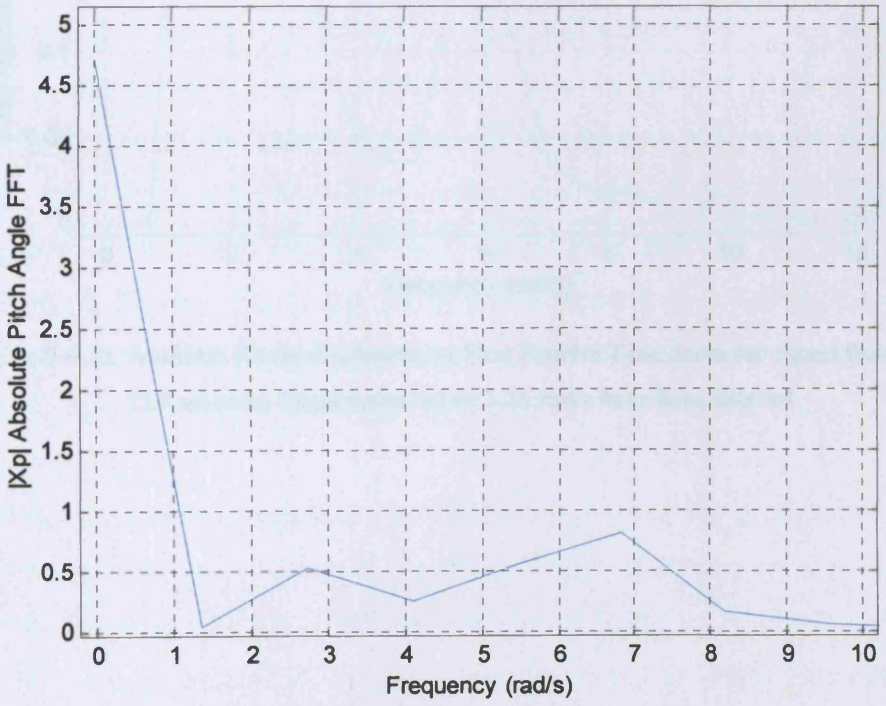

Figure 5-6- 6: Absolute pitch Fast Fourier Transform for signal from 0 – 4.6 seconds

A second window is now considered from 4.6 to 13.5 seconds. The absolute heave displacement DFT is given in Figure 5-6- 7. There are peaks at 1.412, 2.8239 and 5.6478 rad/s and a hollow with significant power between the first two peaks at 2.1179 rad/s. Once again the absolute roll DFT exhibited a single peak frequency at 2.8239 rad/s. So, there are peaks at the roll frequency and both half and double the roll frequency as well as significant energy at 2.1179 rad/s. The absolute pitch DFT is given in Figure 5-6- 8 where there is a peak at the roll frequency and around twice the roll frequency.

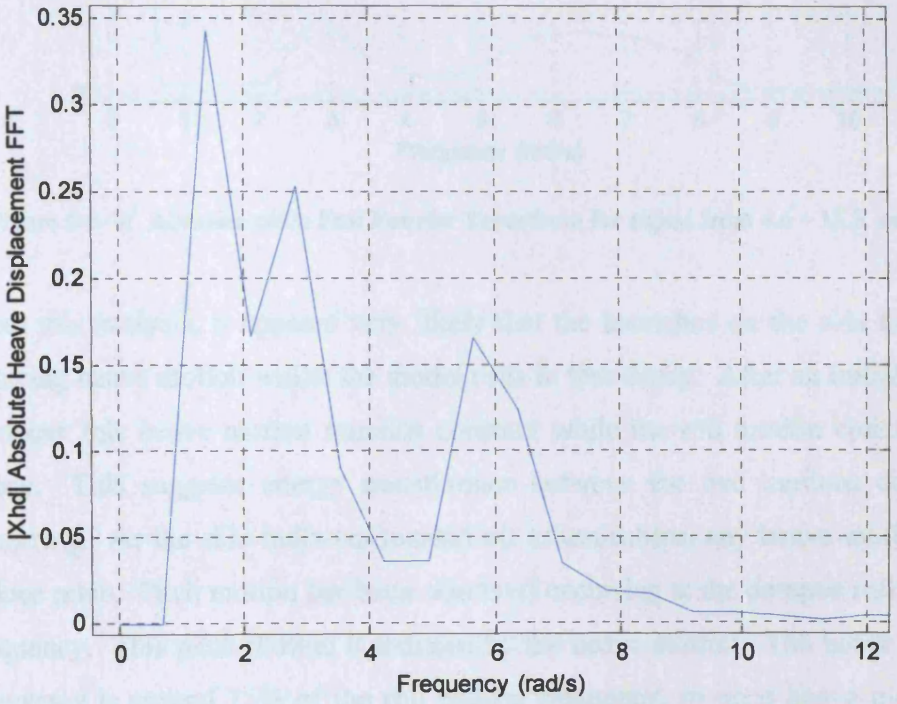

Figure 5-6- 7: Absolute Heave displacement Fast Fourier Transform for signal from 4.6 – 13.5 seconds, frequencies below 1.26 rad/s have been filtered

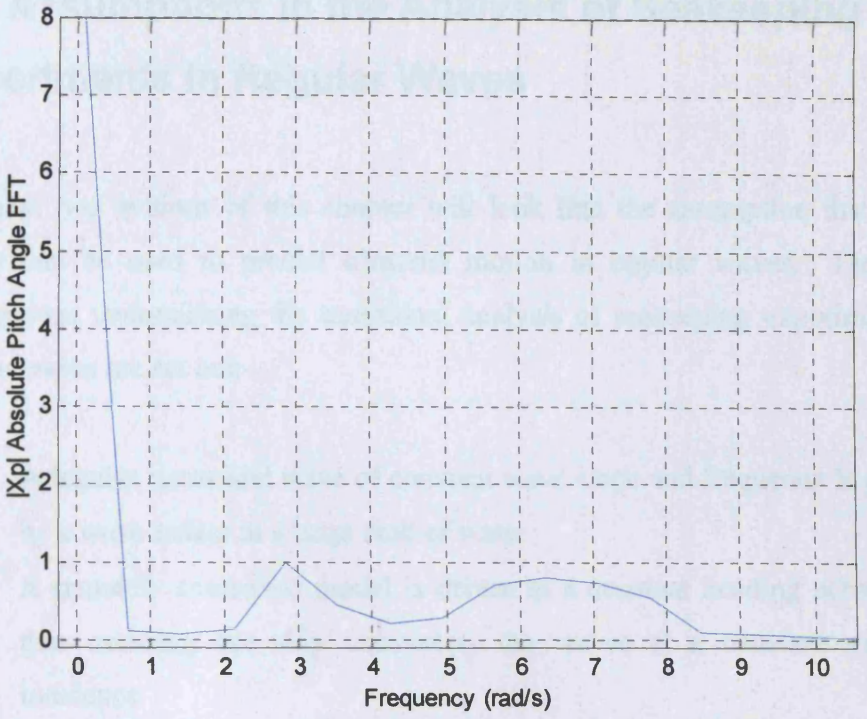

Figure 5-6- 8: Absolute pitch Fast Fourier Transform for signal from 4.6 – 13.5 seconds

From this analysis, it appears very likely that the haunches on the side hulls are inducing heave motion whilst the model rolls in free decay. After an initial period of decay this heave motion remains constant while the roll motion continues to decay. This suggests energy transference between the two motions could be occurring. As the side hulls are located aft of amidships, any heave motion will induce pitch. Pitch motion has been observed occurring at the damped roll natural frequency. This pitch motion is induced by the heave motion. The heave natural frequency is around 75% of the roll natural frequency, so once heave motion is induced it may lead to resonance. This problem would be exacerbated if the two natural frequencies were coincident.

Therefore, it can be concluded that, for trimaran DVZ, the assumption that an uncoupled roll equation adequately models the roll decay does not hold. It seems most likely that roll couples with heave due to the haunches on the side hulls and that this must be accurately modelled if roll decay results are to be successfully analysed. This supports the findings of Section 5.5.

5.7 Assumptions in the Analysis of Seakeeping Experiments in Regular Waves

The next two sections of this chapter will look into the assumption that linear theory can be used to predict trimaran motion in regular waves. First, the assumptions underpinning the traditional analysis of seakeeping experiments in regular waves are set out:-

- A regular sinusoidal wave of constant wave slope and frequency is created by a wave maker in a large tank of water
- A remotely controlled model is driven at a constant heading across tank thus ensuring the ship encounters the waves at a constant angle of incidence
- The sinusoidal waves disturb the model and cause motions in up to six degrees of freedom. These model motions are also regular and sinusoidal with constant amplitude and frequency
- During the passage of the model across the tank there is sufficient time for steady state motions to occur and these are recorded by an onboard data logger.
- A window of the motion – time history is selected for analysis that is considered to represent the steady part of the run. This is selected to ensure that the waves are fully developed and interference effects (such as wave reflection from the edge of the tank) were not affecting ship motions.

From this type of experiment, the relationship between the amplitudes of the input regular sinusoidal wave and the output motion regular sinusoid can be established. This is usually expressed as a motion Response Amplitude Operator, or RAO.

To test the applicability of this theory to trimarans the results of the 2004 seakeeping experiments with trimaran DVZ in regular waves shall be studied in greater depth.

5.8 The Applicability of Linear Theory to a Trimaran in Beam Regular Waves

In this section the same Fourier analysis technique used to determine the frequency components of the 2004 roll decay experiments in Section 5.6 will be applied to the 2004 model experiments results obtained in regular waves.

In the original analysis of the seakeeping experiment results, documented in Section 4.3 of Chapter 4, the RAO's were determined based on the steady amplitude of the ship response in the desired degree of freedom. The procedure adopted was as follows:-

1. Obtain the DFT from the steady roll – time history.
2. Determine the wave power from the absolute value of the DFT and plot this against frequency. Note that in the Fourier analysis in Section 5.6, just the absolute value of the DFT was plotted with no conversion to wave power.
3. Assuming all the power of the wave is located at one dominant frequency reconstruct a regular wave at that frequency and peak amplitude. The peak amplitude is determined from the wave power.
4. Use this amplitude to determine the roll RAO.

The MATLAB computer package (www.mathworks.com) was used for this analysis which is outlined in further detail in this section.

In the next three sub-sections the roll, heave and pitch motions in beam waves will be investigated in greater depth to see if this analysis method and thus the linear theory assumption are applicable to trimaran DVZ.

5.8.1 Rolling in Regular Beam Waves

The roll – time histories used to obtain the roll RAO in Chapter 4 are shown at each of the wave frequencies tested in Figure 5-8- 1 for the model at six knots in beam seas. This was the lowest speed tested and it was at this speed that the largest roll motions were recorded. The wave amplitude – time histories used to determine the constant amplitude of the regular sinusoidal input waves are shown in Figure 5-8- 2.

The damped natural roll frequency was determined from the analysis of the roll decay experiments performed on the model as part of the 2004 experiments in Section 5.6. This was found to be 2.8345 rad/s. Perusal of Figure 5-8- 1 shows that the roll amplitude is greatest at excitation frequencies close to resonance, as would be expected. What is of great interest in these graphs is that the output roll motion of the model is not regular with constant amplitude. The input wave – time histories appear to be approximately sinusoidal, with the amplitude varying slightly at the lower wave frequencies, see Figure 5-8- 2. If linear theory was invoked, the beating in the roll – time histories would be removed as the roll – time history would then be approximated by a regular sinusoidal wave of constant amplitude. To model the observed motion properly in a seakeeping code non-linear theory would need to be used.

We now turn to focus on the significance of the non-linear effects. A Fourier analysis was conducted on each of the output roll – time histories to determine the frequency components influencing the roll motion. The results are shown in Figure 5-8- 3. The absolute value of the DFT has been converted to a scale of roll amplitude in degrees and this is plotted against the frequency in rad/s. If the motion is regular and sinusoidal, one spike would be expected at the excitation frequency and the motion amplitude can be determined from the power in the wave at this spike. For simple harmonic motion, all the power of the wave would be located at this spike. So, if the input wave was a sinusoid a very narrow banded peak would be expected. A very narrow banded spike at one frequency is unlikely to be measured from the experimental results as the wave maker is not

likely to generate perfect sinusoidal waves every cycle (as can be seen from Figure 5-8- 2). The results in Figure 5-8- 3 show narrow banded peaks, with the wave amplitude greatest at wave excitation frequencies near resonance (because the encounter frequency is equal to the wave frequency in beam seas).

At wave frequencies close to resonance a very small second peak occurs at a frequency exactly twice that of the first peak. However, for all six waves, over 90% of the wave power is concentrated at a single frequency coinciding with the location of the first peak, see Table 5-8- 1. This compares to wave powers greater than 97% at the frequency of the peak in the DFT for the input waves. This table also shows that the roll frequency and wave frequency are generally coincident as the linear regular wave theory would suggest.

Wave Frequency (rad/s)	3.788	3.097	2.800	2.574	2.398	2.192
Roll Frequency (rad/s)	3.737	3.091	2.788	2.555	2.388	2.180
Roll Amplitude from Peak of DFT (degrees)	4.340	9.589	14.980	12.768	8.773	7.823
Percentage Power in Peak of Roll Motion DFT (%)	90.6	90.7	94.5	94.6	95.3	94.0
Percentage Power in Peak of Input Wave DFT (%)	98.5	99.4	99.2	99.1	98.9	97.4

Table 5-8- 1: Wave and roll motion data from Fourier analysis of the model experiment results with trimaran DVZ (without roll damping appendages) at a speed equivalent to 6 knots

As shown in Table 5-8- 1, most of the wave power is located at one frequency, therefore the linear regular wave theory can be considered to give a reasonable approximation of the roll motion.

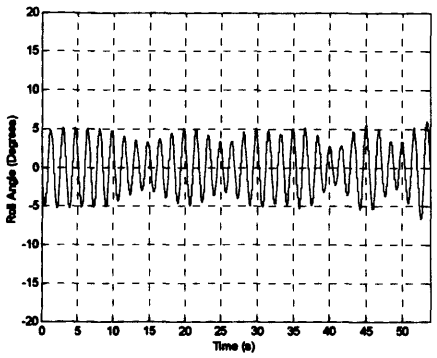

Wave Frequency 3.788 rad/s

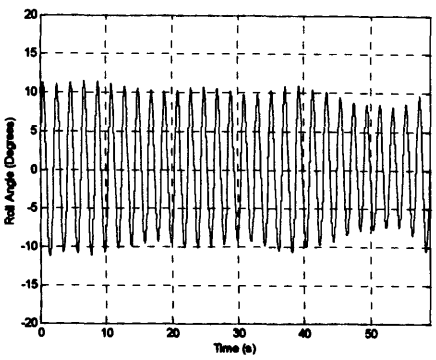

Wave Frequency 3.097rad/s

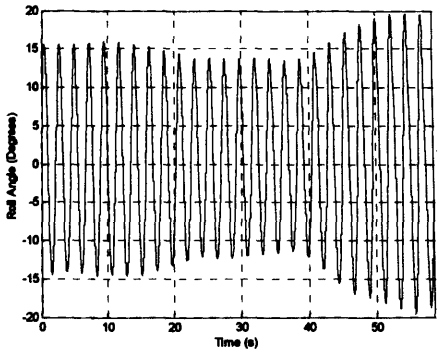

Wave Frequency 2.800 rad/s

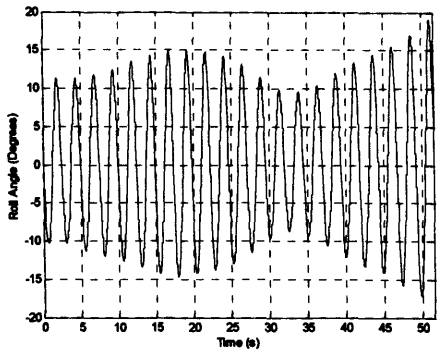

Wave Frequency 2.574 rad/s

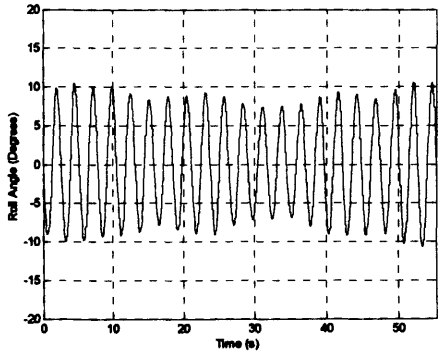

Wave Frequency 2.398 rad/s

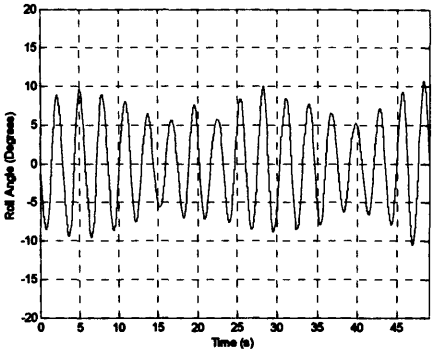

Wave Frequency 2.192 rad/s

Figure 5-8- 1: Roll angle – time history from model experiment in regular waves for trimaran DVZ in beam seas at a speed equivalent to 6 knots (with no roll damping appendages fitted)

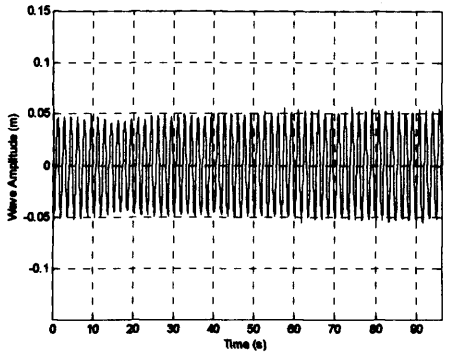

Wave Frequency 3.788 rad/s

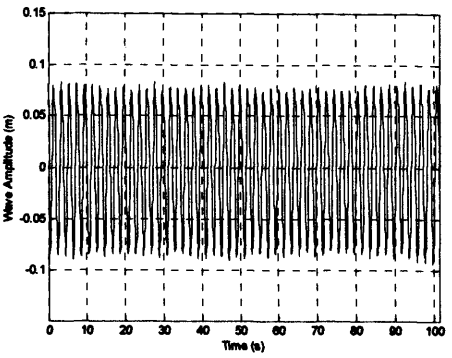

Wave Frequency 3.097rad/s

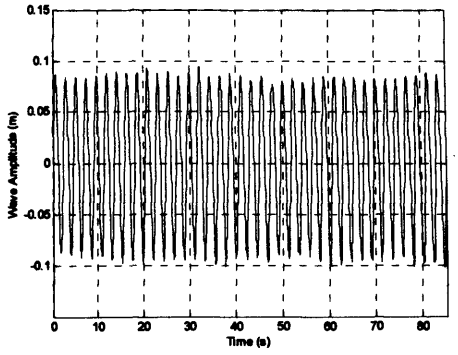

Wave Frequency 2.800 rad/s

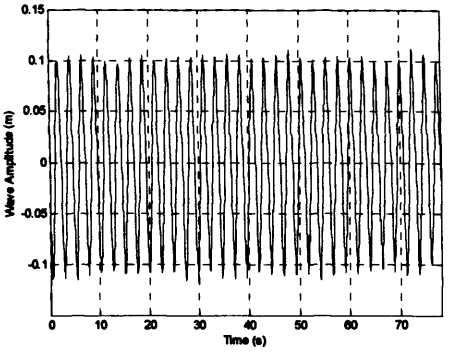

Wave Frequency 2.574 rad/s

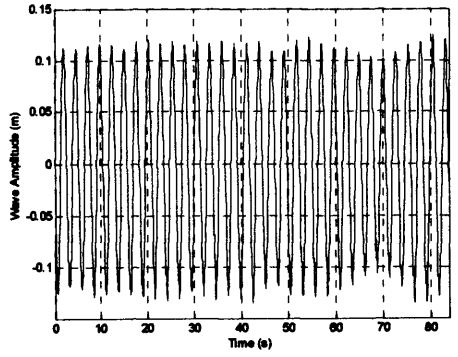

Wave Frequency 2.398 rad/s

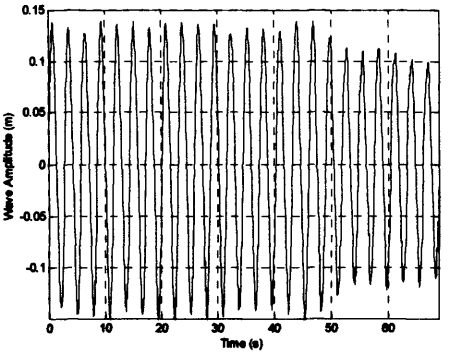

Wave Frequency 2.192 rad/s

Figure 5-8- 2: Wave amplitude – time history from model experiment in regular waves for trimaran DVZ in beam seas at a speed equivalent to 6 knots (with no roll damping appendages fitted)

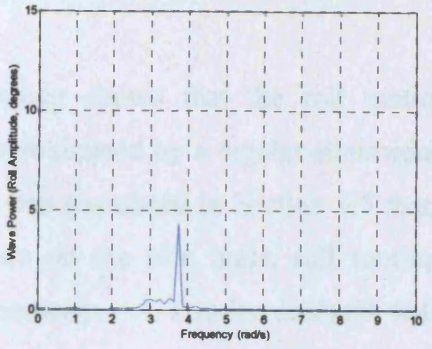

Wave Frequency 3.788 rad/s

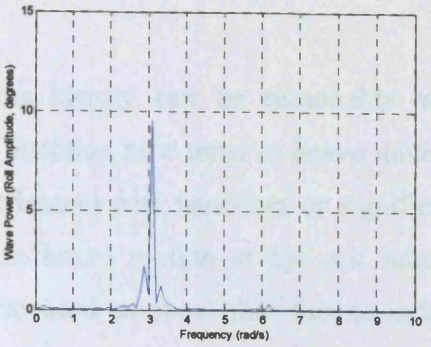

Wave Frequency 3.097rad/s

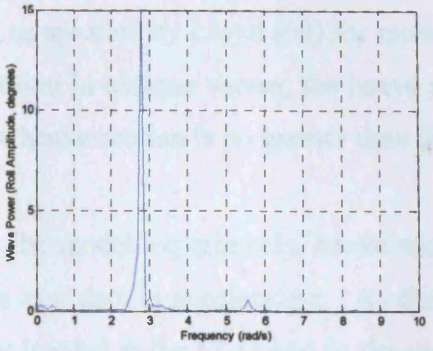

Wave Frequency 2.800 rad/s

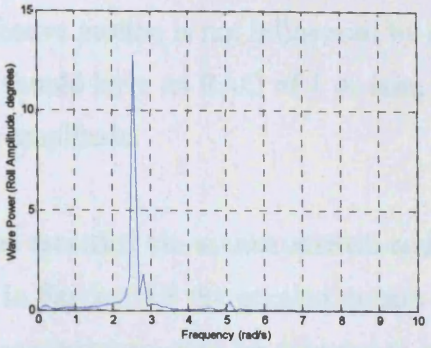

Wave Frequency 2.574 rad/s

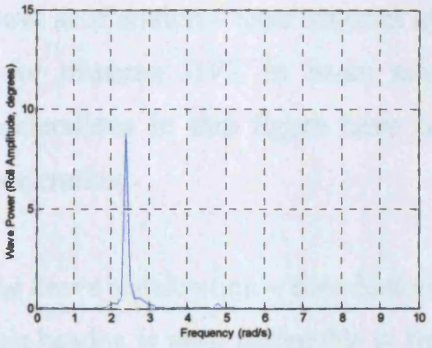

Wave Frequency 2.398 rad/s

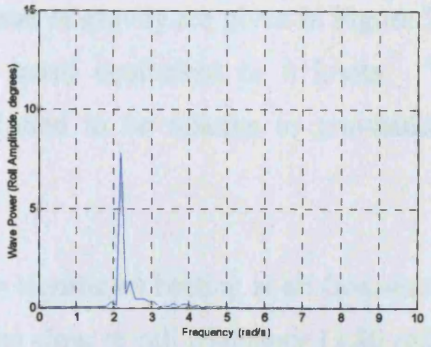

Wave Frequency 2.192 rad/s

Figure 5-8- 3: Discrete Fourier Transform of roll angle – time history with wave power scale (y-axis) converted to represent roll amplitude for trimaran DVZ in beam regular waves at a speed equivalent to 6 knots

5.8.2 Heaving in Regular Beam Waves

Having shown that the roll motion – time history can be reasonably well approximated by a regular sinusoidal wave, attention now turns to heave motion. It was postulated in Section 5.5 that, for a trimaran with haunches or significant flare on the side hulls, roll motion induces heave motion at the roll natural frequency. A Fourier analysis will now be used to show that this is indeed occurring.

If, as asserted by Lloyd (64) for monohulls, heave motion is not influenced by roll motion in oblique waves, the heave motion should have an RAO of 1 or less, i.e. the heave motion is no greater than the wave amplitude.

In the model experiments, heave motion was recorded via accelerometers and so the raw data is acceleration. As discussed in Section 5.6 the accelerometers are not located at the LCG and so the recorded accelerations must be adjusted to give results at the LCG removing acceleration caused by pitch motions. The relevant heave acceleration – time histories at the centre of gravity are given in Figure 5-8-4 for trimaran DVZ in beam seas at a speed equivalent to 6 knots. The accelerations in this figure have been adjusted to be relative to gravitational acceleration.

The heave acceleration – time histories show significant beating at all frequencies. This beating is most noticeable at frequencies close to roll resonance (2.80 rad/s), where the recorded heave acceleration amplitude is greatest. An interesting observation is that, at an excitation frequency of 2.80 rad/s, the heave acceleration is not symmetrical about 0 m/s^2 as would be expected with linear regular wave theory. This shows that the heave restoring is changing as the draught changes. Therefore, the model heaves upwards more than it heaves downwards due to the flare above the still water position on the three hulls. Beating will occur if either the amplitude or frequency is time variant or when the output wave is the summation of a number of different waves with constant amplitude and frequency

but differing phases. The Discrete Fourier Transform is now used to determine which one of these is the case.

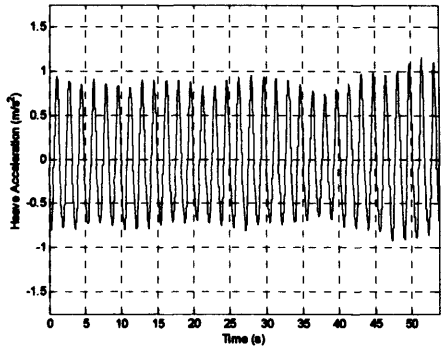

Wave Frequency 3.788 rad/s

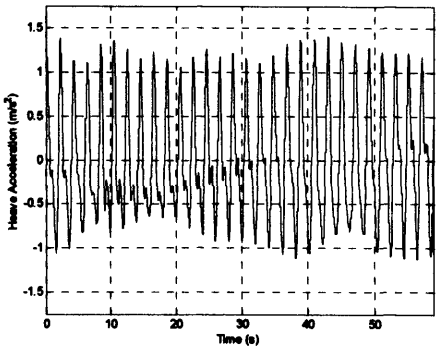

Wave Frequency 3.097rad/s

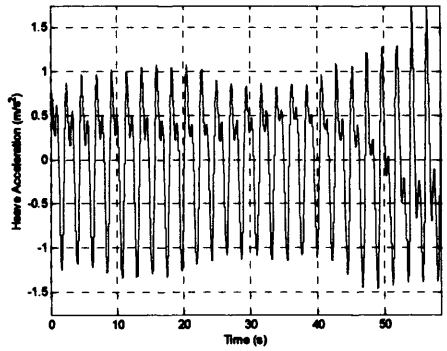

Wave Frequency 2.800 rad/s

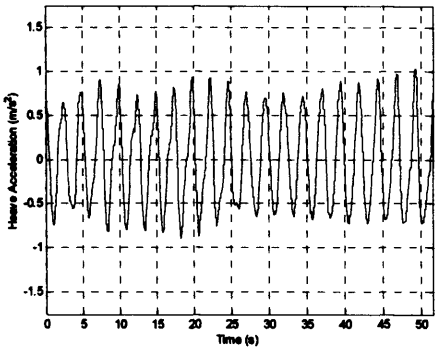

Wave Frequency 2.574 rad/s

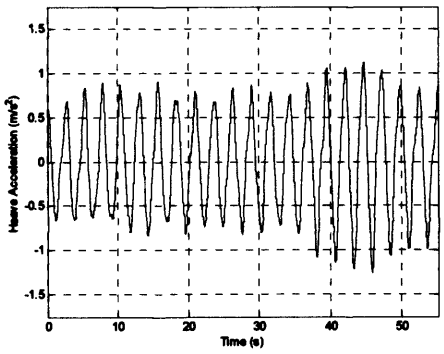

Wave Frequency 2.398 rad/s

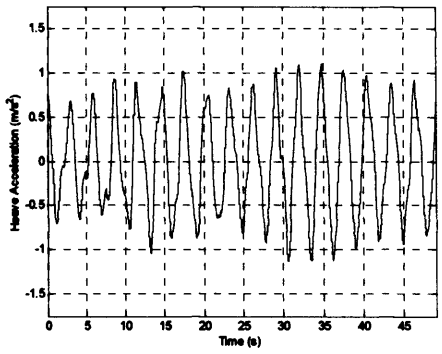

Wave Frequency 2.192 rad/s

Figure 5-8- 4: Heave acceleration – time histories measured at the LCG for trimaran DVZ in beam seas at a speed equivalent to 6 knots without roll damping appendages

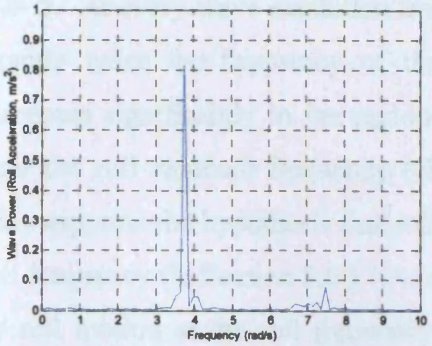

Wave Frequency 3.788 rad/s

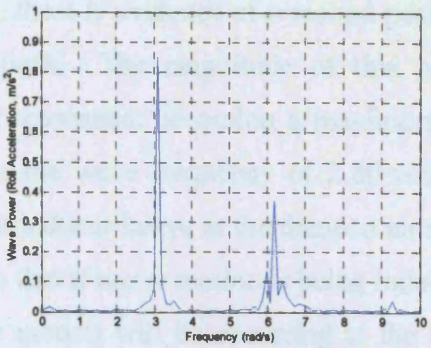

Wave Frequency 3.097rad/s

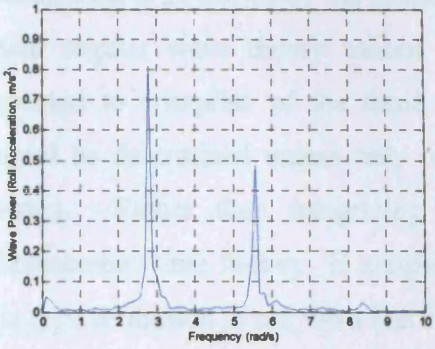

Wave Frequency 2.800 rad/s

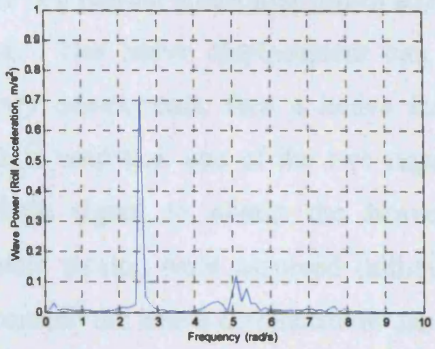

Wave Frequency 2.574 rad/s

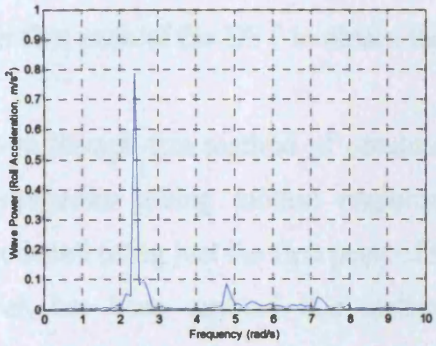

Wave Frequency 2.398 rad/s

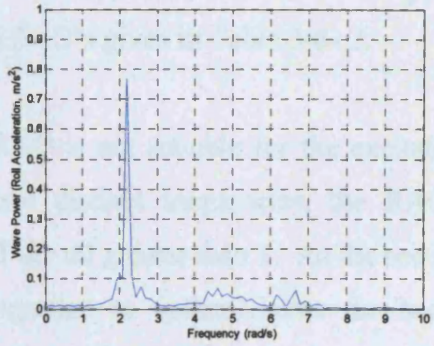

Wave Frequency 2.192 rad/s

Figure 5-8- 5: Discrete Fourier Transform of acceleration – time history for trimaran DVZ in beam seas at a speed equivalent to 6 knots without roll damping appendages

The DFT of the heave acceleration – time history for each wave is given in Figure 5-8- 5. At every wave excitation frequency, there is evidence of a second peak at exactly twice the frequency of the first peak. The magnitude of this peak increases significantly in the region of roll resonance, becoming a maximum at near the roll resonant frequency (closest to the wave frequency of 2.80 rad/s). This supports the hypothesis that roll motion induces heave at the damped natural roll frequency (in Section 5.6.1 it was shown that if heave motion is being induced by roll motion at the roll frequency, heave motion will be occurring at the roll frequency and twice the roll frequency). Twin peaks indicate that the heave acceleration is governed by the summation of two regular sinusoidal waves and so linear regular wave theory cannot be used. The heave displacement can be expected to comprise of the same frequency components, thus a heave RAO cannot be determined unless only one peak is used (i.e. one of the two regular waves). Rather than integrating the whole signal to obtain the heave – displacement time history, if simple harmonic motion were assumed (although this type of motion is not what has been recorded) the heave displacement can be obtained by dividing the peak heave acceleration amplitude by the corresponding peak heave acceleration frequency squared. This approach is followed using just the first peak of the DFT to obtain the heave RAO's given in Table 5-8- 2.

Even though this method of obtaining an RAO is not suitable for the excitation frequencies giving motion responses at two distinct frequencies, the RAO's produced using just the first peak of the DFT are all greater than 1. As the second peak has been omitted this method is expected to underestimate the heave response and so these RAO values are conservative. This is highlighted by considering the percentage power in the DFT at the frequency of the first peak, see Table 5-8- 2, at a wave excitation frequency equal to the damped roll natural frequency, the power at this peak drops to 63.6% whereas away from this roll resonant frequency the power at the frequency of the first peak rises to around 90%.

As mentioned in the previous paragraph, a regular wave constructed using only the first peak of the heave acceleration DFT will not give a good fit to the recorded data when the magnitude of the second peak is large. An example of this

is shown in Figure 5-8- 6 at a wave excitation frequency of 2.80 rad/s (roll resonance). As only 64% of the power of the motion response was located in this first peak a good fit is not expected. Contrast this with the fit of a regular wave constructed using the first peak of the heave acceleration DFT at a wave excitation frequency of 2.192 rad/s (close to heave resonance). Here 87% of the power is located in this first peak and so the fit is much better.

Wave Frequency (rad/s)	3.788	3.097	2.800	2.574	2.398	2.192
Wave Amplitude (mm)	50.6	81.8	89.1	99.3	116.2	128.8
Heave Frequency (rad/s)	3.737	3.091	2.788	2.555	2.388	2.180
Heave Acceleration from Peak of DFT (m/s^2)	0.814	0.846	0.812	0.717	0.790	0.768
Heave Displacement from Peak of the DFT (m)	0.058	0.089	0.104	0.110	0.138	0.162
RAO	1.15	1.09	1.17	1.11	1.19	1.26
Percentage Power at First Peak of the DFT (%)	96.1	77.0	63.6	91.9	92.6	87.3

Table 5-8- 2: Wave, heave acceleration and heave displacement data from model experiment results in regular waves with trimaran DVZ (without roll damping appendages) at a speed equivalent to 6 knots

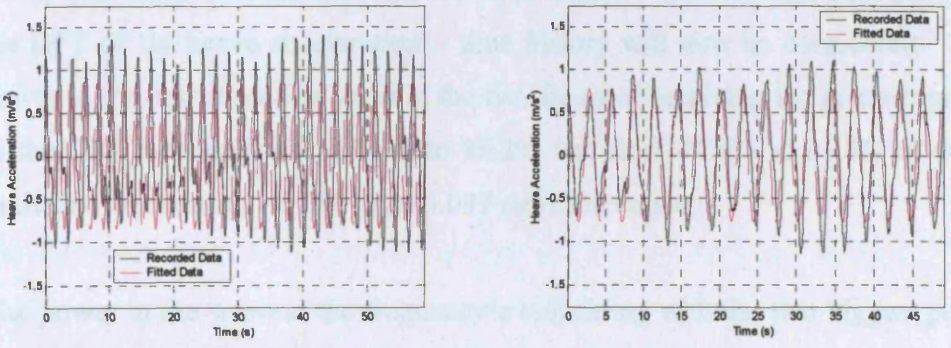

Wave Frequency 2.800 rad/s ***Wave Frequency 2.192 rad/s***

Figure 5-8- 6: Fit of regular wave to recorded heave acceleration – time history using the magnitude of the acceleration of the first peak of the Discrete Fourier Transform for trimaran DVZ without roll damping appendages in beam seas at a speed equivalent to 6 knots

The above analysis shows that, for a trimaran with a similar hull shape to trimaran DVZ, the heave RAO will not be accurately determined using linear regular wave theory at excitations close to the roll resonance frequency. In this condition the heave RAO will be under predicted.

There is some other experimental evidence that would appear to support this. Vassilos, Helvacioglou and Jasionowski (13) conducted experiments using a scale model of a 150 metre 4500 tonne trimaran design. This ship had haunches on the side hulls as well as flare on the outboard side of the side hulls. The hulls of this model were similar to those of trimaran DVZ. However, the $\overline{GM}$ value was lower at 1.90 metres (compared with 3.14 metres). Model test results in regular waves are presented and the roll and heave RAO's are compared with theoretical predictions. The heave RAO was shown to drop significantly at two frequencies close to the damped roll natural frequency. This drop did not occur in the theoretical prediction. Whilst this evidence is compelling, without knowledge of how the RAO was calculated (the process used to determine the steady heave motion amplitude) no firm conclusion can be drawn. This is the only documented example of a drop in the heave RAO obtained from trimaran roll experiment results.

To try and obtain a better fit to the recorded motion – time history, both peaks of the DFT of the heave acceleration – time history will now be considered. The power in the output motion wave at the two frequencies giving the greatest peaks in the DFT increases from 63.6% to 86.2% and from 77.0% to 91.8% at wave excitation frequencies of 2.800 and 3.097 rad/s respectively.

The power in the wave at the frequency's coinciding with the two biggest peaks changes to 91.8% and 86.2% from 77.0% and 63.6% at wave frequencies 3.097 and 2.800 rad/s respectively. If a wave is constructed from the addition of two sine waves, one with the amplitude and frequency measured from the first peak of the DFT of the acceleration – time history, and the other with amplitude and frequency measured from the second peak, the fit between this wave and the output heave acceleration – time history is improved. The fit of a two term sine

wave to the output acceleration – time history at a wave excitation of 2.800 rad/s is given in Figure 5-8- 7 where it can be seen that the fit is indeed much improved (compare this with the left hand graph of Figure 5-8- 6).

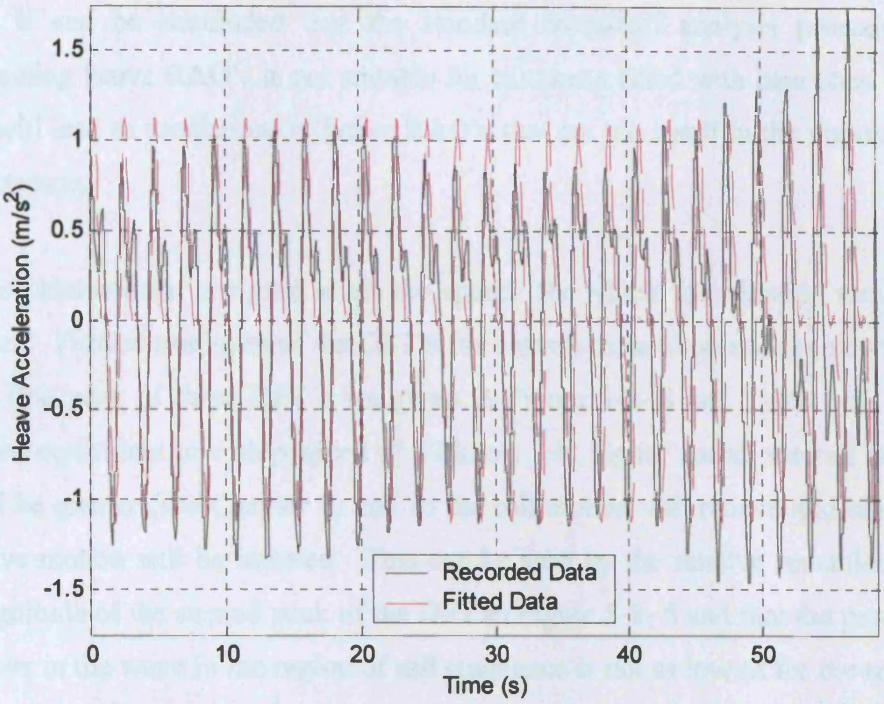

Figure 5-8- 7:- Recorded heave acceleration – time history compared to fit using two sinusoidal varying terms each with constant amplitude and frequency taking from the first and second peak of the Discrete Fourier Transform for wave frequency 2.80 rad/s for trimaran DVZ in beam seas at a speed equivalent to 6 knots

In Figure 5-8- 7 the phase difference between the two sinusoidal terms has been taken as zero. It can be seen from the shape of the recorded heave acceleration - time history that there is likely to be some phase difference because the shape of the fitted two term sine wave is not identical to this recorded motion – time history. The phase difference could be determined by a least squares fit of a two term sine wave with phase difference to the recorded data.

In Figure 5-8- 7, towards the end of the time window, the amplitude of the recorded motion – time history is greater than the amplitude of the sum of the two sine waves (without phase difference) measured from the relevant DFT. This could indicate that coupling with another motion could be occurring as well. The

most likely is pitch because the side hulls are located aft of midships and their centre of buoyancy will be aft of the LCF and LCB of the centre hull. So, when rolling in beam seas, the heave motion of the side hulls could induce pitch motion. This possibility is investigated in Section 5.8.3.

So, it can be concluded that the standard monohull analysis procedure for obtaining heave RAO's is not suitable for trimarans fitted with haunches. To do so will lead to predictions of heave RAO's that are too small in the region of roll resonance.

This phenomenon occurred at all the speeds for which the trimaran model was tested. Further examples of the DFT's for heave acceleration and the power from the first peak of these DFT's are given in Figure 5-8- 8 and Table 5-8- 3 for a speed equivalent to a ship speed of 12 knots. At higher speed, the roll damping will be greater (see Chapter 2) and so the roll motion will reduce and hence less heave motion will be induced. This can be seen by the relative reduction in the magnitude of the second peak of the DFT in Figure 5-8- 8 and that the percentage power in the wave in the region of roll resonance is not as low as for the results at 6 knots presented previously.

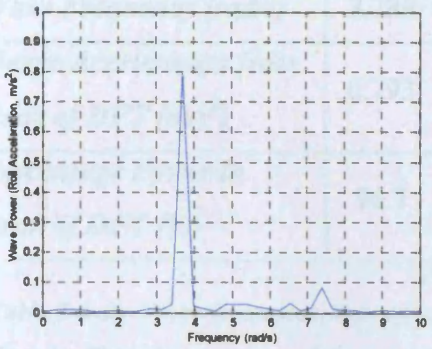

Wave Frequency 3.788 rad/s

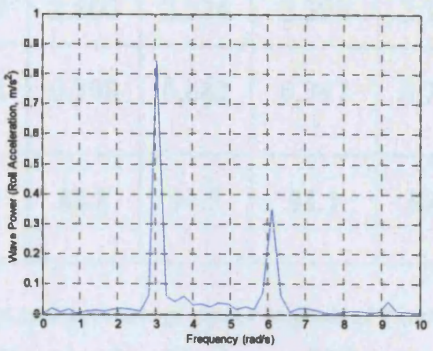

Wave Frequency 3.097rad/s

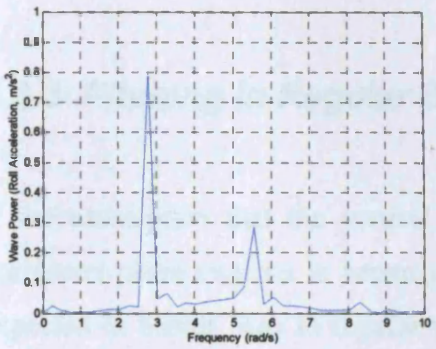

Wave Frequency 2.800 rad/s

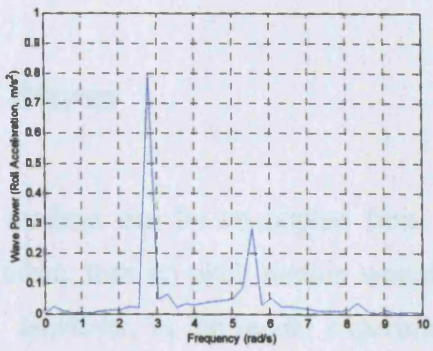

Wave Frequency 2.574 rad/s

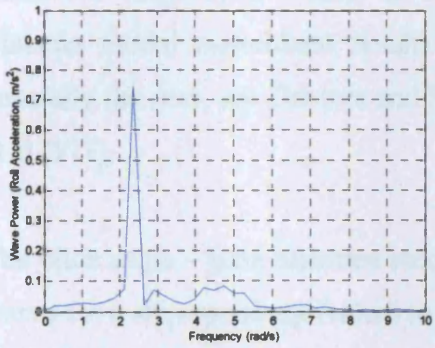

Wave Frequency 2.398 rad/s

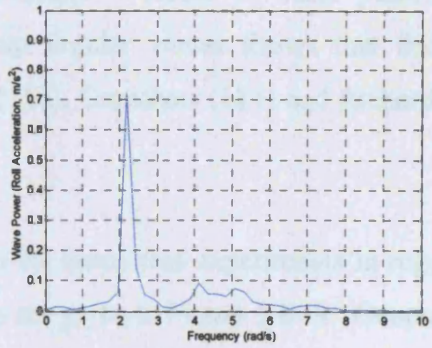

Wave Frequency 2.192 rad/s

Figure 5-8- 8: Discrete Fourier Transform of heave acceleration – time history for trimaran DVZ in beam seas at a speed equivalent to 12 knots without roll damping appendages

Wave Frequency (rad/s)	3.788	3.097	2.800	2.574	2.398	2.192
Heave Acceleration from Peak of DFT (m/s^2)	0.793	0.844	0.798	0.682	0.747	0.724
Percentage Power in Peak of DFT (%)	96.7	81.0	83.8	91.3	91.1	88.6

Table 5-8- 3: Wave frequency, heave acceleration and percentage power in peak of Discrete Fourier Transform measured from model experiment results with trimaran DVZ (without roll damping appendages) at a speed equivalent to 12 knots

5.8.3 Pitching in Regular Beam Waves

If the assumption that the vertical plane motions can be uncoupled from the horizontal plane motions in beams seas is taken, then no pitch motion would be expected in beams seas in regular waves. However, in the model experiments with trimaran DVZ, pitch motions were recorded and these were greatest at wave excitation frequencies closest to roll resonance. Perusal of other published trimaran model experiment results in beam regular waves shows that this is generally the case, see Doctors and Scrace (166), Granshaw (181) and Richardsen et al (171).

The pitch angle – time histories recorded in the beam seas experiments in regular waves for a ship speed equivalent to 6 knots are given in Figure 5-8- 9. Generally speaking, the greatest pitch angles occur at wave excitation frequencies closest to roll resonance, with the exception of a few cycles giving large pitch angles at an excitation frequency of 2.192 rad/s.

The DFT of these pitch angle – time histories is given in Figure 5-8- 10. These DFT plots show a narrow banded peak of large amplitude for excitation frequencies around roll resonance, whereas at excitation frequencies away from roll resonance the magnitude of the peak is much smaller and the peak is not so narrowly banded. In all cases, there is a second peak just after the first and this is likely to represent the pitch natural frequency. From this analysis it can be

concluded that if roll motion induces heave motion it is also quite likely the pitch motion is induced as well if the side hulls are located such that when they heave the model will also pitch.

The percentage power at the frequency causing the largest peak in the pitch angle DFT is given in Table 5-8- 4. Only the first two frequencies in the table have a power at this frequency greater than 70%, for the other frequencies a single regular wave at this peak frequency would not provide a good fit to the experimental data and thus accurate RAO's would not be able to be produced.

Wave Frequency (rad/s)	3.788	3.097	2.800	2.574	2.398	2.192
Pitch Frequency (rad/s)	3.737	3.091	2.788	2.555	2.729	1.923
Pitch Angle from Peak of DFT (degrees)	0.341	0.830	0.686	0.211	0.282	0.374
Percentage Power in Peak of DFT (%)	84.1	73.9	64.7	42.5	34.6	29.6

Table 5-8- 4: Wave frequency, pitch frequency, pitch amplitude and percentage power in peak of Discrete Fourier Transform measured from model experiment results with trimaran DVZ (without roll damping appendages) at a speed equivalent to 6 knots

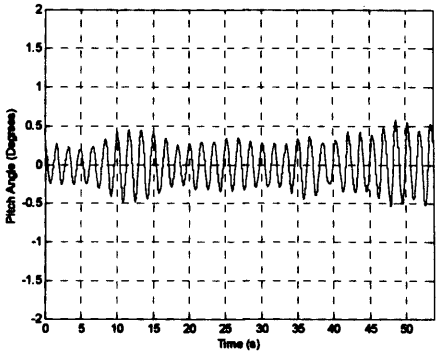

Wave Frequency 3.788 rad/s

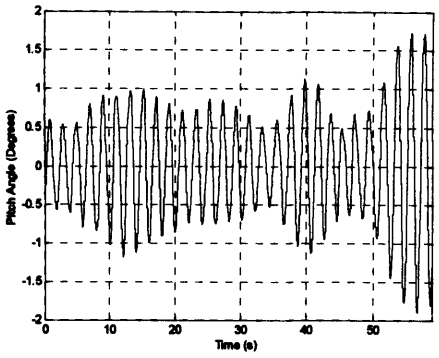

Wave Frequency 3.097rad/s

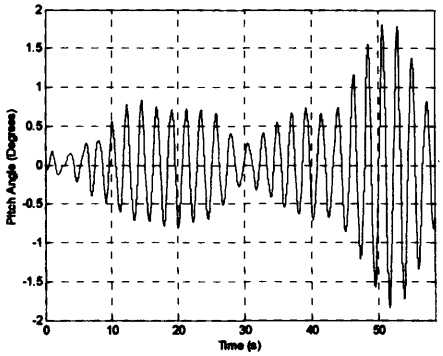

Wave Frequency 2.800 rad/s

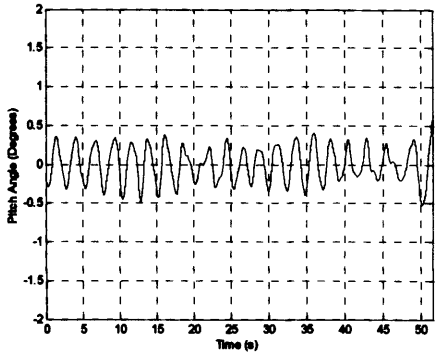

Wave Frequency 2.574 rad/s

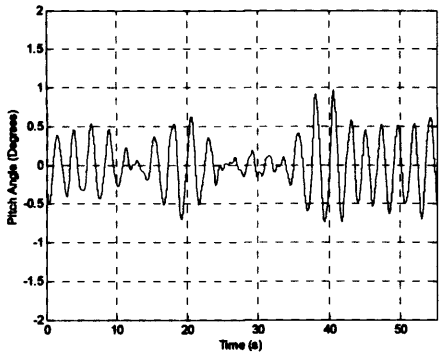

Wave Frequency 2.398 rad/s

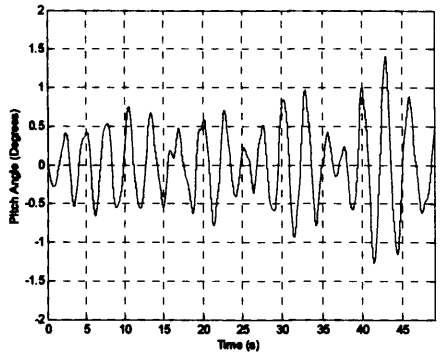

Wave Frequency 2.192 rad/s

Figure 5-8- 9: Pitch angle – time histories for trimaran DVZ in beam seas at a speed equivalent to 6 knots without roll damping appendages

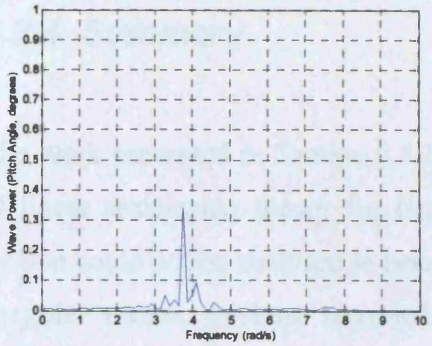

Wave Frequency 3.788 rad/s

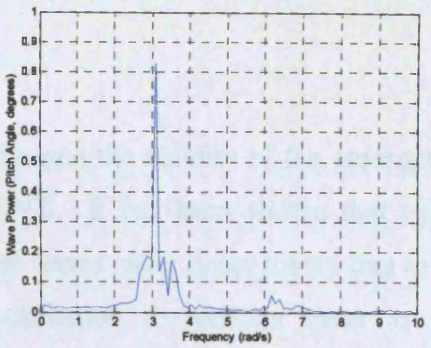

Wave Frequency 3.097rad/s

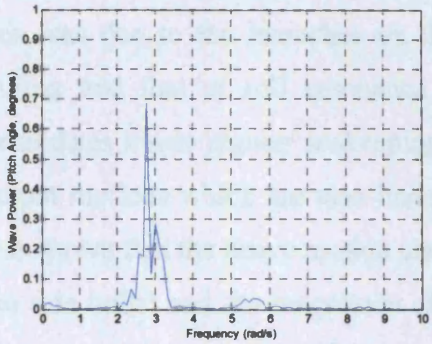

Wave Frequency 2.800 rad/s

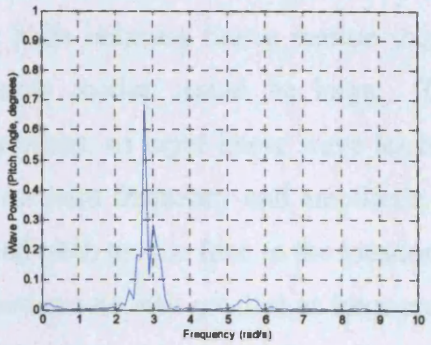

Wave Frequency 2.574 rad/s

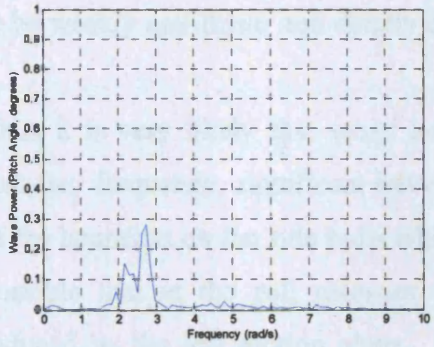

Wave Frequency 2.398 rad/s

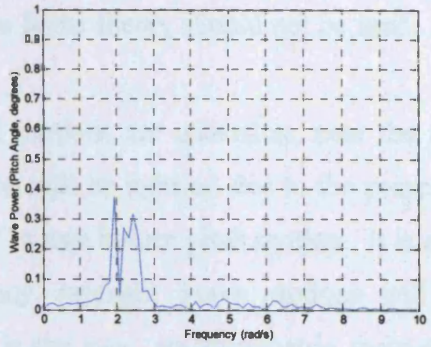

Wave Frequency 2.192 rad/s

Figure 5-8- 10: Discrete Fourier Transform of pitch angle – time history for trimaran DVZ in beam seas at a speed equivalent to 6 knots without roll damping appendages

5.8.4 Summary

The work presented in Section 5.8 has challenged the validity of the assumption of linear seakeeping theory for trimaran DVZ. It has been shown that heave motion could not be analysed in beam regular waves using linear theory due to the irregular output motions recorded. At excitation frequencies close to roll resonance, heave motion was occurring at two predominant frequencies (the excitation frequency and twice the excitation frequency). It was postulated that this was due to the haunches on the side hulls inducing heave motion during rolling and that at roll resonance this heave motion would be large. This invalidates linear regular seakeeping theory where an input linear wave leads to output motions which are also linear with constant frequency and amplitude. It was shown that the heave motion also induced pitch motion (due to the location of the side hulls) and the magnitude of this motion was also greatest at frequencies close to roll resonance. Whilst a reasonable approximation of the roll motion could be obtained using the linear assumption, the output roll motion was shown to be weekly non-linear and strictly therefore linear theory should not be used.

Thus it is very likely that when large roll motions are occurring, near the roll resonant frequency, significant heave motion will be induced due to the presence of the haunches on the side hulls which will in turn induce pitch motion. It is also possible that at the roll resonant frequency, resonant heave motions will be induced by the roll motion alone. If this is the case, autoparametric resonance occurs between the two modes and then there is continuous energy exchange between them. This idea is explored for monohulls by Nayfeh, Fung, Haji and Mook (182). An autoparametric resonance is said to occur when resonance in one degree of freedom, driven by external forcing of the system, causes resonant motion in another degree of freedom. A parametric resonance occurs when energy from a degree of freedom excited by external forcing, *not leading to resonance in that degree of freedom*, causes resonance in a different degree of freedom. Autoparametic resonance of trimarans would appear to be an interesting topic for future theoretical studies.

5.9 Conclusions

In this chapter the assumptions underpinning the analysis of trimaran roll motion have been explored through focused studies based on research conducted on a single trimaran model. This work has shown that many of these assumptions, which to date have been considered acceptable for trimarans, are erroneous when applied to this trimaran model. The key conclusions from this work are outlined in the following paragraphs. Further, more complete, studies are required to investigate this assertion in greater depth and in particular to understand whether the results are applicable to all trimarans. A plan for further studies is developed in Chapter 6.

This chapter started with further analysis of the trimaran roll decay experiments. The start point was to see whether a quadratic or cubic damping model fitted the measured data best. From the roll decrement, the equivalent linear roll damping was calculated over half a roll period and plotted against the average roll amplitude of the two peaks defining the half roll cycle so that the spread of the data around the chosen damping model could be investigated. After least squares fitting the two damping models to the data (quadratic or cubic) the spread of equivalent linear damping results around the line representing the fitted damping model was large in both cases. For roll decay at zero speed, the spread of data could be so large that some values of equivalent linear damping were negative even though the linear and quadratic or cubic damping coefficients are positive. Negative damping, that is motion amplification in proportion to roll velocity, is physically most unlikely. This trend was shown to occur in both the sets of zero speed roll decay experiments carried out on trimaran DVZ (undertaken in 2002 and 2004).

Analysis of the two sets of zero speed roll decay experiments allowed the repeatability of the results to be checked. In both sets of experiments the plots of peak decrement against time were well matched (allowing for slight variations in the initial roll angle), however there was a great variation between the linear and quadratic damping coefficients determined in 2002 compared with those from

2004, this was due to the considerable spread of the damping data described in the previous paragraph. Thus, due to the spread of the damping data, the damping coefficients cannot be determined with any level of confidence.

Having questioned the appropriateness of the chosen damping model, the next series of investigations, still focused on the analysis of roll decay results, were focused on the assumption that the decay could be modelled by a single degree of freedom roll equation with constant coefficients. To start with, the assumption of a single degree of freedom equation of motion was accepted and the studies just explored the assumption of constant coefficients. Studies were undertaken using time domain simulations of the roll decay (of trimaran DVZ) with a time varying roll stiffness term (after dividing the equation of motion through by the summation of the roll inertia and added inertia). These simulations showed that, when the roll decrement was analysed in the same way as before, a spread of equivalent linear damping data could be obtained. It was postulated that, for a trimaran with significant flare or haunches on the side hulls, roll motion would induce heave motion due to the immersion and emergence of the side hulls during one roll cycle. A second heave component is introduced in any roll decay experiment when a force is applied to the edge of the model to instigate the roll decay. These effects were incorporated in the roll decay simulations by modifications to the roll stiffness of the model (due to the change of waterplane whilst heaving). It was shown that, for trimaran DVZ, the only way a spread of damping could be obtained which was similar to that occurring in the previous roll decay analysis was when there was little or no heave damping.

Having shown for trimaran DVZ that stable roll damping coefficents could not be achieved if the decay was analysed using a single degree of freedom roll equation with constant coefficients, and by using simulations of the roll decay of trimaran DVZ shown that the assumption of constant coefficients may be erroneous, it remained to see if the assumption of uncoupled roll was correct. This assumption was investigated by looking at results of heave, pitch and roll motions recorded in the 2004 series of roll decay experiments. This showed that roll motion did infact induce heave motion during roll decay and that this heave motion did not decay away. The recorded heave component did not occur at one distinct frequency,

Fourier analysis showed it to comprise of a number of frequency components including the roll frequency and twice the roll frequency. Due to the location of the side hulls on trimaran DVZ, the heave motion also induced pitch motion. Thus, the assumption of uncoupled roll during roll decay was shown to be incorrect for trimaran DVZ.

Having thoroughly explored the roll decay, the next step was to look at the assumptions underpinning roll motion prediction. These were challenged by analysing the results of seakeeping experiments carried out on trimaran DVZ in beam waves. The assumption of linear theory, where a regular sinusoidal wave of constant amplitude and frequency leads to output motions which are also regular and sinusoidal with constant amplitude and frequency, was shown to be invalid for heave motion and somewhat questionable for roll motion. The heave results showed that there was strong coupling between roll and heave at excitation frequencies close to roll resonance, and at these frequencies the heave motion was irregular and comprised of two distinct frequency components. If this heave motion was being driven by roll motion then two peaks in the decomposition of the frequency response would be expected. This is because one heave cycle occurs for every half a roll cycle (i.e. heave up and back down when the model rolls to port and up and back down again when the model rolls to starboard). Therefore, if heave motion is being induced by roll motion at the roll frequency, heave motion will be occurring with half the period of the roll motion (i.e. at twice the frequency). This leads to an irregular output heave motion.

Theoretical seakeeping prediction codes have not been investigated in this chapter. However, many of the important conclusions outlined in the previous paragraphs, strictly applicable only to the roll motion of trimaran DVZ (and possibly all similar trimaran hull shapes), question the appropriateness of most modern theoretical seakeeping codes. The inability to obtain stable roll damping coefficients from roll decay experiments affects the accuracy of seakeeping computer predictions in both the frequency and time domains that reply upon them. The work in Chapter 4 showed that, at the current time, there are no theoretical methods suitable for predicting roll damping coefficients for trimarans. The assumption of constant coefficients in the equation of motion was questioned.

If this assumption were to be invalid, solutions of the equation in the frequency domain would be inappropriate and it would complicate analysis in the time domain. Finally, the questioning of the appropriateness of linear theory also makes all but the most sophisticated mathematical formulations in the time domain inappropriate.

Chapter (6) A Path to Improved Predictions of Trimaran Roll Motions

Chapter (6) A Path to Improved Predictions of Trimaran Roll Motions 371
6.1 Introduction 372
6.2 Overview of the Key issues 373
6.2.1 The Problems 373
6.2.2 Proposal for the Solution 375
6.3 Process to Further the Understanding of Trimaran Roll Motion 377
6.4 Model Tests and Theoretical Studies in Support of the Process 380
6.4.1 Model Experiments and Theory at Zero Speed 380
6.4.2 Model Experiments and Theory with Forward Speed 390
6.4.3 Future Work 396
6.5 Conclusions 397

6.1 Introduction

The research documented in Chapters 4 and 5 has demonstrated that currently the physics of trimaran roll motion is poorly understood, both at zero speed and with forward speed. The coupling between roll motion and other motions and the significance of any coupling effects on the roll motion are not very well understood at all. Experimental studies and simulation of the roll equation of motion in Chapter 5 have demonstrated that coupling between heave and roll is most likely for a trimaran with haunches on the side hulls. The research in Chapter 4 has shown that current theoretical approaches based on monohull roll analysis processes are inadequate for trimarans. However, all these conclusions are based on research with just one trimaran model and one analysis tool (TRISKP).

A programme of work is required that will provide answers to these questions and to provide data to inform the development of theoretical roll damping and roll motion prediction methods. This work must be carried out so that conclusions which are applicable to all trimarans can be made.

Studies can sensibly be split into two parts: The first task is to understand the physics of roll motion at zero speed for a trimaran without appendages (Section 6.4.1); the second is to understand the physics of trimaran roll motion at forward speed without appendages and then to determine the roll damping contribution of any roll damping appendages (Section 6.4.2). Each part will need to be supported by model experiments and theoretical studies covering a range of trimaran geometries and configurations.

The purpose of this part of the thesis is to draw up a process that encapsulates these studies and to identify the model experiments and theoretical studies required to aid development of new theory to accurately predict the roll motion of trimarans. The completion of this proposed research is left as future work to be taken forward by other researchers.

6.2 Overview of the Key issues

6.2.1 The Problems

The issues identified in Chapters 4 and 5 can be distilled down into four key points, each of which needs to be addressed if accurate roll motion predictions are to be obtained for trimarans.

1) Existing computer seakeeping prediction codes do not predict trimaran roll motion with sufficiently accuracy.

Predictions with existing linear frequency domain seakeeping computer programs are generally poor, being particularly so at zero speed. Furthermore, theoretical roll motion predictions, obtained using linear frequency domain seakeeping computer programs with experimentally derived linear and quadratic damping coefficients, do not correlate particularly well with model experiment results.

2) Stable measurements of roll damping coefficients cannot be obtained from roll decay experiment results using analysis techniques based on an uncoupled single degree of freedom equation of motion.

When the 2002 and 2004 free roll decay experiment results on trimaran DVZ were re-analysed in Chapter 5, there was considerable variability in the damping coefficients obtained from each set of results. The analysis showed that neither a quadratic or cubic damping model (with linear and quadratic or cubic damping coefficients) fitted the measured damping data particularly well because of a large spread in the damping data measured in the experiments (assuming an uncoupled linear equation of roll motion). This is part of the reason why poor roll motion predictions were obtained when experimentally derived damping coefficients were input into linear frequency domain seakeeping computer codes.

3) Analysis of results from model experiments show that it is likely that roll couples strongly into heave and to a lesser extent heave couples into pitch for trimarans fitted with haunches and flare on the side hulls.

Further analysis of the 2004 model experiment results, including motion predictions in regular beam waves and zero speed free roll decay, showed that it is most likely that roll motion induces heave and pitch motion. Thus, in the model experiments in waves, whist a regular input wave leads to a predominantly regular output roll response, it causes irregular heave and pitch responses.

It is postulated that this coupling of roll into heave is the reason why analysis of free decay experiments using only a single degree of freedom roll equation does not yield stable or accurate damping coefficients.

4) Using theory adapted from existing published methods, roll damping calculations based on the summation of a number of components do not give satisfactory predictions for trimarans fitted either with or without roll damping appendages.

In Chapter 4 a roll damping prediction method was developed based on the summation of a number of theoretical components, both linear and non-linear, with respect to the roll velocity. If non-linear components are included they must be converted to an equivalent linear form to allow a linear equation of motion to be solved. These equivalent linear components depend on the steady roll amplitude (requiring the equation of motion to be solved in an iterative manner) and so solution of the equation of motion is only practical in the frequency domain.

In the theoretical method that was developed, the dominant damping components were all linear. Of these linear components, three contributed the majority of the roll damping; lift of the appendages, centre hull horizontal lift and damping induced by side hull heave; all the contributions from the other components were so small that they could be safely discarded. The accuracy of the appendage lift calculations and damping induced by side hull heave were restricted in the

frequency domain linear analysis because the time varying position of both the appendage and side hulls cannot be considered. For the appendages, the time variance influences the free surface lift losses and the angle of attack, these factors significantly affect the lift and hence therefore the roll damping moment they generate. Whereas, for the roll damping component due to side hull heave, instantaneous immersion of the side hulls will affect the heave damping. It is possible that other mechanisms could be providing roll damping that were not considered in this theoretical method.

A proposal for a method to solve these issues is discussed in the next section.

6.2.2 Proposal for the Solution

In order to solve the problems identified in the previous sub section a more complete understanding of the basic physics of trimaran rolling is required. Attempts to predict the roll motion of a trimaran using accepted methods for analysis of monohulls have met with mixed success. This work was described in Chapter 4. Thus the applicability to trimarans of the assumptions interwoven in the monohull analysis methods has had to be questioned. This work is described in Chapter 5. The end result is that the basic physics of trimaran roll dynamics at zero speed are not properly understood. It has been postulated in Chapter 5 that this is especially the case when flare or haunches are fitted to the side hulls. Furthermore, when appendages were added, leading to significant roll reduction at high speed, theoretical predictions, once again based on tried and tested monohull methods, did not provide accurate estimates of trimaran rolling.

Whilst the desired end result is to be able to theoretically predict trimaran roll motion accurately, this cannot be achieved until the mechanisms influencing rolling of a trimaran hull without appendages are understood, at both zero speed and with forward speed. Furthermore, theoretical methods are required that allow the roll damping contribution of the range of appendages that could be fitted to a trimaran to be predicted.

Thus, the way forward is to first understand the physics of trimaran rolling at zero speed, then to build on this by understanding the additional damping generated by the hull alone at forward speed. Once these are understood the lift generated by appendages can be investigated. This understanding is best gained by experimental and theoretical studies on simplified trimaran hull shapes.

The work outlined so far will not yield a coherent theory which can be applied to computer seakeeping codes, rather it will allow trimaran motion to be better understood and provide a starting point on the route to development of an extensive validated theory. Once the physics of the problem are understood, further experiments and analysis should be conducted that will allow a robust semi-empirical theory to be developed. This completes the first step towards the development of fully theoretical methods.

It is likely that the early investigative experiments will be based on simplified trimaran hull shapes or prismatic hull sections. It is important therefore that any new theory developed is subsequently validated against actual trimaran hulls.

In summary, what is required is a proper understanding of the physics of trimaran rolling as well as a route towards new methods for obtaining accurate estimates of trimaran roll motion.

6.3 Process to Further the Understanding of Trimaran Roll Motion

A process towards the development of a fully theoretical method for predicting trimaran roll motion is outlined in Figure 6-3- 1. A good precursor to a theoretical method is a robust semi-empirical method using data from model experiments. This is the central box in the figure. This semi-empirical method is fed by two streams of research. The first is work required to gain a complete understanding of the physics of roll motion of a trimaran at zero speed (the box with the dashed outline at the top of Figure 6-3- 1), the other is work required to understand what is happening at forward speed (the box with the dashed outline at the bottom of Figure 6-3- 1).

Looking at each of these two research activities in turn, the first point to address to understand roll motion at zero speed is the possible coupling between roll and heave identified in Chapter 5. It has been postulated that this is due entirely to flare or haunches on the side hulls. As the purpose of the side hulls on a trimaran is to provide stability, they will also be expected to have a significant effect on the roll motion. The next step is to understand how the geometry and location of the side hulls affects roll motion and then to understand the roll damping they provide.

Focusing on the second option, trimaran motion analysis at forward speed, theoretical methods for predicting monohull roll damping suggest that the extra damping that occurs is due to the horizontal lift force generated by the hull due to an angle of attack developed between the hull and the inflow whilst rolling. The magnitude of this term should be investigated for a trimaran and in particular the contribution of the side hulls to this form of damping needs to be understood.

Once all the mechanisms influencing the roll motion of a trimaran hull at both zero and forward speed have been identified semi-empirical theory can be

developed to predict them. Finally, the lift developed by appendages must be investigated so that theoretical predictions can be made.

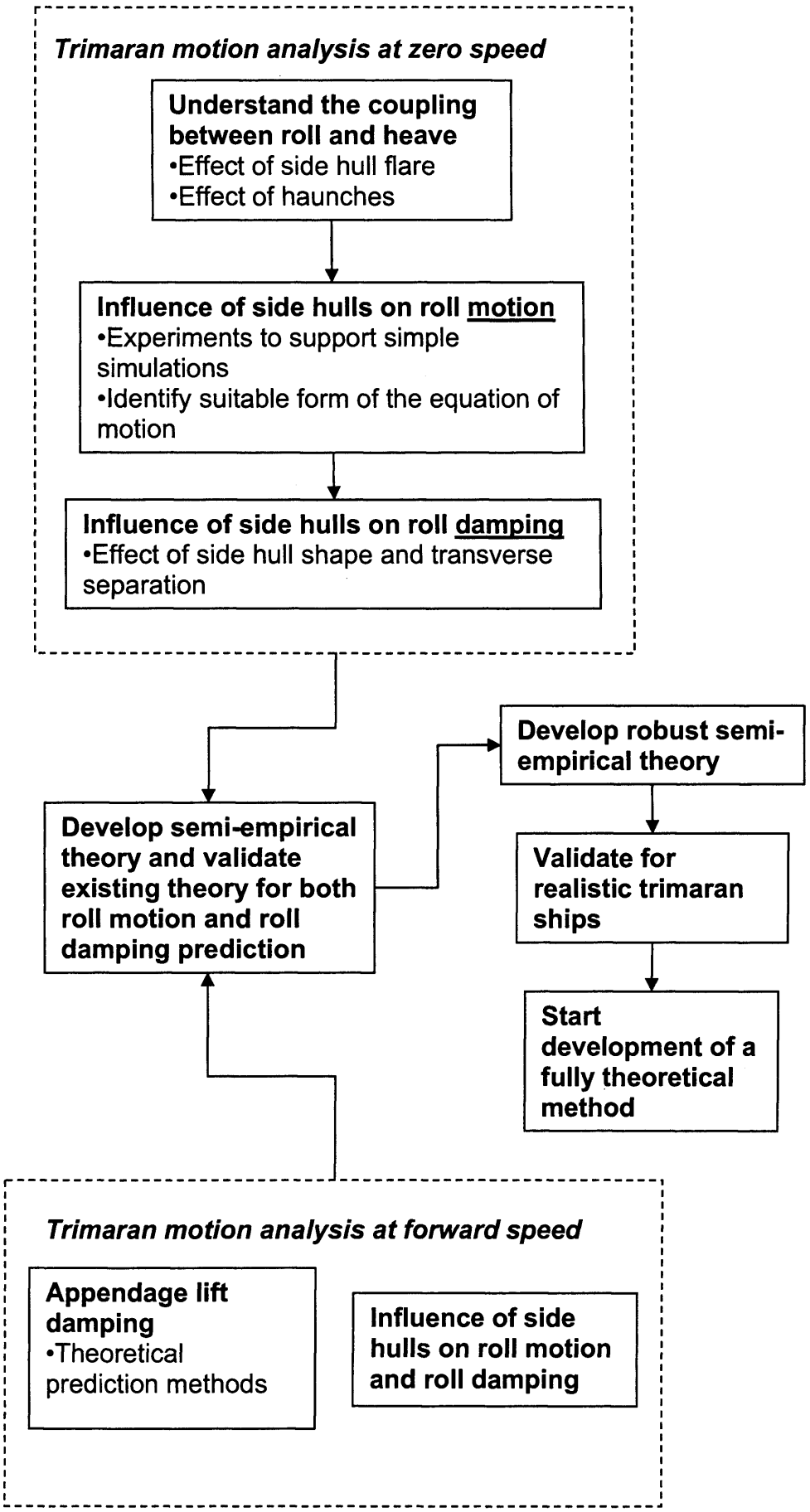

Figure 6-3- 1: Process to further the understanding of trimaran rolling

6.4 Model Tests and Theoretical Studies in Support of the Process

Based on the process outlined in Section 6.3, a number of model experiments, simulations and computational analyses are discussed in the next two sub sections to address the problems outlined in Section 6.2.1. It is beyond the scope of this thesis to research these topics in any depth. However, they must be addressed if trimaran roll motion is to be understood. This work forms a basis for the development of theoretical methods which will allow accurate predictions of trimaran roll motion and roll damping.

The initial focus of these studies is to fully understand the physics of trimaran roll motion at zero speed. Building on this knowledge the roll damping components which were put forward for trimarans in Section 4.4.1 of Chapter 4 can then be validated or their relative contribution investigated further.

6.4.1 Model Experiments and Theory at Zero Speed

Experiment One: The nature of roll and heave coupling

The purpose of this experiment is to understand when roll motion induces heave motion for a trimaran. In Chapter 5 it was postulated that when rolling, trimarans fitted with haunches and flare on the side hulls heave. This causes regular wave theory and any analysis with a single degree of freedom roll equation to become invalid.

To investigate this effect a trimaran model is required with a centre hull shape that will not induce any heave motion during rolling. This allows heave motion, caused purely by the change of side hull immersion during rolling, to be investigated. As this experiment will be conducted at zero forward speed the hulls do not need to be shaped to minimise resistance, therefore simple prismatic hull

shapes are to be used. Thus the trimaran model will comprise a prismatic centre hull of circular section and thickened flat plate side hulls of rectangular section. The model shall be set up so that the transverse position and draught of the side hulls can be varied. The side hulls should be manufactured so that a series of simple triangular sectioned haunches can be fitted to the inboard face. The cross structure connecting the three hulls should be designed so that it does not enter the water for the range of roll angles likely to be recorded in the experiments. The model arrangement is shown in Figure 6-4- 1.

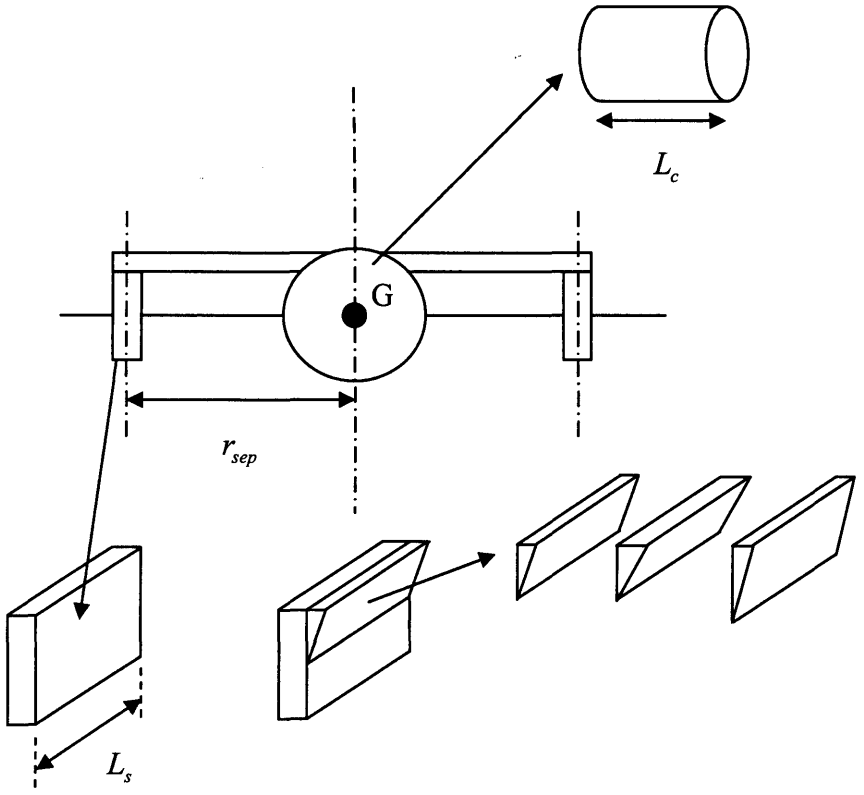

Figure 6-4- 1: Set up for experiment one

The model shall be set up so that the centre of gravity, and thus the roll centre, are located at the mid point of the circular sectioned centre hull and this shall be coincident with the waterline. When setup in this way, the centre hull hydrostatic properties will not change during roll motion, thus the centre hull will not cause the model to heave. So, whilst the side hulls remain in the water, the waterplane area of the model will not change appreciably during roll motion (so long as there

are no haunches fitted). The model should be instrumented so that roll angle and heave acceleration are measured. Due to the simple shape of the model, motion in degrees of freedom other than roll and heave (only likely when the haunches are fitted), should not be encountered.

The model should be small enough to allow the roll radius of gyration to be determined using a compound pendulum, see Chapter 16 of Lloyd (64).

The test rig will need to be set up so that the following tests can take place:-

1. Roll decay with heave constrained.
2. Heave decay with roll constrained
3. Free roll decay

In the first series of experiments, heave motion can be constrained by fixing the model longitudinally through the centre of gravity. Free decay experiments can then be conducted for various values of side hull separation and beam to draught ratio. The initial heel angle should be selected so that both side hulls remain submerged at all times. As this is measuring purely roll motion, a single degree of freedom uncoupled roll equation will model the decay and so the equivalent linear roll damping per half cycle can be obtained from the decrement using one of the approaches outlined in Section 2.4.2 of Chapter 2. The mass distribution of the model should be arranged to ensure that the resulting roll radius of gyration gives a sensible roll period. A suitable form of the damping model can then be proposed. A large spread in the equivalent linear damping values should not be expected. Experiments can then be conducted at larger heel angles so that one side hull comes out of the water during the decay. This will allow a qualitative analysis of the effect that this has on the decay. Finally, the haunches can be added to the side hulls and the effect of these on the roll motion can be investigated by comparing peak decrements for the model with and without haunches.

In the second series of experiments the pure heave decay can be measured by constraining the model so that it cannot roll. Decrements can be compared for

different values of side hull beam to draught ratio both with and without the haunches fitted. The haunches should reduce the heave motion as the heave stiffness will increase when they are submerged.

Finally, the model should be subjected to a free "roll" decay experiment. Once again, experiments should be conducted for the same range of side hull separations and beam to draught ratios used in the first set of experiments, taking care to ensure that the side hulls remain immersed for the duration of the decay. Without the haunches fitted, heave motion should not be induced and the results should be almost identical to those from the experiments where the model was restrained. The experiments should then be repeated with the haunches fitted. Heave motion will be expected and so both heave and roll time histories should be recorded. The initial heel angle on the model can then be increased so that the side hulls come out of the water during the decay. The effect this has on the roll and heave motion can be investigated qualitatively.

The results of Experiment One will allow the hypothesis that for a trimaran fitted with haunches (or considerable flare) roll motion induces heave motion to be proved or disproved.

Experiment Two: Establishing a suitable form for the equation of motion

The purpose of this experiment is to examine the roll motion of a simple trimaran to determine an appropriate form of the equation of motion to use for future analysis. Once a form for the equation of motion has been established, time domain simulations can be performed and the results compared to the model experiments. This will allow the chosen form of the equation of motion to be validated.

The results of Experiment One are expected to show that for the simple trimaran model, coupling between roll and heave only occurs when either the side hulls are fitted with haunches or if the side hulls exit the water. Thus, without the haunches (or flared side hulls) the motion of the model can be examined using an uncoupled

single degree of freedom roll equation with constant coefficients (so long as the side hulls do not exit the water).

However, if when rolling in calm water the haunches on the side hulls induce heave motion, a moment will be created that opposes the roll moment. This extra moment could be included on the right hand side of a single degree of freedom roll equation. In order to continue with the simple single degree of freedom approach, the stiffness term will now be time variant, depending on the change in displacement due to heave and the roll angle. The change in displacement will also affect the roll inertia.

As shown in Chapter 5, examining trimaran roll motion using a free decay experiment is not ideal as a heave moment has to be applied to the model to instigate the decay. This heave moment will decay at the natural heave frequency whereas any heave motion induced by rolling will occur at the roll frequency. This complicates the heave response, which comprises of more than one frequency component. The problem can be avoided if a forced roll experiment is conducted instead. Here a steady sinusoidal roll moment is applied to the model of amplitude m_{a4} per unit roll inertia and frequency ω. If the model's restoring characteristics are linear, the output roll motion will be sinusoidal but there will be a phase difference between the roll angle and the roll moment. The equation of motion can then be described by:-

$$\ddot{x}_4 + b_{44}\dot{x}_4 + \frac{\rho\nabla\overline{GM}}{(I_4 + A_{44})}x_4 = m_{a4}\cos(\omega t) \qquad \textbf{6-4-1}$$

The equation can be further expanded by replacing the roll damping term with a suitable damping model, for example a quadratic model with linear and quadratic damping coefficients:-

$$\ddot{x}_4 + (b_1 + b_2|\dot{x}_4|)\dot{x}_4 + \frac{\rho\nabla\overline{GM}}{(I_4 + A_{44})}x_4 = m_{a4}\cos(\omega t) \qquad \textbf{6-4-2}$$

For the simple trimaran model used in Experiment One, equation 6-4- 2 should be adequate to describe the output motion without the haunches fitted to the side hulls so long as the $\overline{GZ}$ curve remains linear over the range of roll angles observed in the experiment (with the right hand side of the equation set to zero). However, as discussed above, addition of the haunches will cause an extra heave moment and will make the stiffness term time variant. Thus, if the assumption is made that the roll inertia and added inertia are constant, the equation can be recast as follows:-

$$\ddot{x}_4 + \left(b_1 + b_2|\dot{x}_4|\right)\dot{x}_4 + \frac{\rho\nabla(t)\overline{GM}(t)}{\left(I_4 + A_{44}\right)}x_4 = m_{a4}\cos(\omega t) + h_a(t)\cos(\omega t) \qquad \textbf{6-4-3}$$

Where $h_a(t)$ is the time varying heave moment amplitude caused by immersion of the haunches on the side hulls of the model per unit roll inertia. This term will depend on the roll angle, x_4, and the heave displacement, x_3. In addition, if the model is heaving as well as rolling, the magnitude of $\overline{GM}$ and the displaced volume, ∇, will vary with both the roll angle and heave displacement.

The equation of motion is now much more complex but remains in just a single degree of freedom. A coupled heave and roll equation of motion would be more appropriate, but this requires knowledge of the coupling terms and the added mass and damping in heave. To obtain these further experimentation would be required or theoretical estimates would have to be used which introduce additional sources of error.

Using this new equation of motion, estimates of the roll damping coefficients can be obtained from the results of forced roll experiments. Because of the time varying terms in the equation of motion, accurate estimates of the roll damping will only be obtained if the complete roll – time history is used. Damping coefficients can be determined in this way using a Parameter Identification Technique. A brief discussion on these methods was given in Section 2.4.2.2 of Chapter 2. The damping coefficients can be obtained using the following procedure:-

1. Obtain measurements for the roll angle and heave displacement from the forced roll experiments
2. Create a lookup table for $\overline{GM}$ and displacement covering the range of roll angles and mean draughts (calculated using the heave displacement data) observed in the experiments
3. Use the lookup table to determine the time varying roll stiffness term in equation 6-4-3 assuming the roll inertia and added inertia remain constant
4. For the given roll angle use the lookup table to determine the extra buoyancy due to the change in immersion of the side hulls and hence calculate $h_a(t)$, the time varying heave damping moment
5. Use a parameter identification technique to obtain values for the unknown damping coefficients
6. Re-simulate the equation of motion (equation 6-4-3) using a Runge Kutta technique and check the accuracy of the damping coefficients

The above procedure can be tried with different roll damping models if the fit of the simulated data to the recorded data is not satisfactory. Based on the conclusions of the theoretical studies in Section 4.4 of Chapter 4 the linear coefficient should be greater than the non-linear coefficient.

The heave moment damping roll motion caused by the haunches on the side hulls of the simple trimaran model varies with roll velocity. This moment is dependent on the side hull heave damping which depends on the roll angle. Thus, only changes in the heave *damping* of the side hulls will influence roll damping. This was discussed in Section 4.4.1.2 of Chapter 4 where the damping component due to side hull heave damping, B_{SHH}, was developed. Therefore, damping coefficients obtained for the trimaran model without haunches should be almost identical to those obtained when the haunches are added so long as the waterplane area of the model in the still water condition does not change (haunches positioned above the still waterline). The analysis should be repeated for the trimaran without haunches fitted using equation 6-4-2 (without heave forcing and time varying stiffness) to model the resulting roll motion and the damping

coefficients obtained should be compared to those obtained when the haunches were fitted. For the simple trimaran model the two sets of damping coefficients should be almost identical. This expected trend can be further proved by repeating the analysis with haunches with different amounts of flare.

Some further qualitative information about the physics of trimaran roll motion can be gleaned from this experiment. If, when haunches are fitted to the model, heave motion couples with roll motion when a regular forced sinusoidal input roll moment is applied, a sinusoidal output motion will not be recorded. The level of irregularity in the output roll motion should increase as the flare on the haunches is increased.

Experiment Three: Influence of side hulls on roll damping

The purpose of this experiment is to determine the contribution of the side hulls to the roll damping term in the equation of motion.

For the simple trimaran model used in the previous two experiments, the circular sectioned centre hull when rolling around its central axis will not radiate waves or shed eddies when rolling. Thus, if the roll damping is considered to be made up of a number of additive components as asserted by Ikeda, Himeno and Tanaka (114) and Schmitke (81) the only damping the centre hull will provide is due to hull friction. As shown in Section 2.5.2 of Chapter 2 this component us usually very small. Thus, the majority of the roll damping for this model will come from the side hulls.

In Chapter 4, a roll damping component was developed based on the heave damping of the side hulls in vertical motion. An assumption was made that, when the side hull transverse separation is large, the motion of the side hulls during rolling can be considered to be approximated by movement in the vertical plane only. Thus, the heave damping in the vertical plane will provide roll damping depending on the magnitude of the vertical component of the roll velocity. For large side hull separation the vertical component of the roll velocity will be much larger than the horizontal component and so it can be approximated by

multiplying the roll velocity (in rad/s) by the separation of the side hull from the centre hull. For the theory in Chapter 4, the heave damping of the side hulls was estimated using linear Potential Flow Theory. This only considers the hull shape below the still water position and does not account for the vertical movement of the side hull when rolling. The quality of the roll motion predictions will depend on the accuracy of the heave damping term. Thus a series of experiments are proposed to gain an improved understanding of the heave damping of the side hulls.

Forced heave tests should be conducted using flat plate side hulls of the same geometry as those used in the previous two sets of experiments. Once again the side hull should be designed so that a series of haunches can be attached. The experimental setup is shown in Figure 6-4- 2. Forced heave experiments should be conducted for a range of side hull beam to draught ratios both with and without haunches fitted. The range of heave force amplitudes applied to the model in the experiments should be carefully selected so that the resulting heave velocity is representative of the vertical component of the roll velocity at the side hull position observed in the previous experiments ($\approx r_{sep}\dot{x}_4$). In addition, a series of experiments should be conducted where the magnitude of the applied force is enough to move the side hull clear of the water. This will allow a qualitative investigation on the effect this has on the steady heave damping of the side hulls. The frequency of the forced heave should be set to be equal to the roll resonant frequency of the model used in the first two experiments. An estimate of this can be made from the roll decays recorded in Experiment One. The equation of motion describing forced heave is:-

$$\ddot{x}_3 + b_{33}\dot{x}_3 + \frac{C_{33}}{(M + A_{33})}x_3 = f_{30}\cos(\omega t) \qquad \textbf{6-4- 4}$$

Where f_{30} is the steady heave force amplitude per unit mass. For monohull ships conventional wisdom suggests that the heave damping is linear, see Crossland, Wilson and Bradburn (173). Using the same approach that would be used to analyse the results of a forced roll test, see Spouge (95), a quasi-linear method

will allow the damping for each steady forced heave to be estimated using the following equation:-

$$b_{33}(x_{30}) = \frac{1}{\omega}\sqrt{\left(\frac{f_{30}}{x_{30}}\right)^2 - \left(\omega^2 - \frac{C_{33}}{(M + A_{33})}\right)^2} \qquad \textbf{6-4-5}$$

Where x_{30} is the output steady heave amplitude from the forced heave experiment. Forced heave tests should be conducted for a range of values of f_{30} and the resulting values of b_{33} should be plotted against x_{30}. If the heave damping is linear this will yield a straight line with a gradient equal to zero. These plots can be used to determine how the heave damping is affected by changes in beam to draught ratio of the side hulls, the addition of haunches with differing amounts of flare and when the side hull comes out of the water during the experiment. If in any of these cases the heave damping becomes non-linear then the term $h_a(t)$ in equation 6-4-3 will be a non-linear function of the heave amplitude x_3.

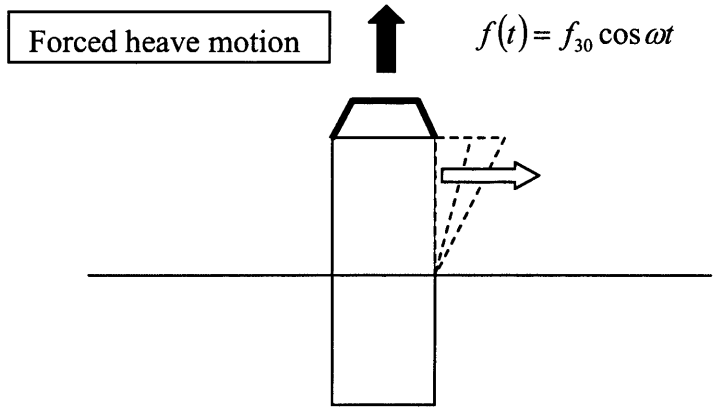

Figure 6-4- 2: Setup for experiment three, forced heave experiments on simple side hull shapes with and without haunches

Semi-empirical Prediction of Roll Motion

Having accurately measured the heave damping of side hull geometries used in Experiment Two, the roll damping of the simple trimaran model can now be

calculated theoretically. For this simple model, using the theoretical method of Section 4.4 of Chapter 4, the total roll damping can be considered to consist of the following components only:-

$$B_{44} = B_F + B_{SHH} \qquad \textbf{6-4-6}$$

Note that there is no wave radiation damping or eddy shedding for a circular sectioned hull. The wave radiation damping of the side hulls is considered to be small and the friction damping, B_F, can be calculated using the theory of Schmitke (81). The roll damping coefficients obtained using the Parameter Identification Technique and the series of forced roll experiment results from Experiment Two can then be compared with theoretical predictions using equation 6-4-6. The side hull heave damping component, B_{SHH}, can be estimated using the measured heave damping values from Experiment Three. Strictly speaking, the damping in equation 6-4-6 is linear and so should only be compared with the linear damping coefficient obtained using the results of Experiment Two. However, if for some of the side hull configurations tested the side hull heave damping proved to be non-linear, then the damping from equation 6-4-6 should be compared with both the linear and non-linear roll damping coefficients. In this case the non-linear damping should be converted to equivalent linear form using the method given in Section 2.2.3.2 of Chapter 2.

The correlation between the theoretical method (using experimentally derived side hull heave damping) and measured roll damping will highlight whether prediction by summation of a number of components is sensible as a basis for future theoretical predictions of trimaran roll damping.

6.4.2 Model Experiments and Theory with Forward Speed

Having suggested a number of experiments linked with theoretical analysis that should enlighten the physics of roll damping of trimarans at zero speed culminating with an embryonic semi-empirical theory, the focus now switches to predictions at forward speed. Investigations will be split into two areas; the first

is gaining an understanding of the magnitude of the lift damping component of a trimaran and then looking at possible ways of predicting appendage damping.

Experiment Four: Horizontal lift force on a trimaran during rolling

The purpose of this experiment is to determine the effect the side hulls have on hull lift damping at forward speed. The experiment will be based on the work of Haddara and Leung (124) who followed the approach pioneered by Ikeda, Himeno and Tanaka (114), (115). Haddara and Leung measured the horizontal lift force on a model towed obliquely (with a fixed yaw angle) down a towing tank with the model free to heel at different Froude Numbers. The horizontal lift force measured in this sort of experiment can be used to predict the horizontal lift damping component for a rolling ship, B_L. The large profile area of the hull of a ship ($\approx L \times T$) generates large forces and moments and these can be far greater than the control forces and moments generated by the rudders. Thus the lift force and associated moment developed by the hull in rolling are important and provide a significant portion of the total roll damping, see Section 2.5.5 of Chapter 2.

For this experiment, a model is towed down a towing tank obliquely at a fixed yaw angle, x_6, with the model free to heel. Once again a trimaran with simple geometry is to be used. This time the side hulls are to be thickened flat plates with rounded ends. The side hulls should have a constant vertical section shape. The centre hull is to be symmetrical about the x and y axes. A hull with semi-circular section below the waterline and wall sided above tapered fore and aft to form the bow and stern is proposed. The taper at the ends of the centre hull must be sufficiently long so that the flow around the hull is similar to that on an actual trimaran hull; care must be taken to ensure that the flow does not separate from the hull too close to the bow. The model is to be setup so that the lift force and moment on the hull can be measured. The hull and experimental test rig are shown in Figure 6-4- 3.

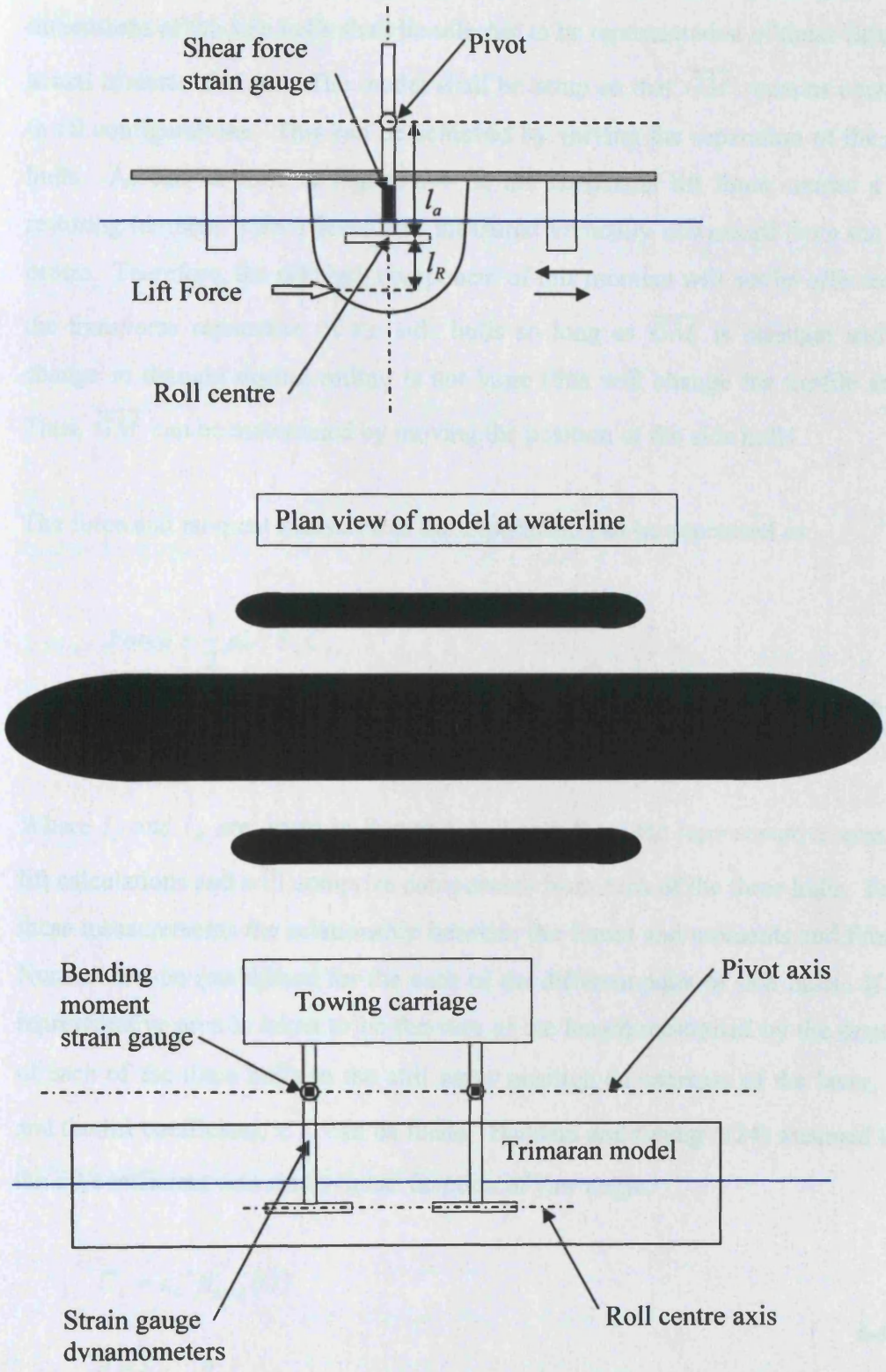

Figure 6-4- 3: Experimental setup for hull lift calculations

The same centre hull will be used for all of the experiments, with a range of different side hulls with varying length, draught, beam and displacement. The dimensions of the side hulls shall be selected to be representative of those fitted to actual trimaran designs. The model shall be setup so that $\overline{GM}$ remains constant in all configurations. This can be achieved by varying the separation of the side hulls. As can be seen in Figure 6-4- 3, the horizontal lift force creates a roll restoring moment, with a lever arm measured vertically downward from the roll centre. Therefore, the side hull component of this moment will not be effected by the transverse separation of the side hulls so long as $\overline{GM}$ is constant and the change in draught during rolling is not large (this will change the profile area). Thus, $\overline{GM}$ can be maintained by moving the position of the side hulls.

The force and moment measured in the experiment can be expressed as:-

$$Force = \frac{1}{2}\rho U^2 S_L C_L$$

$$Moment = Force(l_a + l_R) \qquad \textbf{6-4- 7}$$

Where l_a and l_R are given in Figure 6-4- 3 and S_L is the representative area for lift calculations and will comprise components from each of the three hulls. From these measurements the relationship between the forces and moments and Froude Number can be established for the each of the different pairs of side hulls. If the representative area is taken to be the sum of the length multiplied by the draught of each of the three hulls in the still water position an estimate of the lever, l_R, and the lift coefficient, C_L, can be made. Haddara and Leung (124) assumed that the lift coefficient was a non-linear function of yaw angle:-

$$C_L = x_6{}^n \beta_{H-L}(U)$$

$$n = 1,.....,n \qquad \textbf{6-4- 8}$$

Where $\beta_{H-L}(U)$ is a coefficient varying with forward speed which can be determined by fitting the measured lift coefficient values to equation 6-4-8. If this

expression proves to be unsuitable for a trimaran, another expression would need to be proposed. Haddara and Leung then related the steady yaw angle to the roll velocity using the following expression:-

$$x_6 = \frac{l_R \dot{x}_4}{U} \qquad \textbf{6-4-9}$$

Thus from equations 6-4-7, 6-4-8 and 6-4-9 an expression can be gained for the roll damping moment due to hull lift:-

$$Moment = \frac{1}{2}\rho U^{(2-n)} S_L l_R{}^{(1+n)} \beta_{H-L} \dot{x}_4{}^n \qquad \textbf{6-4-10}$$

If $n > 1$ this is a non-linear expression rather than the linear lift damping expression proposed by Ikeda, Himeno and Tanaka (114) (115).

Using equation 6-4-10, insight can be gained into the magnitude of the roll damping moment due to horizontal lift for a trimaran. One would expect long side hulls with large draughts to have a significant effect on this, however with smaller side hulls it may be that this moment is dominated by the centre hull component. In the theoretical method developed in Chapter 4 only the centre hull contribution was considered.

From these simple experiments it may be possible to propose a semi-empirical formula to predict the roll damping component due to hull lift for a trimaran with different side hull geometries.

Understanding the Contribution of Appendages

As pointed out in Section 6.2.1, accurate predictions of the lift of appendages will only be obtained if the time varying angle of attack and submergence of the appendage with respect to the free surface during rolling can be determined. Thus accurate appendage lift calculations will only be obtained in the time domain.

The work in the previous section on roll dynamics at zero speed focused on experiments that could be used to either validate or further develop theoretical methods that allowed the equation of motion to be solved in either the frequency or the time domain. This focus was necessary to allow the vast array of existing work based on solution of the equation of motion in the frequency domain to be built upon. However, as accurate appendage calculations require time domain theoretical methods it will not be possible to draw upon much of the existing work on predicting the roll damping of appendages. Instead, more complex methods involving Computational Fluid Dynamics (CFD) will be required. Model experiments will only give a limited insight due to the difficulty in maintaining the ship scale Reynolds number for the appendage on the model.

The purpose of the theoretical studies will be to understand how the time varying angle of attack and time varying immersion of an appendage affect the lift developed. This is to be achieved using modern CFD computer codes. The start point will be a detailed review of current CFD codes focusing, in particular, on their ability to accurately model the free surface, there are currently two approaches: Interface Tracking methods and Interface Capturing methods. In the former, the free surface is defined as a sharp interface, moving grids are fitted to the free surface and only the flow of the liquid is modelled. In the latter method, no distinct boundary is defined between the water and the air and grids exist with both liquid and gas filled regions. Either marker particles, or a transport equation for the void fraction of the liquid phase, are used to capture the free surface. For further enlightenment see Bertram (66) and (183). Once a suitable code has been identified the following investigations can be carried out.

1. Test the suitability of the CFD code by modelling a two-dimensional hydrofoil (with a two-dimensional grid) deeply submerged in water with a forward speed oscillating vertically up and down. The heave velocity and frequency should be chosen to be representative of a trimaran at roll resonance. The time varying lift can then be determined from the pressure distribution.
2. Repeat the above analysis introducing the free surface. Oscillate the hydrofoil below the free surface at different depths.

3. Create a three dimensional model of a hydrofoil moving with forward speed below a free surface which rolls around a fixed position. The location of both the roll centre and position of the hydrofoil with respect to the roll centre should be representative of an appendage fitted to a trimaran. The roll velocity and frequency should be chosen to be represent a trimaran at roll resonance.
4. The effect of the trimaran hull on the hydrofoil can be considered by modelling the side hull and if necessary the centre hull and repeating the above simulation. This is likely to require a very complex mesh geometry and may take some time to solve. However, it is mentioned here as in time it is hoped that such a simulation will be viable.

The CFD analysis will give an insight into how the lift varies during rolling. It may be possible to develop simple semi-empirical methods using this analysis that could be coded into time domain seakeeping codes.

6.4.3 Future Work

In the previous two sub sections a number of experiments, theoretical studies and analyses have been identified that will increase the understanding of the physics of trimaran rolling. Once these investigations have been completed the knowledge gained must be put to use to identify a route towards the eventual aim of developing new theoretical methods that accurately predict trimaran roll motion. This will not be an easy task, but the work in the thesis provides a good background for other researchers on the route down the long dark tunnel towards this eventual aim.

6.5 Conclusions

In this sixth chapter of the thesis, a process has been developed that, when followed through, will give a much improved understanding of trimaran roll motion. This process includes a series of model experiments using both simple trimaran sections and representative ship models. These experiments can be tailored so that they can be used, in addition, to develop and validate new semi-empirical roll damping theory.

There will be little progress in understanding and accurately predicting trimaran roll motion unless the work identified in this chapter is completed. Current prediction methods must be extensively validated before they can be accepted as representative for all trimarans, and new theories must be developed and validated that cover a wide range of side hull geometries and roll damping appendage configurations. Existing methods and simple adaptations of them have been shown (in Chapter 4) not to provide accurate roll motion predictions for trimarans.

Chapter (7) Conclusions

Chapter (7) Conclusions 398
7.1 General 399
7.2 Roll Motion Prediction 400
7.3 Disproving the Hypothesis 402
7.4 Testing the Assumptions Supporting the Hypothesis 404
7.5 Limitations 406
7.6 Recommendations for Future Work 408
7.7 Concluding Comments 410

7.1 General

When embarking on this research thesis it was thought that the science of trimaran roll motion prediction was mature and hence the focus of the research would be on further characterisation of trimaran rolling and on the reduction of roll motion. However, the literature review (contained in Chapters 1 to 3) shows that roll motion prediction is not an exact science for monohulls let alone for trimarans. In fact, nearly all the researchers who reported on trimaran roll motions had used methods adapted from those commonly applied to monohulls.

As the thesis unfolds, it is shown that the methods accepted for trimaran roll motion prediction to date (by previous researchers) are lacking and many of the assumptions that underpin them are not appropriate for trimarans. The primary cause of this difference is believed to be due to the presence of considerable flare above the still water position on the side hulls. This flare is necessary in order to achieve satisfactory large angle stability as discussed in Chapter 1. As the research in this thesis is only based on theoretical and experimental research using a single trimaran which has sidehulls with flare above the still water position, general conclusions for all trimarans cannot be drawn at this stage.

The key conclusions of this work, based on the research conducted on this single trimaran hull, are discussed in the following sub sections.

7.2 Roll Motion Prediction

Monohulls

A thorough review of the literature showed that the preference of most researchers is to use Potential Flow methods to solve a linear equation of motion with constant coefficients for each of the six degrees of freedom: - surge, sway, heave, roll, pitch and yaw. As Potential Flow theory neglects viscosity in the fluid and cannot account for the contribution of appendages or lift generated by the hull during rolling at forward speed it cannot be used in isolation to obtain adequate predictions of roll motion. The Potential Flow roll motion solution is improved by adopting one of two methods:-

- The magnitude of the roll damping is determined by using semi-empirical theory, generally using the methods developed by either Schmitke (81) or Ikeda and others at the University of Osaka, see Himeno (80).

- The roll damping is measured in a model experiment where the roll damping term in the equation of motion can be represented using both linear and non-linear coefficients.

In either of these methods non-linear terms are converted to an equivalent linear format to allow the equation of motion to be solved using linear Potential Flow methods. A linear equation of motion can be solved rapidly in the frequency domain whereas a non-linear equation must be solved in the time domain which requires considerably greater computational effort. If a non-linear equation is used, all existing formulations still assume that the relationship between the wave forcing and roll damping is linear and thus any non-linear roll damping terms have to be converted to an equivalent linear form. Roll motion results using the more complex non-linear theory have not been shown to be vastly superior to results obtained using the more simple linear theory, except when the hull shape varies considerably above the still water position or for motion predictions in

large amplitude waves. Therefore, linear methods are still used in preference to non-linear methods.

Trimarans

Although there have been many papers published which discuss theoretical prediction of the seakeeping performance of trimarans, few researchers have conducted detailed investigations into trimaran roll motion. Of those who have investigated roll motions, only a few discuss the prediction of roll damping in any detail. All the published research on theoretical seakeeping predictions use Potential Flow methods with either a linear or a quasi non-linear equation of motion (for the quasi-non-linear method particular terms in the equation of motion are made non-linear). The non-linear methods require solution in the time domain and have identical limitations to those discussed for monohull ships above.

The published papers, which include details of trimaran roll predictions, rely on roll decay coefficients which can be obtained from either model experiments or by adapting semi-empirical methods developed for monohulls. These damping coefficients have been used with both linear and non-linear formulations of the equation of motion adapted to allow solution using Potential Flow methods. The more complex non-linear analysis was shown to be no more accurate than the linear analysis when theoretical predictions were compared with model experiment results in regular waves (although there are very few published experimental results to compare with). Therefore, the conclusion was drawn that trimaran motion in regular waves could be predicted to an acceptable level using the monohull best practice approach – solving a linear equation of motion in frequency domain using Potential Flow methods. The first part of the research in this thesis set out to prove this conclusion by testing the following hypothesis:-

> *Accurate trimaran roll motion predictions can be obtained using linear Potential Flow Seakeeping theory with the roll damping term either obtained from a roll decay experiment or augmented with empirically based theoretical roll damping components developed for monohulls.*

7.3 Disproving the Hypothesis

Having established the hypothesis, a package of research was conducted to test the validity of this hypothesis. This involved the comparison of theoretical predictions of roll motion which supported the hypothesis with seakeeping model experiment results in regular waves with a small number of different wave incident angles. As previously mentioned, all the model experiments were completed using one single trimaran model. A Linear Potential Flow seakeeping code which solves the equation of motion in the frequency domain developed at University College London (TRISKP) was used by the author to predict roll motion. The code was adapted so that roll motion could be predicted using either measured decay coefficients or a suitable range of semi-empirical roll damping prediction formulae which included, in a simplistic way, the contribution of roll damping appendages. This research disproved the hypothesis for the reasons set out in the following important conclusions:-

- The highest roll response measured in the experiments occurs at the wave excitation frequency closest to roll resonance. Theoretical roll motion predictions in the region of this excitation frequency are not well matched to the experimental results. This occurred regardless of the method used to obtain roll damping coefficients although, of the two methods, the semi-empirical approach produced the least accurate roll motion predictions which were significantly under damped, in particular at low forward speed. When the experimentally derived roll damping coefficients were used in the theoretical prediction there was no observable trend, the theoretical roll motion predictions were not consistently greater or less than the experimental results.

- When roll damping appendages were fitted to the model, whose purpose is to reduce roll motions in the region of resonance, the accuracy of theoretical predictions was not improved, sometimes too much extra damping was predicted (giving an over damped theoretical result) and at other times too little extra damping was predicted. The theoretical

appendage damping predictions which were used as part of the semi-empirical roll damping method were found to be very sensitive to assumptions about lift losses and enhancements. Due to the simplistic method used to predict the lift of these appendages these effects could not be properly accounted for. Particular difficulties were encountered for appendages that during one roll cycle would become close to, or pass through, the free surface.

- Theoretically derived roll responses at high excitation frequencies above the resonant region were always less than the response measured in the seakeeping experiments. Recalling the theory of a dynamic spring – mass – damper system this indicates that any or all of the following have not been correctly predicted: - the roll inertia, the roll added inertia or roll stiffness.

- Thus, the simple conclusion is that the linear frequency domain method does not yield accurate trimaran roll motion predictions for the particular trimaran under investigation.

During the seakeeping model experiments, at wave encounter frequencies close to resonance, one of the side hulls of the trimaran could come completely out of the water. Any appendages attached to the side hull would then either partially emerge or be very close to the water surface. In the development of a theoretical method to predict the damping contribution of the appendages it was shown that free surface lift losses were significant. Thus, the lift of any appendage attached to a side hull which is not deeply immersed will vary significantly throughout the roll cycle. Furthermore, if a side hull is coming out of the water the roll stiffness will vary during one roll cycle along with the total roll inertia and added inertia of the three hulls. This variation will be further affected by the haunches and any flare on the side hulls. These experimental observations support the conclusion that the linear frequency domain method cannot be used to accurately predict trimaran roll motion. In addition, they suggest that accurate predictions will require the solution of the equation of motion in the time domain.

7.4 Testing the Assumptions Supporting the Hypothesis

Having shown that the fundamental hypothesis which underpins the work of many previous researchers who investigated trimaran rolling was false, the subsequent parts of this thesis aimed to understand why this was the case. The start point was to re-analyse the existing experimental results, both free roll decay and seakeeping in regular waves, coupled with focused theoretical investigations in order that the assumptions behind the hypothesis could be tested in turn. This is not a complete analysis which fully explores the topic; more in depth studies are required and these are discussed in more detail in the next section which proposes future work. The first set of investigations focused on the measurement of roll damping coefficients in free roll decay experiments. Once again, using the results of model experiments on a single trimaran hullform, the following important conclusions were reached:-

- When comparing the two separate series of free roll decay experiments on the same trimaran model (one series from model experiments in 2002 and the other from experiments in 2004), whilst the roll decrements were repeatable, the roll damping coefficients varied considerably. This trend was observed regardless of whether a quadratic or cubic roll damping model was assumed.

- For the trimaran in question, the assumption that the roll decay can be modelled by an uncoupled (partially non-linear) equation of roll motion with constant coefficients was shown to be invalid.

Firstly, this conclusion was reached after discovering that simulations of the roll decay with a time varying stiffness term could replicate strange behaviour observed during the analysis of the experiment results. This was believed to be the reason why stable roll damping coefficients could not be obtained. The only logical reason why the stiffness term could be time variant and non-linear with

respect to the roll angle was if the waterplane area of the model was varying significantly during one roll cycle. As the trimaran model was fitted with haunches (above water flare in the side hulls) and the centre hull was wall sided above the still water line over the mid region, significant changes in waterplane area during roll motion could only occur if the waterplane area of the side hulls was changing significantly due to heaving, pitching or a combination of heaving and pitching. If this was the case the assumption of uncoupled roll during roll decay would be invalid. This was investigated by looking at the heave, pitch and roll motions recorded in the 2004 roll decay experiments. This did in fact show that roll motion induced heave motion and that this heave motion did not decay away. Fourier analysis showed it to comprise of a number of frequency components including the roll frequency and twice the roll frequency. Due to the location of the side hulls this heave motion also induced pitch motion. Therefore the assumption that roll decay can be modelled by an uncoupled roll equation was shown to be incorrect.

The second series of investigations focused on the assumptions underpinning roll motion predictions. This was explored through analysis of the results of the seakeeping model experiments in regular beam waves. The results of this work led to the following conclusion:-

- Linear wave theory, where a regular sinusoidal wave of constant amplitude and frequency leads to output motions which are also regular and sinusoidal with constant amplitude and frequency, is not valid for heave motion and questionable for roll motion. Strong coupling between heave and roll was shown to occur at excitation frequencies close to roll resonance and at these frequencies the heave motion was irregular (comprising of two distinct frequency components).

It was postulated that, due to the haunches and flare on the side hulls, roll motion induces heave motion and thus the assumption of linear wave theory breaks down. This then renders analysis based on the traditional linear wave theory inappropriate.

7.5 Limitations

As with all things in life, there is a limit to the time one can spend pursuing any particular topic extensively. Therefore, it is important to understand, and in particular to clarify, the limitations of one's work. This allows future researchers to understand the context of the work and makes it easier for them to pick up the baton and move the state of the art of the topic further forward.

The principal limitations of this work are listed in the following bullet points:-

- All the research conducted in this thesis, both experimental and theoretical, is carried out on a single trimaran hull configuration. The extent to which the conclusions of this work can be generalised for all trimarans is not known.

- The model experiments used to understand the physics of trimaran roll motion were not developed specifically for that purpose. When the experiments were devised it was incorrectly thought that the physics behind the problem was understood well enough. A series of experiments have been developed in Chapter 6 which are designed for this purpose. The completion of these studies is left to other researchers whom it is hoped will prove the conclusions set out in this thesis apply to all trimarans fitted with haunches or flare on the side hulls.

- The work in Chapter 4 on the theoretical prediction of the lift of trimaran roll damping appendages is very basic indeed. As the thesis unfolded it was asserted that only solution in the time domain would allow accurate lift predictions due to the considerable vertical displacement of the appendages during one roll cycle. As these appendages (and the side hull to which they are attached) have the propensity to emerge from the water at excitation frequencies near resonance any prediction method must also model the free surface and side hull. Such theoretical modelling is

currently at the cutting edge of three dimensional computational fluid dynamics.

- In Chapter 4, the author attempted to develop a semi-empirical theory for the prediction of roll damping components for trimarans. This theory was developed from existing monohull methods with only one new term specific to a trimaran (the roll damping term due to side hull heave). The theory was not extensively validated by model experiments, nor was it developed using the results of simple experiments that clarify the physics. Any further attempt at developing a theory should be supported by experimentation that can be used both to illuminate the physics of the problem as well as being suitable for use in support of validation of new methods. Chapter 6 set out a series of experiments which should allow the physics to be explored more fully.

7.6 Recommendations for Future Work

Future work should focus initially on understanding the physics of trimaran roll motion. This work should start by considering a trimaran rolling at zero speed without roll damping appendages fitted. Research should be conducted in order to understand:-

a) The coupling between roll and heave, including the effect of side hull flare and haunches.
b) The influence of the side hulls on roll motion. Studies should be carried out with different shape side hulls and for various side hull separations.
c) The influence of the side hulls on roll damping. Once again this should consider the effect of side hull shape and separation.

Once the physics of trimaran rolling at zero speed have been illuminated, a suitable formulation for the equation of motion of a trimaran should be proposed and then validated using model experiment results on simple trimaran hull shapes. A package of work whose purpose is to address these three issues is identified in Chapter 6.

Having developed a suitable formulation for the equation of motion for a trimaran, this equation should then form the basis for theoretical seakeeping prediction methods which should solve the equation in the time domain. It is suggested that this work starts by modelling a simplified non-linear roll and heave coupled equation of motion in the time domain.

Once motions at zero speed are fully understood the focus can then move to accurate motion predictions with forward speed. There are two key themes to address:-

a) The influence of the side hulls on both roll motion and roll damping. The lift force developed by the side hulls during rolling at forward speed should be the primary focus of this work.

b) The contribution of roll damping appendages. At forward speed the lift damping of the appendage will provide a significant proportion of roll damping, therefore accurate, validated, methods are required to predict the lift generated by the appendage. Computational methods using the Reynolds Averaged Navier Stokes Equations in the time domain are thought to be the best approach.

Some initial thoughts on research required on these topics were given in Chapter 6. The results of all this work should be bought together to support the development and validation of theoretical methods for determining the roll motion applicable to all trimarans. This may require a series of semi-empirical methods to account for some of the unknowns in the equation of motion. To achieve this, a large number of model experiments coupled with focused theoretical studies are required. Thus there is still a considerable amount of work to be completed before the goal of accurate rapid prediction of trimaran motion can be achieved.

7.7 Concluding Comments

It is easy to convince ourselves when analysing a new hullform that existing theories can be used to adequately predict the response of the new hullform. If predictions for the new hullform using existing theory correlate reasonable well to model experiment results, it is even easier to convince ourselves that we understand the physics of the problem. However, until a great number of the new hull type have been analysed, this confidence may prove to be unfounded. The careful analysis in this thesis has shown that the physics of trimaran rolling are not well understood and that existing methods cannot be used to determine the nature of trimaran rolling.

This thesis has highlighted that, based on results from experiments on a single trimaran hull fitted with haunches and flare on the side hulls, heave motion will be induced due to the change of buoyancy of the side hulls during rolling. For most trimarans, due to the location of the side hulls, this heave motion will further induce pitch motion. This coupling was shown to cause heave motion comprising more than one frequency component. Hence this invalidates the principal assumption of linear regular wave theory that an input sinusoidal wave will cause output sinusoidal motion in all degrees of freedom. As this coupling is caused by a time varying phenomenon accurate trimaran motion prediction will only be possible in the time domain using a non-linear equation of motion.

Furthermore, it has been identified that, using adaptations of current monohull methods, trimaran roll damping cannot be predicted accurately. Difficulties arise in predicting the contribution of the side hulls and that of appendages. These problems are best addressed using time domain methods.

If the postulation that heave and roll couple for trimarans with flare and haunches on the side hulls is proved to be true for all trimarans, care must be taken to ensure that the natural frequencies in these two motions are not coincident or nearly coincident, otherwise synchronous roll and heave motion will occur at similar

frequencies and energy may be swapped between the two motions leading to auto-parametric resonance.

References

1. Pattison, D. R. and Zhang, J-W.
Trimaran Ships.
Transactions of the Royal Institution of Naval Architects, Volume 136, 1994.

2. Irens, N.
Notes and Observations Resulting from Practical Experience Gained in the Operation of Small Sized Power Trimarans (1988-2004).
RINA International Conference on the Design and Operation of Trimaran Ships, 29th - 30th April 2004, London, UK, ISBN 0 903055 99 6.

3. Bastisch, C. and Peters, T.
Advanced Technology Frigate - Mk II.
MSc in Naval Architecture, Ship Design Exercise Report, Mechanical Engineering Department, University College London, 1990.

4. Bastisch, C.
An Advanced Technology ASW Frigate for the Year 2000.
RINA International Symposium on Affordable Warships, 1992.

5. Summers, A. B. and Eddison, J. F. P.
Future ASW Frigate Concept Study of a Trimaran Variant.
Procedings of IMDEX 1995, International Maritime Defence Exhibition and Conference, Greenwich, London, March 1995.

6. Andrews, D. J. and Hall, J. H.
The Trimaran Frigate - Recent Research and Potential for the Next Generation.
Procedings of IMDEX 1995, International Maritime Defence Exhibition and Conference, Greenwich, London, March 1995.

7. Andrews, D. J. and Zhang, J-W.
Considerations in the Design of a Trimaran Frigate.
RINA International Conference on High Speed Vessels for Transport and Defence, 1995.

8. Zhang, J-W. and Andrews, D. J.
Roll Damping Characteristics of a Trimaran Displacement Ship.
International Shipbuilding Progress, Volume 46, No 448, 1999.

9. Zhang, J-W. and van Griethuysen, W. J.
Trimaran Design.
Naval Platform Technology Seminar, Singapore, 1998.

10. Zhang, J-W.
Design and Hydrodynamic Performance of Trimaran Displacement Ships.
A Thesis Submitted for a Degree of Doctor of Philosophy, Department of Mechanical Engineering, University College London, 1997.

11. Chan, H. S., Incecik, A., Hall, J. H., and Bate, J.
On the Dynamic Motion Behaviour of Trimaran Ships.
IMDC '97, 6th Intl Marine Design Conference, 23-25 June 1997, Newcastle upon Tyne, ISBN 0-9518806-7.

12. Chan, H. S., Incecik, A., and Ireland, N.
Seaworthiness Assessment of a Trimaran Ship.
RINA International Conference on High Speed Craft Motions and Manoeuvrability, London, 1998.

13. Vassilos, D., Helvacioglou, I., and Jasionowski, A.
An Investigation of the Stability and Survivability of Trimarans.
STAB 2000, 7th International Conference on the Stability of Ships and Ocean Vehicles, 7-11 February 2000, Launceston, Tasmania, ISBN 0 9585990 4.

14. Bingham, A. E., Hampshire, J. K., Miao, S. H., and Temarel, P.
Motions and Loads of a Trimaran Travelling in Regular Waves.
FAST 2001, 6th International Conference on Fast Sea Transportation, 4-6 Sept 2001, Southampton, ISBN 0 903055 70 8.

15. Hampshire, J., Erskine, S., Halliday, N., and Arason, M.
Trimaran Structural Design and Assessment
RINA International Conference on the Design and Operation of Trimaran Ships, 29th - 30th April 2004, London, UK.ISBN 0 903055 99 6.

16. Cheng, F., Mayoss, C., and Blanchard, T.
The Development of Trimaran Rules
RINA International Conference on the Design and Operation of Trimaran Ships, 29th - 30th April 2004, London, UK.ISBN 0 903055 99 6.

17. Douglas, A. and Dodkins, A.
The Structural Design of RV Triton.
RINA International Conference on R V 'TRITON': Trimaran Demonstrator, 18th and 19th April 2000, Southampton UK, ISBN 0 903055 58 9.

18. Helgesen, P.
Classification of RV Triton.
RINA International Conference on R V 'TRITON': Trimaran Demonstrator, 18th and 19th April 2000, Southampton UK, ISBN 0 903055 58 9.

19. Pattison, N. and Searle, G.
The Design and Construction of RV Triton - The Trimaran Demonstrator.
RINA International Conference on R V 'TRITON': Trimaran Demonstrator, 18th and 19th April 2000, Southampton UK, ISBN 0 903055 58 9.

20. Scrace, R. J.
Model Experiments to Investigate the Hydrodynamic Performance of RV Triton.
RINA International Conference on R V 'TRITON': Trimaran Demonstrator, 18th and 19th April 2000, Southampton UK, ISBN 0 903055 58 9.

21. Short, R.
R V Triton - Project Outline, Aims and Objectives the Integrated Project.
RINA International Conference on R V 'TRITON': Trimaran Demonstrator, 18th and 19th April 2000, Southampton UK, ISBN 0 903055 58 9.

22. Simmons, B., Russel, P., and Carlisle, C.
RV Triton: The Total Evaluation of a Novel Hullform.
RINA International Conference on R V 'TRITON': Trimaran Demonstrator, 18th and 19th April 2000, Southampton UK, ISBN 0 903055 58 9.

23. Renilson, M. R., Scrace, R. J., Johnson, M. C., and Richardsen, C.
Trials to Measure the Hydrodynamic Performance of RV Triton.
RINA International Conference on the Design and Operation of Trimaran Ships, 29th - 30th April 2004, London, UK, ISBN 0 903055 99 6.

24. Short, R. J. and Burgess, J.
Triton - The Operators View.
RINA International Conference on the Design and Operation of Trimaran Ships, 29th - 30th April 2004, London, UK, ISBN 0 903055 99 6.

25. Scott, R.
UK Studies Trimaran Hull for Future ASW Frigate.
Jane's Navy International, March/April Edition 1995.

26. Galtiev, B.
The Highly Streamlined Monohull with Lateral Wings.
Carenes-Le Magazine due Bassin D'Essais des Carenes, Volume No 2, December 1994.

27.
Performance of Fast Multi Hull Vessels: Model Tests for the 'Telakka 2000' R and D Project.
Maritime Research News, Vol.8, Maritime Institute of Finland, 1994.

28. Gee, N., Dudson, E., Marchant, A., and Steiger, H.
The Pentamaran, A New Concept for Fast Freight and Car Ferry Applications.
13th Fast Ferry International Conference, 25-27 Feb 1997, Singapore.

29. Chacon, J. R., Ollero, P., Gee, N., and Dudson, E.
The Pentamaran Ro-Ro: The Solution for Modal Shift from Land to Sea.
RINA International Conference on the Design and Operation of Trimaran Ships, 29th - 30th April 2004, London, UK, ISBN 0 903055 99 6.

30. Roy, J., Bonafoux, J., Kimber, A., and Dand, I.
A Technical Comparison Between Monohull and Pentamaran Platforms for High Speed Operation and Future Naval Warships.
RINA International Conference on the Design and Operation of Trimaran Ships, 29th - 30th April 2004, London, UK, ISBN 0 903055 99 6.

31. Armstrong, N. A.
Coming Soon to a Port Near You - The 126 Metre Austal Trimaran.
RINA International Conference on the Design and Operation of Trimaran Ships, 29th - 30th April 2004, London, UK, ISBN 0 903055 99 6.

32. Tulk, R. J. and Quigley, S. G.
Development of the North West Bay Ships Trimaran.
RINA International Conference on the Design and Operation of Trimaran Ships, 29th - 30th April 2004, London, UK, ISBN 0 903055 99 6.

33.
The DAT Concept (Dynamically Assisted Trimaran)
Ship and Boat International, Editor Cheryl Saponia, Published by the Royal Institution of Naval Architects, June/July 2003 Edition.

34. Barone, R., Begovic, E., and Bertorello, C.
Multi-attribute Procedure for Basic Design of Trimaran Fast Ferries.
NAV 2003, International Conference on Ship and Shipping Research, Palermo, Italy, 24-27 June 2003.

35. Brizzolara, S., Capasso, M., Ferrando, M., Podenzana Bonvino, C., Cardo, A., and Francescutto, A.
Trimaran hull design for fast ferry applications
NAV 2003, International Conference on Ship and Shipping Research, Palermo, Italy, 24-27 June 2003.

36. Francescutto, A.
On the Roll Motion of a Trimaran in Beam Waves.
ISOPE 2001 - The Proceedings of The 11th International Offshore and Polar Engineering Conference - CD-ROM, Volume 3, Stavanger, 2001.

37. Francescutto, A. and Cardo, A.
Dynamic Stability and Roll Motion Modelling of Multihulls.
FAST 2001, 6th International Conference on Fast Sea Transportation, 4-6 Sept 2001, Southampton, UK, 2001.

38. Begovic, E., Bertorello, C., and Boccadamo, G.
Seakeeping Assessment of Trimaran Hulls.
FAST 2003, 7th International Conference on Fast Sea Transportation, 7-10 Oct 2003, Ischia, Italy, 2003.

39. Coppola, T., Mandarino, M., and Simeonw, F.
Trimaran Structural Analysis.
NAV 2003, International Conference on Ship and Shipping Research, Palermo, Italy, 24-27 June 2003.

40. Li, P-y., Feng, T-c., and Qiu, Y-m.
Investigation of Trimaran Roll Motion Characteristics.
Shipbuilding of China, Vol 44, No 1, March 2003.

41. Kang, K. J., Lee, C. J., Kim, S. Y., and Cho, Y. J.
Design and Hydrodynamic Performance of a Frigate Type Trimaran.
RINA International Conference on the Design and Operation of Trimaran Ships, 29th - 30th April 2004, London, UK, ISBN 0 903055 99 6.

42. Hall, J. H.
Investigations into the Wetted Surface Area of Slender Hulls.
DERA Haslar Report for the UK Ministry of Defence, 1995.

43. Greig, A. R. and Bucknall, R. W. G.
Marine Engineering the Trimaran Hull Form: Opportunities and Constraints.
Transactions of the Institution of Marine Engineers, Volume 110, Part 3, 1998, ISSN 0309-3948.

44. Bricknell, D. and Carlisle, C.
Power and Propulsion Systems for the New Naval Trimarans.
RINA International Conference on the Design and Operation of Trimaran Ships, 29th - 30th April 2004, London, UK, ISBN 0 903055 99 6.

45. Skarda, R. K. and Walker, M.
Merits of the Monohull and Trimaran Against the Requirement for Future Surface Combatant.
RINA International Conference on the Design and Operation of Trimaran Ships, 29th - 30th April 2004, London, UK, ISBN 0 903055 99 6.

46. Greig, A. R., Bucknall, R. W. G., Grafton, T. J., and Rusling, S. C.
A High Speed Trimaran Corvette.
NATO Applied Vehicle Technology Panel (AVT) Symposium on Novel and Emerging Vehicle and Vehicle Technology Concepts, Brussels, Belgium, 7-9 April, 2003.

47. Brizzolara, S. and Grossi, L.
Design Aspects and Applications of Deep-V Hull Forms to High Speed Crafts.
Proceedings of IMDEX 1997, International Maritime Defence Exhibition and Conference, Greenwich, London, October 1997.

48. Sarioz, K. and Narli, E.
Seakeeping Performance of High Speed Warship Hullforms: Deep Vee Versus Round Bilge.
RINA International Conference on High Speed Craft Motions & Manoeuvrability, 20 Feb 1998, London, U.K.

49. Andrews, D. J. and Zhang, J-W.
A Novel Design Solution to Stability - The Trimaran Ship.
RINA International Conference on Watertight Integrity and Ship Survivability, London, November 1995.

50.
2000 HSC Code: International Code of Safety for High-Speed Craft 2000.
International Maritime Organization, 4 Albert Embankment, London, SE1 7SR, ISBN 92-801-5122-3.

51.
Stability Standards for Surface Ships
Ministry of Defence, Naval Engineering Standard, NES 109, Issue 4, 1999.

52. Jordan, D. W. and Smith, P.
Nonlinear Ordinary Differential Equations: An Introduction to Dynamical Systems.
Oxford University Press, Third Edition, 1999, Reprinted 2004.ISBN 0 19 856562 3.

53. Ribeiro e Silva, S., Santos, T. A., and Guedes Soares, C
Parametrically Excited Roll in Regular and Irregular Head Seas.
International Shipbuilding Progress, Volume 52, No 1, 2005.

54. Hashimoto, H. and Umeda, N.
Nonlinear Analysis of Parametric Rolling in Longitudinal and Quartering Seas with Realistic Modelling of Roll-Restoring Moment.
Journal of Marine Science and Technology, Volume 9, No 3, 2004.

55. Hua, J.
A Representation of a Ships GM Variation in Waves by the Volterra System.
Department of Vehicle Technology, Naval Architecture Report 9549, Royal Institute of Technology, Stockholm, 1995.

56. Roberts, J. B.
Effect of Parametric Excitation on Ship Rolling Motion in Random Waves.
Journal of Ship Research, Volume 26, No 4, 1982.

57. Hamamoto, M. and Munif, A.
A Mathematical Model of Ship Motions Leading to Capsize in Astern Waves.
Contemporary Ideas on Ship Stability, Edited by D.Vassalos et al, Published by Elsevier Science Ltd, Oxford, UK; 2000; ISBN 0-08-043652-8.

58. Hua, J-b.
Fast Simulation of Nonlinear GM - Variation of a Ship in Irregular Waves.
Journal of Ship Mechanics, Volume 4, No 3, June 2000.

59. Francescutto, A. and Bulian, G.
Nonlinear and Stochastic Aspects of Parametric Rolling Modelling.
Proceedings of the 6th International Ship Stability Workshop, Webb Institute, October 2002.

60. Francescutto, A., Bulian, G., and Lugni, C.
Nonlinear and Stochastic Aspects of Parametric Rolling Modelling.
Marine Technology, Volume 41, No 2, April 2004.

61. Francescutto, A.
An Experimental Investigation of Parametric Rolling in Head Waves.
International Offshore & Arctic Engineering Conference, OMAE 2000, New Orleans, Louisiana, USA, February 14-17 2000.

62. Levadou, M. and Gaillarde, G.
Operational Guidance to Avoid Parametric Roll.
RINA International Conference on Design and Operation of Container Ships; 23-24 April, London, UK, 2003.

63. France, W., Levadou, M, Treakle, T., Paulling, J., Michel, R., and Moore, C.
An Investigation of Head-Sea Parametric Rolling and its Influence on Container Lashing Systems.
Marine Technology, Volume 40, No 1, 2003.

64. Lloyd, A. R. J. M.
Seakeeping: Ship Behaviour in Rough Weather.
Ellis Horwood Limited, First Edition, IBSN 0-7458-0230-3, 1989.

65. Newman, J. N.
Marine Hydrodynamics.
The MIT Press, Cambridge, Massachusetts, 1977, ISBN 0-262-14026-8.

66. Bertram, V.
Practical Ship Hydrodynamics.
Butterworth-Heinemann, ISBN 0 7506 4851 1, 2000.

67. Jensen, J. J., Mansour, A. E., and Olsen, A. S.
Estimation of Ship Motions Using Closed-Form Expressions.
Ocean Engineering, Volume 31, 2004.

68. Journee, J.
Quick Strip Theory Calculations in Ship Design.
PRADS 92, International Symposium on Practical Design of Ships and Mobile Units, 1992.

69. Bruzzone, D., Gualeni, P., and Sebastiani, L.
Different Three Dimensional Formulations for Evaluating Forward Speed Effects in Seakeeping Calculations of High Speed Hulls.
FAST 2001, 6th International Conference on Fast Sea Transportation, 4-6 Sept 2001, Southampton, ISBN 0 903055 70 8.

70. Stredulinsky, D. C., Pegg, N. G., and Gilroy, L. E.
Motion, Load and Structural Response Predictions and Measurement on CFAV Quest.
Transactions of the Royal Institution of Naval Architects, Volume 141, 1999.

71. Stredulinsky, D. C., Pegg, N. G., and Gilroy, L. E.
Motion and Wave Load Predictions and Measurements on HMCS Nipigon.
Transactions of the Royal Institution of Naval Architects, Volume 142, 2000.

72. Kent, J. S.
Comparison of Methods for Estimating the Fatigue Life of a Naval Frigate.
3rd International ASRANet Colloquium, Glasgow, July 2006.

73. Kring, D., Huang, Y-F., Sclavounos, P., Vada, T., and Braathen, A.
Nonlinear Ship Motions and Wave Induced Loads by a Rankine Method.
21st Symposium on Naval Hydrodynamics, 24-28 June 1996, Trondheim, Norway.

74. Nakos, D. and Sclavounos, P.
Ship Motions by a Three Dimensional Rankine Panel Method.
18th Symposium on Naval Hydrodynamics, 1991.

75. Pastoor, W., van't Veer, R., and Harmsen, E.
Seakeeping Behaviour of a Frigate-Type Trimaran.
RINA International Conference on the Design and Operation of Trimaran Ships, 29th - 30th April 2004, London, UK, ISBN 0 903055 99 6.

76. Kim, Y. and Weems, K. M.
Motion Responses of High Speed Vessels in Regular Random Waves.
RINA International Conference on the Hydrodynamics of High Speed Craft: Wake Wash and Motions Control, London, 2000.

77. Lin, W-M. and Yue, D.
Numerical Solutions for Large-Amplitude Ship Motions in the Time Domain.
18th Symposium on Naval Hydrodynamics, 1991.

78. Salvesen, N. and Lin, W-M.
Extreme-Sea Response Simulation for Ship Design.
SAIC, Science and Technology Trends II, 1998.

79. Froude, W.
The Papers of William Froude.
The Institution of Naval Architects, 1955.

80. Himeno, Y.
Prediction of Ship Roll Damping - State of the Art.
Report Number 239, Department of Naval Architecture and Marine Engineering, University of Michigan, Ann Arbor, Michigan, 1981.

81. Schmitke, R. T.
Ship Sway, Roll and Yaw Motions in Oblique Seas.
Transactions of the Society of Naval Architects and Marine Engineers, Volume 87, 1978.

82. Kat, J. O.
The Numerical Modelling of Ship Motions and Capsizing in Severe Seas.
Journal of Ship Research, Volume 34, No 4, December 1990.

83. Bass, D. W. and Haddara, M. R.
Non-linear Models of Ship Roll Damping.
International Shipbuilding Progress, Volume 35, No 401, 1998.

84. Haddara, M. R.
On the Stability of Ship Motion in Regular and Oblique Waves.
International Shipbuilding Progress, Volume 18, No 207, 1971.

85. Mathisen, J. B. and Price, W. G.
Estimation of Ship Roll Damping Coefficients.
Transactions of the Royal Institution of Naval Architects, Volume 126, 1984.

86. Haddara, M. R. and Bennett, P.
A Study of the Angle Dependence of Roll Damping Moment.
Ocean Engineering, Volume 16, No 4, 1989.

87. Haddara, M. R. and Bass, D. W.
On the Form of Roll Damping Moment for Small Fishing Vessels.
Ocean Engineering, Volume 17, No 6, 1990.

88. Spouge, J. R.
Non-linear Roll Damping Measurements.
Transactions of the Royal Institution of Naval Architects, Volume 132, 1990.

89. Renyuan, D.
An Improvement in the Analysis of Roll Decay Tests.
Selected Papers of the Chinese Society of Naval Architecture and Marine Engineering, No 2, 1986.

90. Roberts, J. B.
Estimation of Nonlinear Ship Roll Damping from Free Decay Data.
Journal of Ship Research, Volume 29, No 2, 1985.

91. Chan, H. S. Y, Xu, Z., and Huang, W. L.
Estimation of Nonlinear Damping Coefficients from Large-amplitude Ship Rolling Motions.
Applied Ocean Research, Volume 17, No 4, August 1995.

92. Francescutto, A., Nabergoj, R., and Hsiu, T. C.
Nonlinear Ship Rolling: Identification of Damping Model.
Tecnica Italiana, Volume 3, September 1991.

93. Bulian, G.
Estimation of Nonlinear Roll Decay Parameters Using an Analytical Approximate Solution of the Decay Time History.
International Shipbuilding Progress, Volume 51, No 1, 2004.

94. Cotton, B. and Spyrou, K. J.
An Experimental Study of Nonlinear Behaviour in Roll and Capsize.
International Shipbuilding Progress, Volume 48, No 1, April 2001.

95. Spouge, J. R.
Non-linear Analysis of Large Amplitude Rolling Experiments.
International Shipbuilding Progress, Volume 25, No 403, 1988.

96. Bailey, P. A., Hudson, D. A., Price, W. G., and Temarel, P.
Comparisons Between Theory and Experiment in a Seakeeping Validation Study.
Transactions of the Royal Institution of Naval Architects, Volume 144, 2002.

97. Hudson, D. A., Price, W. G., and Temarel, P.
Seakeeping Performance of High Speed Displacement Craft.
FAST 95, 3rd International Conference on Fast Sea Transportation, 25-27 Sept 1995, Lubeck-Travemunde, Germany, 1995.

98. Maury, C., Delhommeau, G., Ba, M., Boin, J. P., and Guilbaud, M.
Comparison Between Numerical Computations and Experiments for Seakeeping on Ship Models with Forward Speed.
Journal of Ship Research, Volume 47, No 4, 2003.

99. Takaki, M., Lin, X., Gu, X., and Mori, H.
Theoretical Prediction of Seakeeping Qualities of High Speed Vessels.
FAST 95, 3rd International Conference on Fast Sea Transportation, 25-27 Sept 1995, Lubeck-Travemunde, Germany, 1995.

100. Ballard, E. J., Hudson, D. A., Temarel, P., and Du, S. X.
Motions of Mono- and Multi-hulled Vessels in Regular Waves Using a Partly Non-linear Time Domain Method.
FAST 2001, 6th International Conference on Fast Sea Transportation, 4-6 Sept 2001, Southampton, UK, 2001.

101. Fan, Y. T. and Wilson, P. A.
Time-Domain Non-Linear Strip Theory for Ship Motions
Transactions of the Royal Institution of Naval Architects, Volume 146, 2004.

102. Vassilos, D., Jasionowski, A., and Cichowicz, J.
Issues Related to the Weather Criterion.
International Shipbuilding Progress, Volume 50, No 2/3, 2004.

103. Ballard, E. J., Hudson, D. A., Price, W. G., and Temarel, P.
Time Domain Simulation of Symmetric Ship Motions in Waves.
Transactions of the Royal Institution of Naval Architects, Volume 145, 2003.

104. Holloway, D. S. and Davis, M. R.
Green Function Solutions for the Transient Motion of Water Sections.
Journal of Ship Research, Volume 46, No 2, 2002.

105. Kara, F. and Vassalos, D.
Time Domain Prediction of a Steady and Unsteady Marine Hydrodynamics Problem.
International Shipbuilding Progress, Volume 50, No 4, 2003.

106. Westlake, P. C. and Wilson, P. A.
Time Domain Simulation of Ship Motions.
Transactions of the Royal Institution of Naval Architects, Volume 142, 2000.

107.
Numerical Recipes in FORTRAN 77: The Art of Scientific Computing.
Cambridge University Press, 1992, ISBN 0-521-43064-X.

108. Francescutto, A.
Roll-Heave-Sway Coupling in Beam Waves.
ISOPE 2002, 12th International Offshore and Polar Engineering Conference, 26-31 May 2002, Kitakyushu, Japan, ISBN 1-880653-58-3, Vol III, 2002.

109. Gawn, R. W. L.
Rolling Experiments with Ships and Models in Still Water.
Transactions of the Royal Institution of Naval Architects, Volume 82, 1940.

110. Salvesen, N., Tuck, E. O., and Faltinsen, O.
Ship Motions and Sea Loads.
Transactions of the Society of Naval Architects and Marine Engineers, Volume 78, 1970.

111. Roberts, J. B., Kountzeris, A., and Gawthrop, P. J.
Parametric Identification Techniques for Roll Decrement Data.
International Shipbuilding Progress, Volume 38, No 415, September 1991.

112. Contento, G., Francescutto, A., and Piciullo, M.
On the Effectiveness of Constant Coefficients Roll Motion Equation.
Ocean Engineering, Volume 23, No 7, October 1996.

113. Francescutto, A., Contento, G., Biot, M., and Schiffrer, L.
The Effect of Excitation Modelling in the Parameter Estimation of Nonlinear Rolling.
ISOPE 98, 8th International Offshore and Polar Engineering Conference, 24-29 May 1998, Montreal, Canada, ISBN 1- 880653-37-0, Vol III.

114. Ikeda, Y., Himeno, Y., and Tanaka, N.
A Prediction Method for Ship Roll Damping.
Report of Department of Naval Architecture, University of Osaka Prefecture, No 00405, December 1978.

115. Ikeda, Y., Himeno, Y., and Tanaka, N.
Components of Roll Damping of a Ship at Forward Speed.
Report of Department of Naval Architecture, University of Osaka Prefecture, No 00404, August 1978.

116. Ikeda, Y., Komatsu, K., Himeno, Y., and Tanaka, N.
On the Roll Damping Force of Ship:- Effect of Hull Surface Pressure Created by Bilge Keels.
Report of Department of Naval Architecture, University of Osaka Prefecture, No 00402, April 1979.

117. Ikeda, Y., Himeno, Y., and Tanaka, N.
On Eddy Making Component of Roll Damping. Force on Naked Hull.
Report of Department of Naval Architecture, University of Osaka Prefecture, No 00403, July 1978.

118. Ikeda, Y., Himeno, Y., and Tanaka, N.
On the Roll Damping Force of Ship:- Effect of Friction of Hull and Normal Force of Bilge Keels.
Report of Department of Naval Architecture, University of Osaka Prefecture, No 00401, December 1978.

119. Ikeda, Y.
Prediction Methods of Roll Damping of Ships and their Application to Determine Optimum Stabilisation Devices.
Marine Technology, Volume 41, No 2, 2004.

120. Chakrabarti, S.
Empirical Calculation of Roll Damping for Ships and Barges.
Ocean Engineering, Volume 28, No 7, July 2001.

121. Brook, A. K.
Evaluation of Theoretical Methods for Determining Roll Damping Coefficients.
Transactions of the Royal Institution of Naval Architects, Volume 132, 1990.

122. Kat, J. O. and Paulling, J.
The Simulation of Ship Motions and Capsizing in Severe Seas.
Transactions of the Society of Naval Architects and Marine Engineers, Volume 97, 1989.

123. Ikeda, Y., Tanaka, N., and Himeno, Y.
Effect of Hullform and Appendage on Roll Motion of a Small Fishing Vessel.
STAB 82, International Conference on Stability of Ships and Ocean Vehicles, Tokyo, Japan, 1982.

124. Haddara, M. R. and Leung, S. K.
Experimental Investigation of the Lift Component of Roll Damping.
Ocean Engineering, Volume 21, No 2, February 1994.

125. Kato, H.
On the Frictional Resistance of Ships to Rolling.
Journal of the Society of Naval Architects of Japan, Volume 102, 1958.

126. Tamiya, S. and Komura, T.
Topics on Ship Rolling Characteristics with Advance Speed.
Journal of the Society of Naval Architects of Japan, Volume 132, 1972.

127. Tanaka, N.
A Study on the Bilge Keels (Part 4 - On the Eddy Making Resistance to the Rolling of a Ship).
Journal of the Society of Naval Architects of Japan, Volume 109, 1960.

128. Chaplin, J. R. and Ikeda, Y
Viscous Forces on Offshore Structures and their Effects on the Motion of Floating Bodies.
ISOPE 99, 9th International Offshore and Polar Engineering Conference, 30 May-4 June 1999, Brest, France, ISBN 1- 880653-42-7.Vol III.

129. Ikeda, Y., Fujiwara, T., and Katayama, T.
Roll Damping of a Sharp Cornered Barge and Roll Control by a New Type of Stabiliser.
3rd International Offshore and Polar Engineering Conference, Singapore, 1993.

130. Standing, R. G.
Prediction of Viscous Roll Damping and Response of Transportation Barges in Waves.
ISOPE 91, 1st International Offshore & Polar Engineering Conference, 11-16 Aug 1991, Edinburgh, U.K, ISBN 0-9626104-61, Vol III.

131. Standing, R. G., Jackson, G. E., and Brook, A. K.
Experimental and Theoretical Investigation into the Roll Damping of a Systematic Series of Two-Dimensional Barge Sections.
BOSS 92, 6th International Conference on the Behaviour of Offshore Structures, 7-10 July 1992, London, U.K.

132. Ikeda, Y. and Katayama, T.
Roll Motion Characteristics of High Speed Slender Vessels.
STAB 94, 5th International Conference on Stability of Ships and Ocean Vehicles, 7-11 Nov 1994, Florida, USA.

133. Yumuro, A. and Mizutani, I
A Study on Anti-Rolling Fins Part (2).
Ishikawajima-Harima Engineering Review, Volume 10, No 2, 1970.

134. Blok, J. J. and Aalbers, A. B.
Roll Damping Due to Lift Effects on High Speed Monohulls.
FAST 91, 1st International Conference on Fast Sea Transportation, 17-21 June 1991, Trondheim, Norway.

135. Ikeda, Y. and Katayama, T.
Roll Damping Prediction Method for a High Speed Planing Craft.
STAB 2000, 7th International Conference on the Stability of Ships and Ocean Vehicles, 7-11 February 2000, Launceston, Tasmania, Australia, ISBN 0 9585990 4.

136. Kato, H.
Effect of Bilge Keels on the Rolling of Ships.
Journal of the Society of Naval Architects of Japan, Vol 117, 1965.

137. Whicker, L. F. and Fehlner, L. F.
Free-Stream Characteristics of a Family of Low-Aspect-Ratio, all Moveable Control Surfaces for Application to Ship Design. Revised Edition.
David Taylor Model Basin (DTMB) Report 933, 1958.

138. Klaka, K., Krokstad, J., and Renilson, M. R.
Prediction of Yacht Roll Motion at Zero Forward Speed.
14th Australian Fluid Mechanics Conference, Adelaide, 2001.

139. Klaka, K. and Renilson, M. R.
Roll motion of yachts at anchor
YachtVision02 Conference, Auckland, New Zealand.2002

140. Klaka, K., Penrose, J., Horsley, R., and Renilson, M. R.
Roll Motion of Yachts at Anchor.
RINA Modern Yacht Conference, Southampton, 2003.

141. Klaka, K.
Response of a Vessel to Waves at Zero Ship Speed: Preliminary Full Scale Experiments.
Curtin University Centre for Marine Technology, Interim Report, 2000.

142. Klaka, K.
Model Tests on a Circular Cylinder with Appendages.
Curtin University Centre for Marine Technology, Interim Report, 2001.

143. Klaka, K. and Renilson, M. R.
Experimental Study of the Influenence of Appendages on a Yacht Rolling at Zero Froude Number.
Marine Technology, Volume 41, No 4, 2004.

144. Tanaka, N. and Himeno, Y.
Study on Roll Characteristics of a Small Fishing Vessel.
Naval Architecture and Ocean Engineering, Volume 24, 1982.

145. Ikeda, Y. and Umeda, N.
A Prediction Method of Roll Damping of a Hardchine Boat at Zero Forward Speed.
Kansai Society of Naval Architects of Japan, No 213, March 1990.

146. Ikeda, Y. and Kawahara, Y.
Studies on Roll Characteristics of a High Speed Hardchine Craft.
Proceedings of the Second Japan-Korea Joint Workshop on Ship and Marine Hydrodynamics, 1993.

147. Chan, H. S.
Dynamic Structural Response of a Monohull Vessel to Regular Waves.
International Shipbuilding Progress, Volume 39, No 419, 1992.

148. Dallinga, R. P.
Hydromechanic Aspects of the Design of Fin Stabilisers.
Transactions of the Royal Institution of Naval Architects, Volume 135, 1993.

149. Lloyd, A. R. J. M. and Crossland, P.
Motions of a Steered Model Warship in Oblique Waves.
Transactions of the Royal Institution of Naval Architects, Volume 132, 1990.

150. Lee, C. M. and Curphey, R. M.
Prediction of Motion, Stability, and Wave Load of Small-Waterplane-Area Twin-Hull Ships.
Transactions of the Society of Naval Architects and Marine Engineers, Volume 86, 1977.

151. Centeno, R., Varyani, K. S., and Guedes Soares, C.
Experimental Study on the Influence of Hull Spacing on Hard-Chine Catamaran Motions.
Journal of Ship Research, Volume 45, No 3, 2001.

152. Centeno, R., Fonseca, N., and Guedes Soares, C.
Prediction of motions of catamarans accounting for viscous effects
International Shipbuilding Progress, Vol 47, no 451, 2000

153. Fang, C. C., Chan, H. S., and Incecik, A.
Investigation of Motions of Catamarans in Regular Waves - I.
Ocean Engineering, Volume 23, No 1, January 1996.

154. Chan, H. S.
On the Calculations of Ship Motions and Wave Loads of High Speed Catamarans.
International Shipbuilding Progress, Volume 42, No 431, 1995.

155. Chan, H. S.
Prediction of Motion and Wave Loads of Twin-Hull Ships.
Marine Structures 6, 1993.

156. Schellin, T. E. and Rathje, H.
A Panel Method Applied to the Hydrodynamic Analysis of Twin-Hull Ships.
FAST 95, 3rd International Conference on Fast Sea Transportation, 25-27 Sept 1995, Lubeck-Travemunde, Germany, 1995.

157. Rathje, H. and Schellin, T. E
Viscous Effects in Seakeeping Prediction of Twin-Hull Ships.
Ship Technology Research, Volume 44, No 1, February 1997.

158. Hermundstad, O. A., Aarsnes, J. V., and Moan, T.
Linear Hydroelastic Analysis of High Speed Catamarans and Monohulls.
Journal of Ship Research, Volume 43, No 1, 1999.

159. Faltinsen, O.
On the Seakeeping of Conventional and High Speed Vessels.
Journal of Ship Research, Volume 37, No 2, 1993.

160. Davis, M. R. and Holloway, D. S.
Motion and Passenger Discomfort on High Speed Catamarans in Oblique Seas.
International Shipbuilding Progress, Volume 50, No 4, 2003.

161. Holloway, D. S. and Davis, M. R.
Seakeeping Computations for Semi-Swaths at High Froude Number.
Transactions of the Royal Institution of Naval Architects, Volume 146, 2004.

162. Fang, C. C., Chan, H. S., and Incecik, A.
Investigation of Motions of Catamarans in Regular Waves - II.
Ocean Engineering, Volume 24, No 10, November 1997.

163. Fang, M-C. and Lin, B-N.
The Simulation of the SWATH Ship Motion with Fixed Fin in Longitudinal Waves.
ISOPE 95, 5th International Offshore & Polar Engineering Conference, 11-16 June 1995, The Hague, The Netherlands, ISBN 1-880653-19-2, Vol III.

164. Fang, M-C. and Lin, B-N.
The Simulation of SWATH Ship Motion with Controllable Fin in Longitudinal Waves.
International Shipbuilding Progress, Volume 45, No 443, September 1998.

165. Thwaites, B.
Incompressible Aerodynamics.
First Edition, Oxford University Press, 1960.

166. Doctors, L. J. and Scrace, R. J.
Hydrodynamic Interactions Between the Subhulls of a Trimaran During Roll Motion.
RINA International Conference on the Design and Operation of Trimaran Ships, 29th - 30th April 2004, London, UK, ISBN 0 903055 99 6.

167. Floden, D., Kim, K., and Ottosson, P.
A Computational/Experimental Investigation on Resistance and Seakeeping Characteristics of Trimaran Configuration in Comparison with Monohull.
PRADS 2004, 9th Symposium on Practical Design of Ships and Other Floating Structures, Lubeck-Travemunde, Germany, 2004.

168. Germain, P.
Recent Evolution in Problems and Methods in Aerodynamics.
Journal of the Royal Aeronautical Society, Vol 71, No 682, October 1967.

169. Wu, G. X.
Wave Radiation by an Oscillating Surface-Piercing Plate at Forward Speed.
International Shipbuilding Progress, Volume 41, No 426, 1994.

170. Wu, G. X. and Eatock Taylor, R.
The Numerical Solution of the Motions of a Ship Advancing in Waves.
Numerical Ship Hydrodynamics, 5th International Conference, Vol.II, 25-28 September 1989, Hiroshima, Japan.

171. Richardsen, C., Hall, J. H., Granshaw, D., and Hartley, K. B.
Seakeeping, manoeuvring and resistance experiments on a Trimaran hull form. Comparison of side hull designs.
DERA Report for the UK MoD, DERA/SS/HE/CR971007, December 1997.

172. Grafton, T. J., Zhang, J-W., and Rusling, S. C.
The Design and Hydrodynamic Performance of Trimaran Roll Damping Appendages.
RINA International Conference on the Design and Operation of Trimaran Ships, 29th - 30th April 2004, London, UK, ISBN 0 903055 99 6.

173. Crossland, P., Wilson, P. A., and Bradburn, J. C.
The Free Decay of Coupled Heave and Pitch Motions of a Model Frigate.
Transactions of the Royal Institution of Naval Architects, Volume 135, 1993.

174. Du Cane, P.
High Speed Small Craft - Extract on Lift and Drag of Foils.
High Speed Small Craft, 2nd Edition, David & Charles Ltd, 1974.

175. Fontaine, S., Huberson, S., and Montagne, J.
Numerical Evaluation of Fins Acting Near the Free Surface.
Naval Hydrodynamics, 19th Symposium, 23-28 August 1992, Seoul, Korea.

176. Liut, D., Mook, D., Weems, K. M., and Nayfeh, A.
A Numerical Model of the Flow Around Ship- Mounted Fin Stabilisers.
International Shipbuilding Progress, Volume 48, No1, April 2001.

177. Haddara, M. R., Bass, D. W., and Wang, Z.
Effect of Steady Heel on Damping at Large Roll Amplitudes.
OMAE 1992, 11th International Conference on Offshore Mechanics & Arctic Engineering, 7-12 June 1992, Calgary, Canada, Vol 1.

178. Thompson, J. M. T., Cotton, B., Spyrou, K. J., de Souza, J. R., and Bishop, S. R.
The Nonlinear Dynamics of Ship Roll and Capsize.
Report from the Centre for Nonlinear Dynamics and its Applications, Civil Engineering Building, University College London, 2000.

179. Wright, J. H. G. and Marshfield, W. B.
Ship Roll Response and Capsize Behaviour in Beam Seas.
Transactions of the Royal Institution of Naval Architects, Volume 122, 1980.

180. Newland, D. E.
An Introduction to Random Vibrations, Spectral and Wavelet Analysis.
Third Edition, Longman Singapore, 1997, ISBN 0582 21584 6.

181. Granshaw, D.
A Validation of TRIMO (Version 97_0).
DERA Report for the UK MoD, DERA/SS/HE/CR971023, August 1997.

182. Nayfeh, A. H. and Fung, J.
Parametric Identification for a Roll Instability in a Series S60-70 Ship.
ISOPE 98, 8th International Offshore and Polar Engineering Conference, 24-29 May 1998, Montreal, Canada, ISBN 1- 880653-37-0, Vol III.

183. Bertram, V., Caponetto, M., and El Moctar, O.
RANSE Simulations for Unsteady Marine Two-phase Flows.
RINA CFD 2003: Computational Fluid Dynamics Technology in Ship Hydrodynamics, London, 2003.

184. Shuford Jr, C. L.
A Theoretical and Experimental Study of Planing Surfaces Including Effects of Cross-Section and Plan Form.
Report 1355, National Advisory Committee for Aeronautics (NACA), Langley Aeronautical Laboratory, 1958.

185. Keulegan, G. H. and Capenter, L. H.
Forces on Cylinders and Plates in an Oscillating Fluid.
Journal of Research of the National Bureau of Standards, Volume 60, 1958.

186. Milne Thompson, L. M.
Theoretical Aerodynamics.
4th Edition, Dover Publications Inc, ISBN 0-486-61980-X, 1973.

187. Vladimirov, A. N.
NASA Technical Memorandum 1341: Approximate Hydrodynamic Design of a Finite Span Hydrofoil (Translation).
NACA Technical Memorandum 1344, National Advisory Committee for Aeronautics (NACA), Washington, June 1955.

188. Lloyd, A. R. J. M.
Roll Stabiliser Fins: A Design Procedure.
Transactions of the Royal Institution of Naval Architects, Volume 117, 1975.

Appendix (1) Semi-empirical Roll Damping Components applicable to Monohulls: A Theoretical Review

Appendix (1) Semi-empirical Roll Damping Components applicable to Monohulls: A Theoretical Review 431
A1-1 Introduction 432
A1-2 Skin Friction Damping 433
A1-3 Eddy Damping 436
A1-3.1 Determination of Tanaka's Non-Dimensional Coefficient 437
A1-3.2 Determination of Ikeda et al's Non-dimensional Coefficient 439
A1-4 Lift Damping 444
A1-4.1 Procedure for Determining the Lift Slope, K_N, and Lever Arm, l_0, from Model Experiments 444
A1-4.2 Research at the Maritime Research Institute of the Netherlands (MARIN) 446
A1-4.3 Lift Damping of Planing Craft According to Ikeda and Katayama ... 448
A1-5 Bilge Keel Damping 450
A1-5.1 Schmitke's Method 450
A1-5.2 Ikeda et al's Method 453
A1-6 Miscellaneous 459

A1-1 Introduction

This appendix explains the theory supporting the semi-empirical methods for obtaining roll damping components for monohulls. This theory is reviewed in Section 2.5 of Chapter 2 of this thesis. This appendix is written as a free standing document in support of Section 2.5.

The sections in this appendix have been arranged to match the order the topics are discussed in Section 2.5 of Chapter 2. Therefore, the first section of this appendix concerns Skin Friction Damping (covered in Section 2.5.3 of the main text); the next section covers Eddy Damping (covered in Section 2.5.4); the following section Lift Damping (covered in Section 2.5.5); and the next section Bilge Keel Damping (covered in Section 2.5.6). The final section of this appendix covers all other topics relevant to the thesis.

A1-2 Skin Friction Damping

Both Schmitke (81) and Ikeda (114) developed equivalent linearised damping formula to represent the friction damping based on the work of Kato (125):-

$$B_F = \frac{4}{3\pi}\rho\omega\, x_{40} C_{DF} S_W \bar{r}^3 \qquad \text{A1-2-1}$$

Where S_W is the hull wetted surface area, C_{DF} is the non-dimensional frictional coefficient, ω is the wave frequency and $\bar{r}$ is defined as the average radius of roll. Ikeda proposed that the hull wetted surface and roll radius could be determined using the following empirical formula:-

$$S_W = L(1.7T + C_B B) \qquad \text{A1-2-2}$$

$$\bar{r} = \frac{1}{\pi}\left\{(0.887 + 0.145C_B)\frac{S_W}{L} - 2(\overline{OG})\right\} \qquad \text{A1-2-3}$$

Where C_B is the ship's block coefficient with length L, draught T and beam B, and $\overline{OG}$ is the vertical distance from the origin (at the still water position) to the roll axis (the centre of gravity) measured positive downwards. Schmitke preferred to allow the friction to be calculated element by element and presented equation A1-2-1 as:-

$$B_F = \frac{4}{3\pi}\rho\omega\, x_{40} C_{DF} \int_L dx \int_{C_x} r_f \left(y\frac{dy}{dl} + z\frac{dz}{dl}\right)^2 dl \qquad \text{A1-2-4}$$

Schmitke took an element measured around the girth of the hull, dx, of length l positioned at (x, y, z) a distance $r_f = \sqrt{y^2 + z^2}$ away from the centre of gravity (assumed to be the roll centre), L and C_x on the integrals are over length and

around the girth respectively. This allows the hull wetted surface shape to modelled more accurately than with equation A1-2-2.

In the case when forward speed is non-zero Schmitke proposed that the Schoenherr line based on smooth turbulent flow is used to calculate C_{DF}:-

$$C_{DF} = 0.0004 + (3.46\log\left(\frac{UL}{\upsilon}\right) - 5.6)^{-2} \qquad \textbf{A1-2-5}$$

Where υ is the kinematic viscosity, 0.0004 is the standard hull roughness coefficient.

If forward speed is zero then Schmitke suggested that a method developed by Kato (125) should be used:-

$$C_{DF} = 1.328R_n^{-0.5} + 0.014R_n^{-0.114} \qquad \textbf{A1-2-6}$$

The first part of equation A1-2-6 is due to laminar flow (which is a linear damping component) whereas the second part is due to turbulent flow (which is a non-linear damping component). The Reynolds number is obtained from:-

$$R_n = \frac{3.22}{T_4\upsilon}(\bar{r}x_{40})^2 \qquad \textbf{A1-2-7}$$

Ikeda used Kato's method (equation A1-2-6) and modified the whole formula (equation A1-2-1) by the following factor to account for speed effects:-

$$B_F = B_{F0}\left(1 + 4.1\frac{U}{\omega L}\right) \qquad \textbf{A1-2-8}$$

The empirical coefficient of 4.1 was proposed by Tamiya et al (126) based on theoretical modelling and experimental results for rolling ellipsoid models.

Himeno (80) quoted equation A1-2-1 using Kato's formula for the friction coefficient, equation A1-2-6, in equivalent linear form as:-

$$B_{F0} = 0.787\rho\, S_W \bar{r}^2 \sqrt{\omega\upsilon}\left\{1 + 0.00814\left(\frac{\bar{r}^2 x_{40}{}^2 \omega_d}{\upsilon}\right)^{0.386}\right\} \qquad \textbf{A1-2-9}$$

A1-3 Eddy Damping

Tanaka (127) developed an expression to determine the eddy roll damping component at zero forward speed, B_E. The original work is published in Japanese but has been summarised by Schmitke (81). The equation relies on a non-dimensional coefficient C_{TAN} which can be determined based on empirical data.

$$B_E = \frac{4}{3\pi}\omega\rho\, x_{40} r_{ed}{}^3 S_{W\,sec} C_{TAN} \qquad \text{A1-3-1}$$

Where $S_{W\,sec}$ is the wetted surface area of the transverse section of the hull under consideration, and r_{ed} is the radius from the roll centre (centre of gravity) to the position where eddies are being generated.

Ikeda, Himeno and Tanaka (117) developed the following equation to determine the eddy roll damping component, B_E, at zero forward speed using a non-dimensional coefficient derived from empirical data C_{IKD} :-

$$B_E = \frac{4}{3\pi}\omega\rho\, x_{40} T_{sec}{}^4 L_{sec} C_{IKD} \qquad \text{A1-3-2}$$

Where T_{sec} and L_{sec} are the draught and length of the ship section for which the eddy damping component is being calculated.

In both expressions the ship is split up into a number of transverse sections, the non-dimensional coefficient C_{TAN} or C_{IKD} is determined for the section in question and the eddy damping contribution, B_E, for that section can be determined using equation A1-3-1 or equation A1-3-2. This process is then repeated for all of the sections which represent the ship. The sectional

contributions are then summed together to give the total eddy damping component for the complete hull.

A1-3.1 Determination of Tanaka's Non-Dimensional Coefficient

Tanaka measured the non-linear damping term from forced roll experiments and used this to determine suitable values for C_{TAN}. These values form the basis of a semi-empirical formula that allows the eddy damping to be calculated for different ship sections, equation A1-3-1. Tanaka came up with the following expression:-

$$C_{TAN} = T_1 T_2 \exp\left(-u\frac{r_{eb}}{T_{sec}}\right)$$

$$u = 14.1 - 46.7x_{40} + 61.7x_{40}^{\ 2} \qquad \text{A1-3-3}$$

Where r_{eb} is the effective bilge radius. Tanaka proposed a formula for r_{eb} depending on the ratio between the beam of the section, B_{sec}, and height of the centre of gravity, $\overline{KG}$:-

$$r_{eb} = \begin{cases} \dfrac{B_{sec}}{2}\left[4.12 - 2.69\dfrac{\overline{KG}}{B_{sec}} + 0.823\left(\dfrac{\overline{KG}}{B_{sec}}\right)^2\right] & \dfrac{\overline{KG}}{B_{sec}} < 2.1 \\ 0 & \dfrac{\overline{KG}}{B_{sec}} \geq 2.1 \end{cases} \qquad \text{A1-3-4}$$

The term T_1 is dependent on the relation between the beam of the section and the height of the centre of gravity whereas T_2 depends on the flare, α_s see Figure A1-3- 1, and the relationship between the effective bilge radius radius, r_{eb}, and the

draught of the two-dimensional ship section under consideration, T_{sec}. The terms T_1 and T_2 can be determined using Table A1-3- 1 and Table A1-3- 2.

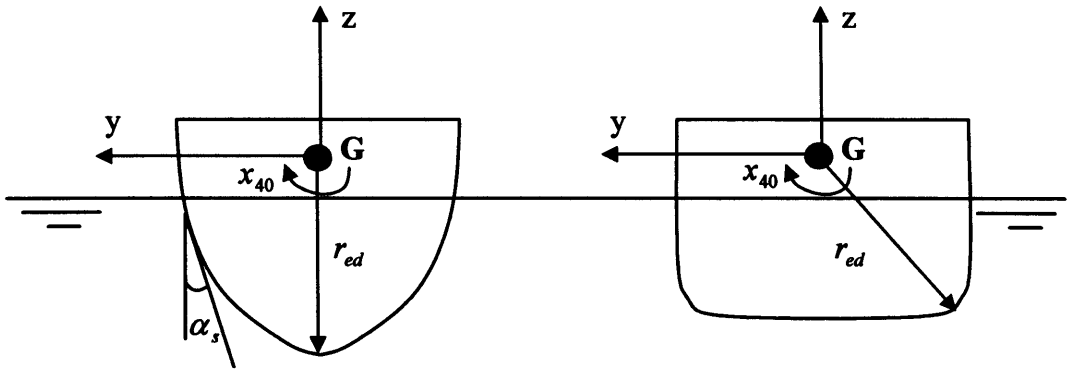

Figure A1-3- 1: Classification of section shapes for eddy damping calculations: "U/V" on left and "Full" on right

$\frac{B_{sec}}{KG}$	T_1
0.00	0.50
0.25	0.61
0.50	0.62
1.00	0.61
1.50	0.53
2.00	0.40
2.50	0.35
3.00	0.32
3.50	0.29
4.00	0.26

Table A1-3- 1: Table of values for Tanaka's T_1 term

α_s (degrees)	$\frac{r_{eb}}{T_{sec}} = 0$	= 0.0571	= 0.1142	= 0.1713
0	1.00	1.00	1.00	1.00
5	0.86	0.75	0.74	0.70
10	0.77	0.67	0.72	0.72
20	0.68	0.75	0.89	1.20
30	0.65	0.92	1.34	1.94

Table A1-3- 2: Table of values for Tanaka's T_2 term

A1-3.2 Determination of Ikeda et al's Non-dimensional Coefficient

Ikeda et al considered the case where either one or two eddies separated from the hull, see Figure A1-3- 2.

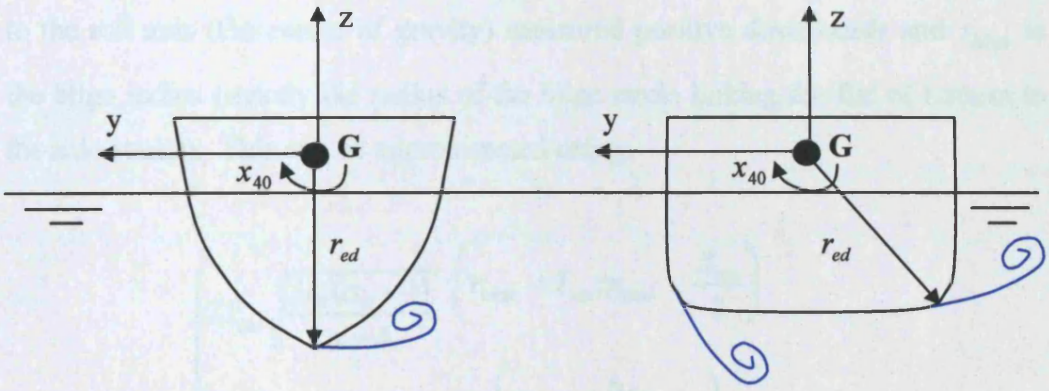

Figure A1-3- 2: Classification of eddy separation conditions: one eddy shed on left and two on right

Through experimentation they determined that the transition from single to double point eddy shedding depended upon the half-breath to draught ratio, H_0, and the area coefficient, σ_S, both defined in equation A1-3-5. Experiments revealed that no eddies were shed from a semi-circular section.

$$H_0 = \frac{B_{sec}}{2T_{sec}}$$

$$\sigma_S = \frac{S_{W\,sec}}{B_{sec}T_{sec}} \qquad \text{A1-3-5}$$

To determine the magnitude of the roll damping moment due to eddy shedding the location of the points (either single or double) of eddy separation had to be determined along with the shape and magnitude of the eddy pressure distribution on the hull. The integral of the pressure distribution multiplied by a suitable rolling lever over the surface gives the eddy damping moment. The following example was proposed by Ikeda et al for two point separation:-

$$Moment = L_{sec}T_{sec}{}^2 \times \left[\left(1-\frac{r_{bilge}}{T_{sec}}\right)\left(1-\frac{\overline{OG}}{T_{sec}}-\frac{r_{bilge}}{T_{sec}}\right)+\left(H_0-\frac{r_{bilge}}{T_{sec}}\right)^2\right]\frac{P_m}{3} \qquad \text{A1-3-6}$$

Where $\overline{OG}$ is the vertical distance from the origin (located at the still waterline) to the roll axis (the centre of gravity) measured positive downwards and r_{bilge} is the bilge radius (strictly the radius of the bilge circle linking the flat of bottom to the side strake). This can be approximated using:-

$$r_{bilge} = \begin{cases} 2T_{sec}\sqrt{\dfrac{H_0(\sigma_S-1)}{\pi-4}} & \left(r_{bilge} < T_{sec}; r_{bilge} < \dfrac{B_{sec}}{2}\right) \\ T_{sec} & \left(H_0 \geq 1; \dfrac{r_{bilge}}{T_{sec}} > 1\right) \\ \dfrac{B_{sec}}{2} & \left(H_0 \leq 1; \dfrac{r_{bilge}}{T_{sec}} > H_0\right) \end{cases} \qquad \text{A1-3-7}$$

P_m is the pressure difference from one side of the hull to the other when the ship is rolling (i.e. the pressure difference between the port and starboard sides of the hull section when the section rolls to port). The constant of 1/3 on the pressure

difference was set depending on the form of the pressure distribution. This pressure distribution was defined as:-

$$\frac{P_m}{3} = \frac{1}{2}\rho\, r_{\max}{}^2 \dot{x}_4 |\dot{x}_4| C_P \qquad \textbf{A1-3-8}$$

Where C_P is the pressure coefficient based on *difference* in pressure between the port and starboard sides of the hull:-

$$C_P = \frac{pressure}{\frac{1}{2}\rho\, r_{ed}{}^2 x_{40}{}^2 \omega^2} \qquad \textbf{A1-3-9}$$

And $r_{\max}$ is the maximum distance from the roll axis to the hull surface and is expressed by an approximate formula (equation A1-3-18).

In Ikeda et al's formulation, the non-linear damping coefficient was defined as:-

$$B_2 = \frac{Moment}{\dot{x}_4|\dot{x}_4|} = \frac{1}{2}\rho\, T_{sec}{}^4 L_{sec} C_{IKD} \qquad \textbf{A1-3-10}$$

Combining equations A1-3-6, A1-3-8 and A1-3-10 allows an expression for the coefficient C_{IKD} to be developed. Adding in further terms proposed by Ikeda et al to account for single point eddy separation the final equation for C_{IKD} is arrived at:-

$$C_{IKD} = \left\{\left(1 - f_1 \frac{r_{bilge}}{T_{sec}}\right)\left(1 - \frac{\overline{OG}}{T_{sec}}\right) + f_2\left(H_0 - f_1 \frac{r_{bilge}}{T_{sec}}\right)^2\right\} C_P \left(\frac{r_{\max}}{T_{sec}}\right)^2 \qquad \textbf{A1-3-11}$$

The factor f_1 is set so that it is equal to one for single point eddy separation and zero for two point separation, it takes the general form:-

$$f_1 = 0.5[1 + \tanh(20\{\sigma_S - 0.7\})] \qquad \textbf{A1-3-12}$$

The correction factor f_2 is determined using:-

$$f_2 = 0.5[1-\cos\pi\sigma_S]-1.5[1-\exp(-5\{1-\sigma_S\})]\sin^2\pi\sigma_S \qquad \textbf{A1-3-13}$$

The pressure coefficient can be obtained using the approximate relationship:-

$$C_p = 0.5[0.87\exp(-\gamma_v)-4\exp(-0.187\gamma_v)+3] \qquad \textbf{A1-3-14}$$

The magnitude of this depends on the strength of eddies shed from the hull which may be affected by the magnitude of the local velocity and pressure gradient. Ikeda et al's representation depends solely on γ_v, the ratio of the maximum to the mean flow velocity around the hull section. The value of C_P becomes zero for a circular cylinder as $\gamma_v = 1$, and approximately 1.5 when $\gamma_v \to \infty$. Ikeda et al developed an approximate formula to determine this ratio based on the potential flow of a cylinder using Lewis forms.-

$$\gamma_v = \frac{\sqrt{\pi f_3}}{2T_{sec}\left(1-\dfrac{\overline{OG}}{T_{sec}}\right)\sqrt{(H_0'\sigma_S')}}\left(r_{max}+\frac{2M_1}{H_1}\sqrt{A_{1E}{}^2+B_{1E}{}^2}\right) \qquad \textbf{A1-3-15}$$

The remaining undefined coefficients are given in equations A1-3-16 to A1-3-18:-

$$M_1 = \frac{B_1}{2(1+a_1+a_3)} \qquad H_0' = \frac{H_0}{1-\dfrac{\overline{OG}}{T_{sec}}} \qquad \sigma_S' = \frac{\sigma_S-\dfrac{\overline{OG}}{T_{sec}}}{1-\dfrac{\overline{OG}}{T_{sec}}} \qquad \textbf{A1-3-16}$$

$$H_1 = 1+a_1{}^2+9a_3{}^2+2a_1(1-3a_3)\cos 2\psi_1-6a_3\cos 4\psi_1$$

$$\begin{aligned} A_{1E} &= -2a_3\cos 5\psi_1+a_1(1-a_3)\cos 3\psi_1 \\ &\quad +\{(6-3a_1)a_3{}^2+(a_1{}^2-3a_1)a_3+a_1{}^2\}\cos\psi_1 \end{aligned} \qquad \textbf{A1-3-17}$$

$$\begin{aligned} B_{1E} &= -2a_3\sin 5\psi_1+a_1(1-a_3)\sin 3\psi_1 \\ &\quad +\{(6-3a_1)a_3{}^2+(3a_1-a_1{}^2)a_2+a_1{}^2\}\sin\psi_1 \end{aligned}$$

The radius to the point at which the distance between the hull and the roll centre becomes a maximum is defined as:-

$$r_{max} = M_1 \left[\begin{matrix} \{(1+a_1)\sin\psi_1 - a_3 \sin 3\psi_1\}^2 \\ + \{(1-a_1)\cos\psi_1 + a_3 \cos 3\psi_1\}^2 \end{matrix} \right]^{\frac{1}{2}} \qquad \textbf{A1-3-18}$$

The coefficients a_1 and a_3 are the Lewis form parameters corresponding to the shape of the modified cylinder below the roll axis and the coefficient ψ_1 represents the argument of the Lewis function on the transformed unit circle (see Lloyd (64)):-

$$\psi_1 = \begin{cases} 0 = \psi_{11} & r_{max}(\psi_{11}) \geq r_{max}(\psi_{22}) \\ \frac{1}{2}\cos^{-1}\frac{a_1(1+a_3)}{4a_3} = \psi_{22} & r_{max}(\psi_{11}) < r_{max}(\psi_{22}) \end{cases}, \qquad \textbf{A1-3-19}$$

And a correction factor for section shapes with a small radius of the bilge circle:-

$$f_3 = 1 + 4\exp\left\{-1.65\times10^5(1-\sigma_S)^2\right\} \qquad \textbf{A1-3-20}$$

A1-4 Lift Damping

Ikeda, Himeno and Tanaka (114) (115) developed the following formula to determine the lift damping of a ship hull:-

$$B_L = \frac{1}{2}\rho ULTk_N l_0 l_R \left[1 - 1.4\frac{\overline{OG}}{l_R} + \frac{0.7\overline{OG}^2}{l_R l_0}\right] \qquad \text{A1-4-1}$$

Where the term in square brackets is an empirically derived applicable when the roll centre is not located on the still waterline. The lift slope is denoted by k_N, $\overline{OG}$ is the vertical distance from the origin (located at the still waterline) to the roll axis (at centre of gravity) measured positive downwards, and the terms l_0 and l_R are moment lever arms. They showed that the product $k_N l_0$ could be determined experimentally from an oblique towing test in which the model is free to heel. In absence of model test results empirical formula were proposed based on a range of model experiment results.

A1-4.1 Procedure for Determining the Lift Slope, K_N, and Lever Arm, l_0, from Model Experiments

For a given steady yaw angle (angle between the ships head and direction of towing) x_6 a transverse lift force will be generated as the model is towed through the water due to the angle of attack x_6. This force will generate a steady heel moment depending on the magnitude of the lever between the centre of gravity and the lift force, l_S. For a steady heel angle this moment will be opposed by a hydrodynamic restoring moment. This restoring moment can be considered to be equivalent to the hydrostatic restoring moment $\rho\nabla\overline{GM}\varphi$, where φ is the steady heel angle. For the oblique towing test, equating the two moments gives:-

$$\frac{1}{2}\rho U^2 S_L C_L l_S = \rho \nabla \overline{GM}\varphi$$

A1-4-2

$$C_L l_S = \frac{2\nabla \overline{GM}\varphi}{S_L U^2}$$

Ikeda et al made the assumption that in roll motion $\alpha_0 \equiv x_6$, that is the moment developed due to steady heeling due to a yaw angle x_6 is equivalent to the moment developed during roll motion caused by an angle of attack α_0:-

$$C_L = k_N \alpha_0$$

$$k_N = \frac{dC_L}{d\alpha_0}$$

A1-4-3

$$\alpha_0 = \frac{l_0 \dot{x}_4}{U}$$

If the lift coefficient in the oblique towing test is the same as the lift coefficient for the rolling model (based on the profile area of the submerged part of the hull) then $l_S \equiv l_0$. Expanding the lift coefficient gives:-

$$k_N l_S = \frac{2\nabla \overline{GM}\varphi}{S_L x_6 U^2}$$

A1-4-4

Model experiments are conducted with different positions of the centre of gravity and the steady heel moment is plotted against $\overline{OG}/T$. Ikeda et al (115) showed that the value of $\overline{OG}/T$ when the static heel moment is zero is equal to l_S. When deriving the lift damping experimentally the correction in the bracket in equation A1-4-1 is not required and can be set to one. Hence, the only remaining unknown is the lever l_R. The only way this can be determined is by measuring the total roll damping moment in a model experiment and isolating the lift component. Ikeda et al did this by running the model at a high enough Froude number so that there was no eddy damping and calculating the friction damping using the procedure outlined in Section A1-2 of this appendix. The remainder of the damping is then

entirely due to hull lift. Having isolated the lift damping the lever can be determined by using equation A1-4-1 without the correction in the square brackets.

A1-4.2 Research at the Maritime Research Institute of the Netherlands (MARIN)

The Maritime Research Institute of the Netherlands (MARIN) conducted research into the seakeeping of a series of fast displacement ships starting in 1979. This work is reported by Blok and Aalbers (134). Roll decay tests were conducted on a number of models in the series and the measured damping was found to be disparate from results using the empirical methods of Ikeda et al (114) (115) (116) (117) (118) and Schmitke (81). A series of 13 models was then tested to allow improvements to the roll prediction methods of Ikeda et al and Schmitke to be made. At high forward speed the total roll damping moment was found to comprise of the wave radiation damping predicted by potential theory and hull lift damping, with the latter contributing the majority. As correlation between the roll damping moment measured in the MARIN roll decay tests and Ikeda et al's theory had been poor at high speed, Blok and Aalbers naturally focused their work on making improved predictions of the lift damping of the hull.

Blok and Aalbers (134) noted that the hull lift damping in the empirical theory of Ikeda et al (114) (115) is derived from the lift of a vertical plate undergoing roll motion. They went on to comment that whilst this assumption may give a reasonable prediction for a merchant ship hull with large block coefficient and low beam to draught ratio it is not realistic for a fast displacement hull form where the beam to draught ratio is much greater. From the large experimental database available to them Blok and Aalbers determined that the hull lift roll damping was dependent on hull shape. This dependence was also reflected in Ikeda et al's formulation (115) in the correction κ to the lift slope k_N, see Section 2.5.5 of Chapter 2.

The basis of the MARIN method reported by Blok and Aalbers is that for flat hulls with high beam to draught ratios the asymmetrical vertical lift force acting on the hull bottom on each side during roll motion creates a much greater roll damping moment than the horizontal lift force acting on the side of the hull used by Ikeda et al (115) to develop a lift damping equation. When the ship has forward speed, the vertical velocity of a transverse section of the hull undergoing roll motion induces an angle of attack to the incoming flow, hence a vertical lift force is developed. The distribution of this lift force along the length of the ship will cause a trim angle to be developed, τ_{ship}. Blok and Aalbers then used the work of Shuford Jr (184) to predict the lift force of a trimmed flat plate and developed a formula for the hull lift roll damping. Using this approach the following formula was proposed for the lift force developed by the flat plate with a trim angle τ_{ship} :-

$$Force/(metre)^2 = \frac{1}{2}\rho U^2 C_L$$

$$C_L = \frac{1}{2}\pi\tau_{ship}\cos^2\tau_{ship}\frac{(1-\beta_{hull})}{L/B+1} \qquad \text{A1-4-5}$$

$$\approx \tau_{ship}\frac{(1-\beta_{hull})}{L/B+1} \quad \tau_{ship} < 5^0$$

Where β_{hull} is the mean hull deadrise angle in radians.. The lift damping component then becomes:-

$$B_L = (k_L)\frac{\rho S_W U B^2}{L/B+1}$$

$$k_L = const \times (1-\sin\beta_{hull}) \qquad \text{A1-4-6}$$

Where k_L is the lift slope coefficient based on trim angle and the constant, *const*, is dependent on frequency and is determined from the MARIN experimental data base. No results for either of these values were published.

A1-4.3 Lift Damping of Planing Craft According to Ikeda and Katayama

Ikeda and Katayama (135) published a paper describing a method for determining the lift damping of a planning craft. This differed from Ikeda et al's (114) (115) original approach in that it considered the asymmetrical vertical lift force acting on the bottom of the planning hull during roll motion would create a much greater roll damping moment than the horizontal lift force acting on the side of the hull.

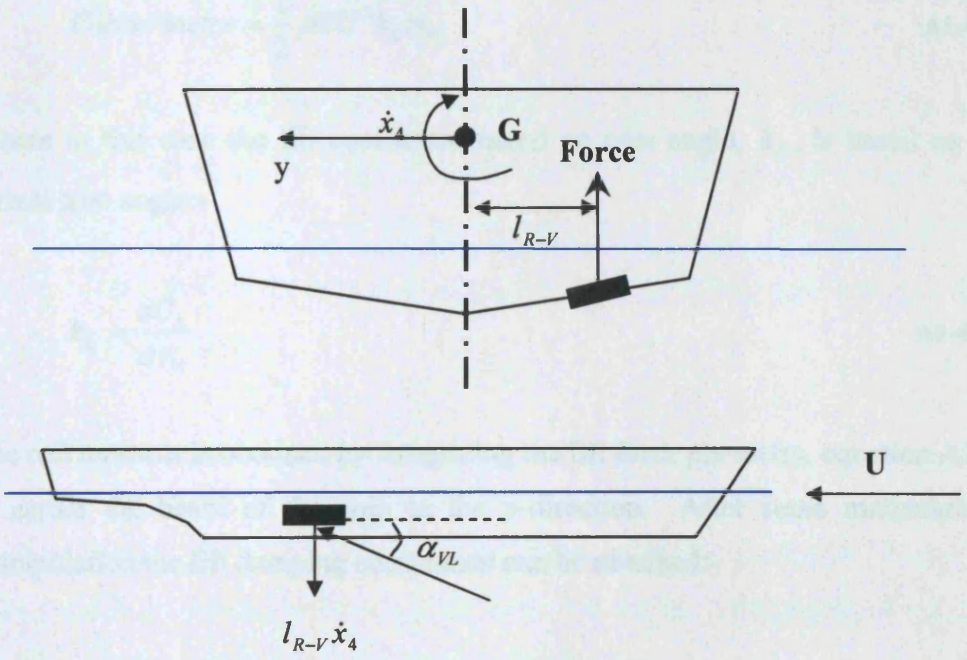

Figure A1-4- 1: Vertical lift force generated during roll motion for a high speed craft with high beam-draught ratio

Consider a section on the underside of the hull of a fast displacement ship with a high beam to draught ratio represented by the black rectangle in Figure A1-4- 1. During roll motion this section moves vertically up and down with velocity $l_{R-V}\dot{x}_4$. This vertical velocity when combined with the forward velocity of the ship induces and angle of attack on this section α_{VL} :-

$$\alpha_{VL} \approx \frac{\dot{x}_4 l_{R-V}}{U} \qquad \text{A1-4-7}$$

Assuming the running trim angle on the ship is τ_{ship}, the virtual trim angle acting on the vertical lift force τ_V can be written:-

$$\tau_V(y) = \tau_{ship} + \alpha_{VL} \approx \tau_{ship} + \frac{\dot{x}_4 l_{R-V}}{U} \qquad \text{A1-4-8}$$

The force per unit metre acting upwards can then be expressed as:-

$$Force/metre = \frac{1}{2}\rho B U^2 k_L \alpha_{VL} \qquad \text{A1-4-9}$$

Where in this case the lift coefficient based on trim angle, k_L, is based on the virtual trim angle:-

$$k_L = \frac{dC_L}{d\tau_V} \qquad \text{A1-4-10}$$

The roll moment is obtained by integrating the lift force per metre, equation A1-4-9, across the beam of the ship in the y-direction. After some mathematical manipulation the lift damping component can be obtained:-

$$B_L = \frac{1}{24}\rho B^4 U k_L \qquad \text{A1-4-11}$$

No empirical formula was offered for the lift coefficient k_L, this had to be determined experimentally.

A1-5 Bilge Keel Damping

A1-5.1 Schmitke's Method

Schmitke (81) reported on a method developed in Japan by Kato (136) for the prediction of a equivalent linear roll damping component due to a pair of bilge keels. He presented an equivalent linear damping terms as:-

$$B_{BK} = \frac{1}{\pi^3}\rho\, l_{bk} b_{bk} r_{bk}{}^3 \omega x_{40} C_{bk} \qquad \text{A1-5-1}$$

Where, the bilge keel length and breadth are l_{bk} and b_{bk} respectively and, assuming the force on the bilge keel acts at the mid span, a lever from the roll centre (the centre of gravity) to this position is defined as r_{bk}. The coefficient C_{bk} can be broken down into a number of components depending upon the ship form and Reynolds number:-

$$C_{bk} = C_0 C_k C_a C_n \breve{B} \breve{F}^{-\alpha_{bk}} \qquad \text{A1-5-2}$$

Kato conducted a large number of model experiments and the results from these were used to determine semi-empirical formulae for the coefficients of equation A1-5-2. These coefficients are defined as follows:-

$$\breve{F} = \frac{3.13 r_{bk} x_{40}}{T_4 \sqrt{g b_{bk}}} \Gamma_{bk}{}^{1.7} \qquad \text{A1-5-3}$$

Where T_4 is the roll period and:-

$$\alpha_{bk} = 0.6 - 2.03 \exp(-25 \xi_{bk}) \qquad \text{A1-5-4}$$

$$\xi_{bk} = \frac{b_{bk}}{\left(r_{bk} \Gamma_{bk}{}^{0.75}\right)} \qquad \text{A1-5-5}$$

$$\breve{B} = \cos\gamma_{bk} + \frac{l_{gbk}}{2b_{bk}r_{bk}}\left[q_{bk} + p_0 - (p_0 - p_1)f(\lambda)\right] \qquad \text{A1-5- 6}$$

Where l_{gbk} is the distance from the root of the bilge keel to the waterline measured around the girth of the hull, see Figure A1-5- 1, and:-

$$q_{bk} = \left[\frac{B_{sec}}{2}\tan\left(\frac{\pi}{4} - \frac{\varepsilon_{bk}}{2}\right) + R_{flr} - \overline{KG}\right]\sin\left(\frac{\pi}{4} - \frac{\varepsilon_{bk}}{2}\right)$$

$$\varepsilon_{bk} = \tan^{-1}\left[\frac{2R_{flr}}{B_{sec}}\right]$$

$$p_0 = \overline{KG} - \frac{B_{sec}}{3} - \frac{2}{3}R_{flr}$$

$$p_1 = 0.88\left\{\overline{KG} - T_{sec} - 0.54\left[\frac{B_{sec}}{2} - (T_{sec} - R_{flr})\tan\left(\frac{\pi}{4} - \frac{\varepsilon_{bk}}{2}\right)\right]\right\}$$

$$f(\lambda) = \frac{1.34\sin\dfrac{\pi\lambda}{3.6}}{1 + 0.162\sin\left[\dfrac{\pi}{1.8}(\lambda - 0.9)\right]} \qquad \text{A1-5- 7}$$

$$\lambda = \frac{r_{bilge}}{T_{sec} - \dfrac{R_{flr}}{B_{sec}}(B_{sec} - 2r_{bilge})}$$

The rise of floor, R_{flr}, is defined by:-

$$R_{flr} = \frac{B_{sec}}{2}\tan\varepsilon_{bk} \qquad \text{A1-5- 8}$$

With γ_{bk}, Γ_{bk} and ε_{bk} defined in Figure A1-5- 1. Where r_{bilge} is the bilge radius (strictly the radius of the bilge circle linking the flat of bottom to the side strake).

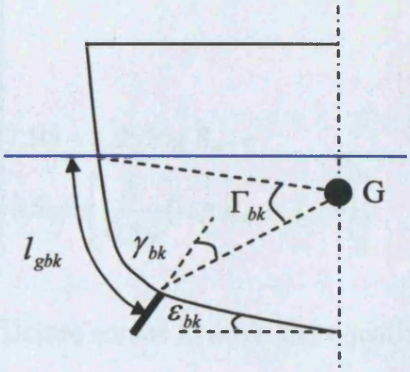

Figure A1-5- 1: Definitions for the bilge keel parameters

C_n is the standard normal force pressure coefficient for a rectangular plate moving with a uniform velocity in the direction perpendicular to its plane, defined by Schmitke (81) as:-

$$C_n = \begin{cases} 1.98\exp\left(\dfrac{-11 b_{bk}}{l_{bk}}\right) & b_{bk}/l_{bk} < 0.048 \\ 1.17 & b_{bk}/l_{bk} \geq 0.048 \end{cases} \qquad \text{A1-5- 9}$$

$$C_k = 1 + 3.5\exp(-9k_{bk}) \qquad \text{A1-5- 10}$$

$$k_{bk} = \frac{r_{bilge}\left(1 + \dfrac{R_{flr}}{B_{sec}}\right)^2}{\sqrt{\dfrac{B_{sec}\overline{KG}}{2}}}$$

The coefficient C_a depends on the Reynolds Number, R_N, defined as:-

$$R_N = \frac{8 b_{bk} r_{bk} x_{40}}{T_4 \upsilon} \qquad \text{A1-5- 11}$$

$$C_a = \begin{cases} 1 & R_N \geq 10^3 \\ 1.95 - 0.25 \log R_N + & \\ 0.2 \sin\left[\frac{\pi}{0.54}(\log R_N - 2.19)\right] & R_N < 10^3 \end{cases} \qquad \text{A1-5- 12}$$

The final coefficient serves to scale the equation:-

$$C_0 = 14.1 + 37.3 \Gamma_{bk}{}^3 \qquad \text{A1-5- 13}$$

A1-5.2 Ikeda et al's Method

Ikeda, Himeno and Tanaka (116) (118) also developed formulae for predicting the roll damping contribution of a pair of bilge keels. They proposed that the total bilge keel roll damping component could be broken down into two parts:-

- One due to the normal force developed by the bilge keel, B_{BKN}, and
- A second due to the modification of the pressure acting on the hull in the region of the bilge keel, B_{BKP}.

The roll damping due to the normal force created by the oscillating bilge keel was:-

$$B_{BKN} = \frac{8}{3\pi} \rho \, r_{bk}{}^3 b_{bk} l_{bk} \omega x_{40} f_{bkn}{}^2 C_D \qquad \text{A1-5- 14}$$

Where, C_D is the drag coefficient of the bilge keel and f_{bkn} a factor to account for the flow speed increase at the bilge in the vicinity of the bilge keels.

The bilge keel roll damping due to the pressure distribution around the bilge keels was determined as:-

$$B_{BKP} = \frac{4}{3\pi}\rho\, r_{bk}{}^2 \omega x_{40} f_{bkn}{}^2 \int_G C_P\, lever.dG \qquad \text{A1-5- 15}$$

Where the term *lever* is a lever arm measured from the centre of gravity to the point of action of the force generated due to the pressure difference across the faces of the bilge keels. The subscript G on the integral indicates that the integration is around the girth (around the outside edge of the hull section). C_p is a pressure coefficient and the integral containing this at the end of the formula was obtained from an empirical formula.

The empirically derived coefficients in equations A1-5-14 and A1-5-15 will now be derived.

The normal force acting from the oscillating bilge keel was assumed to be of the form:-

$$Force = \frac{1}{2}\rho U^2 S C_D \qquad \text{A1-5- 16}$$

Where S represents the maximum area perpendicular to the flow, $l_{bk} b_{bk}$. In unsteady motion the drag coefficient C_D varies with the motion. Keulegan and Carpenter (185) showed that the drag coefficient varied with a period parameter which has become known as the Keulegan-Carpenter Number, KC :-

$$KC = \frac{U_{\max} T_4}{L_{rep}} \qquad \text{A1-5- 17}$$

Where $U_{\max}$ is the maximum speed in oscillatory motion and L_{rep} is the representative length. Taking $U_{\max}$ in angular motion to be $r_{bk}\omega x_{40}$ m/s and the representative length to be $2b_{bk}$, this parameter becomes:-

$$KC = \frac{\pi r_{bk} x_{40}}{b_{bk}} \qquad \text{A1-5- 18}$$

Ikeda et al (118) conducted roll decay experiments and related the energy loss in one period to the drag force on the bilge keel. By making the resulting equation linear (using the equivalent linear method of Section 2.2.3.2 of Chapter 2), an expression for the drag coefficient was obtained:-

$$C_D = \frac{3(\Delta E)}{2\rho b_{bk} l_{bk} r_{bk}^{\ 3} \omega^2 x_{4m}^{\ 3}} \qquad \text{A1-5- 19}$$

Where ΔE is the energy dissipated in one roll cycle and x_{4m} is the mean roll angle (average of the two peaks of the roll decay curve spanning the period under consideration). Having established that the drag varies with Keulegan-Carpenter number, Ikeda et al plotted the Keulegan-Carpenter number against the drag coefficient determined in the experiments. They obtained the following expression for the drag coefficient by applying a least squares fit to the measured data:-

$$C_D = 22.5\left(\frac{b_{bk}}{\pi r_{bk} x_{4m} f_{bkn}}\right) + 2.40 \qquad \text{A1-5- 20}$$

This expression was considered to hold when the Keulegan-Carpenter Number was between 4 and 20. The factor f_{bkn} was added later to account for the flow speed increase at the bilge in the vicinity of the bilge keels. This factor was determined from experiments and should be attached to all the velocity terms in the equations A1-5-14 and A1-5-15. The factor was determined from model experiments on two-dimensional ship sections fitted with bilge keels (116):-

$$f_{bkn} = 1 + 0.3\exp\{-160(1-\sigma_s)\} \qquad \text{A1-5- 21}$$

Ikeda et al (116) stated that this coefficient would be no greater than 1.1, based on model experiment results using a two-dimensional model of the midship section of a Series 60 hullform with block coefficient of 0.80.

Using the process of equivalent linearization, the normal force bilge keel roll damping component for a pair of bilge keels could then be determined. This was given in equation A1-5-14.

Pressure sensors were fitted to the models in the vicinity of the location of the bilge keels. Forced roll experiments were conducted with the free surface covered by a flat plate with a gap around the model large enough to allow it to roll without touching the plate. This was to ensure that free surface effects and hydrostatic pressure effects on the water surface were minimised. The roll axis of the models was set to be located on the still waterline so that wave radiation effects were minimised. A pressure coefficient was calculated using equation A1-3-9 with the pressure defined this time as the difference between the pressures acting on the two faces of the bilge keel when the roll angular velocity was a maximum. The studies showed that the pressure coefficient remained constant when the frequency changed, i.e. the pressure of the bilge keels varies in proportion to the roll frequency squared. Furthermore, changing the roll amplitude only changed the pressure behind the bilge keels as the model rolled; the pressure on the front face of the bilge keel remained the same. Once again the pressure difference across the bilge keels was dependent on the Keulegen-Carpenter Number.

The pressure coefficient on the front face of the bilge keel was assumed to take the empirical value of 1.2, based on experiments on the ellipsoidal model, and to decrease linearly with distance around the hull to a value of zero at the free surface. The distribution of pressure behind the bilge keel was a more complex affair and was assumed to decrease following the profile of a trapezoid with longest length, adjacent to the hull, s_{trapz}, and shorter length $\frac{1}{2}s_{trapz}$. The magnitude of this pressure could be determined by taking the assumption that the pressure coefficient on the front face of the bilge keel minus the pressure coefficient behind the bilge keel is equal to the normal force drag coefficient given in equation A1-5-20. *In order to simplify the calculation the ship section was assumed to have a horizontal bottom (no rise of floor), vertical sides (no flare) both joined together by one quadrant of a circle.* The bilge keels were then located at the centre of the quadrant circle on either side of the hull section. A

further simplification was to take an average length of the pressure distribution behind the bilge keel as $s_{average}$, the distribution of pressure across which is uniform and rectangular:-

$$s_{average} = b_{bk}\left(0.3\frac{\pi\ f_{bkn} r_{bk} x_{40}}{b_{bk}} + 1.95\right) \qquad \textbf{A1-5-22}$$

Under these assumptions, an equivalent linear formula is created by determining the energy dissipated by a rolling moment due to the pressure distribution. This leads to the formula given in equation A1-5- 15. The integral in that equation will now be expanded upon:-

$$\int_G C_P.lever.dG = T_{sec}{}^2\left(-A_{bkp}C_P{}^- + B_{bkp}C_P{}^+\right) \qquad \textbf{A1-5-23}$$

$$C_P{}^+ = 1.2$$
$$C_P{}^- = C_P{}^+ - C_D = -22.5\frac{b_{bk}}{\pi r_{bk} f_{bkn} x_{40}} - 1.2 \qquad \textbf{A1-5-24}$$

Where C_D is taken from equation A1-5-20, and:-

$$A_{bkp} = (m_3 + m_4)m_8 - m_7{}^2$$
$$B_{bkp} = \frac{m_4{}^3}{3(H_0 - 0.215m_1)} + \frac{(1 - m_1{}^2)(2m^3 - m_2)}{6(1 - 0.215m_1)} + m_1(m_3m_5 + m_4m_6) \qquad \textbf{A1-5-25}$$

Where H_0 is the half-breadth to draft ratio (equation A1-3-5). The m coefficients are determined as follows:-

$$m_1 = {}^{r_{bilge}}\!/_{T_{sec}},\quad m_2 = {}^{\overline{OG}}\!/_{T_{sec}},\quad m_3 = 1 - m_1 - m_2,\quad m_4 = H_0 - m_1 \qquad \textbf{A1-5-26}$$

Where r_{bilge} is determined using the expression in equation A1-3-7.

$$m_5 = \frac{\left(0.414H_0 + 0.0651m_1^{\,2} - \left(0.382H_0 + 0.0106\right)m_1\right)}{\left(H_0 - 0.215m_1\right)\left(1 - 0.215m_1\right)}$$

$$m_6 = \frac{\left(0.414H_0 + 0.0651m_1^{\,2} - \left(0.382 + 0.0106H_0\right)m_1\right)}{\left(H_0 - 0.215m_1\right)\left(1 - 0.215m_1\right)}$$

$$m_7 = \begin{cases} s_{average}/T_{sec} - 0.25\pi m_1 & \left(s_{average} > 0.25\pi r_{bilge}\right) \\ 0 & \left(s_{average} \le 0.25\pi r_{bilge}\right) \end{cases}$$

$$m_8 = \begin{cases} m_7 + 0.41m_1 & \left(s_{average} > 0.25\pi r_{bilge}\right) \\ m_7 + \sqrt{2}\left\{1 - \cos\left(s_{average}/r_{bilge}\right)\right\}m_1 & \left(s_{average} \le 0.25\pi r_{bilge}\right) \end{cases}$$

The lever r_{bk} can be estimated using the assumption of a ship section with horizontal bottom and vertical sides joined by quadrant circles as:-

$$r_{bk} = T_{sec}\left[\left\{H_0 - \left(1 - \frac{\sqrt{2}}{2}\right)\frac{r_{bilge}}{T_{sec}}\right\} + \left\{1 - \frac{\overline{OG}}{T_{sec}} - \left(1 - \frac{\sqrt{2}}{2}\right)\frac{r_{bilge}}{T_{sec}}\right\}^2\right]^{\frac{1}{2}} \quad \textbf{A1-5-27}$$

A1-6 Miscellaneous

Ikeda, Tanaka and Himeno (123) (144) investigated the effect of hull shape on roll damping by considering hull shapes typical of small Japanese fishing vessels. The vessels had beam to draught ratios in the range 3.5 – 5.0 with rise of floor and a hard chine joining the bottom of the hull to the side.

For this type of hull shape an improved formula for the eddy damping was proposed (145) (146). The basis of this was model experiments on two-dimensional cylinders with various deadrise angles, α_{hc}. The calculation is per each cross section and must be summed across the number of sections to obtain the complete value for the ship:-

$$B_E = \frac{4}{3\pi}\rho x_{40}\omega C_P s_{hc} L_{sec}(l_{hc-1} + l_{hc-2}) r_{hc}^{\ 2}$$

$$s_{hc} = \left(0.3H_0^* - 0.1775 + \frac{0.0775}{H_0^{*2}}\right) T_{sec} f_{hc-1}(\alpha)$$

$$C_P = \exp\left(K_{hc-1}H_0^* + K_{hc-2}\right) f_{hc-2}(\alpha)$$

$$H_0^* = \frac{B_{sec}}{2\left(T_{sec} - \overline{OG}\right)}$$

$$K_{hc-1} = -\exp\left(-0.114H_0^{\ 2} + 0.584H_0 - 0.558\right)$$

$$K_{hc-2} = -0.38H_0^{\ 2} + 2.264H_0 + 0.748$$

$$f_{hc-1}(\alpha_{hc}) = \exp(-2.145\alpha_{hc})$$

$$f_{hc-2}(\alpha_{hc}) = \exp(-1.718\alpha_{hc}) \qquad \textbf{A1-6- 1}$$

Where C_P is the negative pressure on the surface of the hull distributed over length s_{hc} and r_{hc} is lever from the point where eddies are shed to the centre of gravity. These symbols are defined in Figure A1-6- 1.

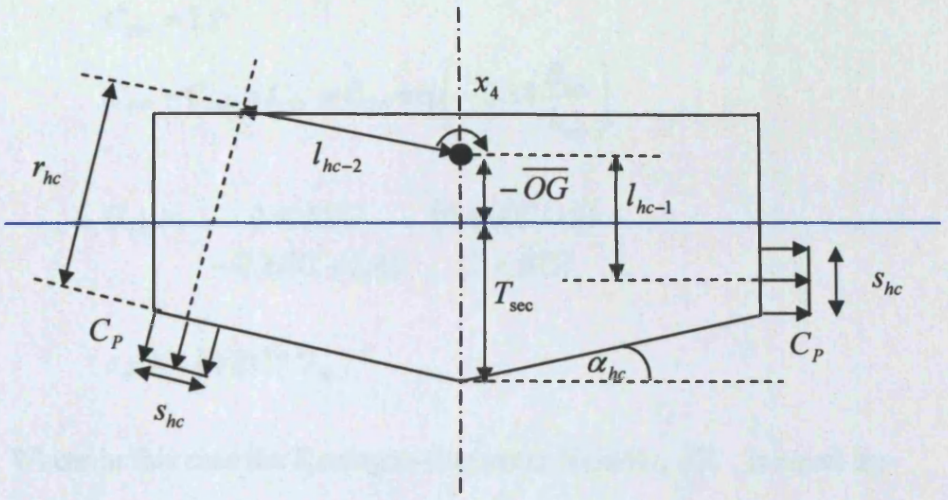

Figure A1-6- 1: Assumed pressure distribution on hard chine hull shape for eddy damping calculation according to Ikeda et al (145) (146)

Another investigation was to consider the effect of a skeg, large examples of which were commonly fitted to Japanese fishing vessels. The damping contribution of two types of skegs was measured in forced roll experiments on three two-dimensional ship shaped sections representative of fishing vessels. From this series of experiments an empirical formula was developed based on the pressure distribution around the skeg. The approach adopted in developing the formula is essentially identical to that used to develop a formula for the roll damping contribution of bilge keels due to the pressure difference around them (see section A1-5.2 of this appendix). The formula developed (146) was:-

$$B_{SK} = \frac{4}{3\pi} x_{40} \omega l_{sk}^{\ 2} \left\{ C_D l_{sk} l_{sk-1} - \frac{1}{2} C_{PF} a_{sk} l_{sk-2} + \frac{3}{4} C_{PR} s_{sk} l_{sk-3} \right\} \qquad \text{A1-6- 2}$$

Expressions for the pressure coefficients on the front and back face of the skeg (see Figure A1-6- 2), C_{PF} and C_{PR}, and the length of the negative pressure region s_{bk} were developed using the results of the model experiments:-

$$C_{PF} = 1.2$$

$$C_{PF} - C_{PR} = C_D = C_{D0} \exp\left(-0.38 \frac{B_{sec}}{L_{sec}}\right)$$

$$C_{D0} = \begin{array}{ll} 2.425KC & (0 \le KC \le 2) \\ -0.3KC + 5.45 & (2 < KC) \end{array} \qquad \text{A1-6- 3}$$

$$s_{sk} = 1.65 KC^{2/3} l_{sk}$$

Where in this case the Keulegan-Carpenter Number, KC, is equal to:-

$$\frac{U_{\max} T_4}{2 L_{sk}} \qquad \text{A1-6- 4}$$

Where L_{sk} is the span of the skeg from root to tip. This can be re-written as:-

$$KC = \frac{l_{sk-1} x_{40} \pi}{L_{sk}} \qquad \text{A1-6- 5}$$

The various symbols are defined in Figure A1-6- 2.

Figure A1-6- 2: Assumed pressure distribution around a skeg for damping calculation according to Ikeda et al (146)

Appendix (3) Lift Force Estimates for Novel Appendages

Appendix (3) Lift Force Estimates for Novel Appendages 484
A3-1 Lift Forces Estimates for Novel Appendages using the Theory of Du Cane 485

A3-1 Lift Forces Estimates for Novel Appendages using the Theory of Du Cane

If an appendage is located near to the free surface it will suffer lift losses. These can be accounted for by using the theory of Du Cane (174) described in the following paragraphs. The approach here is to make corrections to the ideal two dimensional lift slope ($C_{L\alpha}$) of 2π.

In an unbounded fluid, the low pressure generated above the foil acts only to lift the foil, but in the hydrofoil case it also acts on the water surface, which distorts so as to relieve the pressure drop decreasing the lift on the foil. The disturbance of the free surface takes the form of a transverse wave travelling with the hydrofoil, which also curves the flow and introduces a wave drag. The magnitude of these effects varies in a complicated way with the hydrofoil's depth of submergence, h, and speed, U, but since the wave effect becomes negligible at high Froude numbers, a reasonable approximation can be made in two additive terms:-

1. The lift loss due to pressure relief as a function of foil depth calculated at infinite Froude number, and
2. The "tilt" of the lift vector due to the wave effect as a function of foil depth and Froude number.

The first effect is similar to the interference suffered by the lower wing of a biplane and can be estimated using two-dimensional biplane theory, see for example Milne-Thompson (186), taking the wing gap to be twice the submergence depth of the hydrofoil. This gives a correction factor, K_L, that the ideal lift slope curve ($C_{L\alpha}$) of 2π must be multiplied by:-

$$K_L = \frac{\left(4\,h/_{ch}\right)^2 + 1}{\left(4\,h/_{ch}\right)^2 + 2} \qquad \text{A3-1- 1}$$

Where ch is the chord of the appendage. This relationship is shown in Figure A3-1- 1 below.

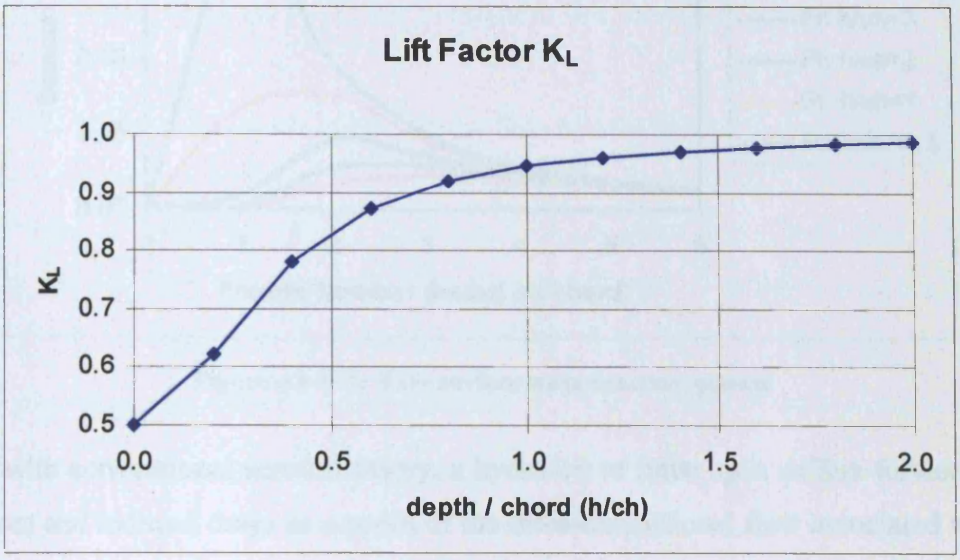

Figure A3-1- 1: Variation of free surface lift loss factor K_L with the ratio of appendage depth to chord

Du Cane quotes an equivalent vortex line approximation to the wave effect derived by Vladimirov from NACA technical memorandum 1341 (187):-

$$\Omega = \frac{1}{2Fn^2}\exp\left(\frac{-2h}{(ch)Fn^2}\right) \qquad \text{A3-1- 2}$$

Where the Froude Number Fn is calculated on the basis of chord:-

$$Fn = \frac{U}{\sqrt{g(ch)}} \qquad \text{A3-1- 3}$$

As speed increases, the lift loss and wave drag at first increase, reaching a peak at $Fn = \sqrt{2h/ch}$. This relationship is shown in Figure A3-1- 2.

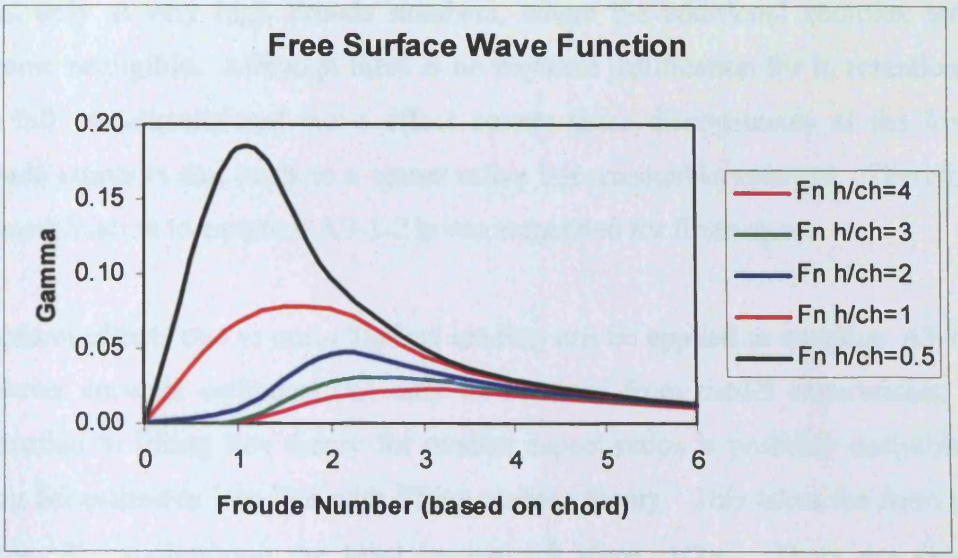

Figure A3-1- 2: Free surface wave function gamma

As with conventional aerofoil theory, a hydrofoil of finite span suffers further lift losses and induced drags as a result of the three-dimensional flow associated with the trailing vortex system. Assuming the simple, but realistic, condition of elliptical spanwise loading, a wing of effective aspect ratio AR_e, has an induced lift angle given by:-

$$\frac{\alpha_{ind}}{C_L} = \frac{1+\sigma_{fs}}{\pi AR_e} \qquad \text{A3-1- 4}$$

Where C_L is the lift coefficient and σ_{fs} is Prandtl's finite span aerofoil factor, where the wing gap is taken as twice the hydrofoil submergence, h. A reasonable approximation to this is given by:-

$$\sigma_{fs} = \frac{AR_e}{AR_e + 12 h/ch} \qquad \text{A3-1- 5}$$

Du Cane notes that this additional σ_{fs} term in the induced effects, equation A3-1-4, accounts for the diverging lateral waves associated with the trailing vortices of a finite span foil. Theoretically, the transverse wave effects given by equation A3-1-2 should be reduced in the finite span case, but if this is done, the overall lift loss and drag tend to be underestimated. This is because the σ_{fs} correction is

valid only at very high Froude numbers, where the additional complex terms become negligible. Although there is no physical justification for it, retention of the full two-dimensional wave effect covers these discrepancies at the lower Froude numbers and leads to a conservative but reasonable estimate. Therefore, no modification to equation A3-1-2 is recommended for finite span.

Planform effects due to non-elliptical loading can be applied to equation A3-1-4, however accurate estimates can only be obtained from model experiments. A correction to lifting line theory for modest aspect ratios is probably desirable to bring lift estimates into line with lifting surface theory. This takes the form of a factor, E_P, multiplying the ideal inverse lift slope, $1/2\pi$. There are several theories proposing different expressions for E_p, but a simple empirical expression that lies between them and fits experimental data is:-

$$E_p = 1 + \frac{2}{AR_e{}^2} \qquad \textbf{A3-1-6}$$

This formula should be corrected further if there is a sweep angle on the foil.

If an appendage is attached to the centre and/or side hull of a trimaran it will be partially immersed in the boundary layer of the hull(s). This causes a reduction in the flow velocity near the connection between the appendage and the hull(s) and the lift developed in this region will be reduced. Using the theory of Lloyd (188), who conducted experiments on an isolated fin mounted at various locations along a backboard, measuring the boundary layer thickness, δ_{bl}, and the lift developed. The results of this work can be approximated by the empirical expression:-

$$E_{BL} = 1.0 - 0.21\frac{\delta_{bl}}{s} \qquad \textbf{A3-1-7}$$

Which is the ratio of the lift developed by the part of the fin inside the boundary layer divided by the nominal lift (with no boundary layer). s is the span of the appendage. The boundary layer thickness can be estimated using:-

$$\delta_{bl} = 0.377 x_{FP} (R_n)^{-0.2} \qquad \text{A3-1-8}$$

Where x_{FP} is the distance from the fore perpendicular of the hull in question to the mid point of the appendage and the Reynolds number is then determined as:-

$$R_n = \frac{U x_{FP}}{\upsilon} \qquad \text{A3-1-9}$$

If an appendage touches both the centre and one side hull then the respective boundary layer thicknesses calculated using equation A3-1-8 must be added together to obtain the value of δ_{bl} for equation A3-1-7.

So, in summary, taking the contributions reducing lift from the previous paragraphs, the inverse of the lift slope curve $C_{L\alpha}$ is defined as:-

$$\frac{\alpha_{ind}}{C_L} = \left\{ \frac{1/K_L + 2/AR_e^{\,2}}{2\pi} + \Omega + \frac{1+\sigma_{fs}}{\pi AR_e} \right\} \frac{1}{E_{BL}} \qquad \text{A3-1-10}$$

Where the 2π in the denominator of the first term in the curly brackets is the ideal lift slope curve for a two-dimensional foil. $C_{L\alpha}$ is the inverse of equation A3-1-10. If free surface lift losses are not thought to be significant then the method put forward by Whicker and Felhner (137) can be used to calculate the lift slope, see Section 2.5.7 of Chapter 2.

Appendix (4) The Effect of Including Different Roll Damping Components on the Roll Response

Appendix (4) The Effect of Including Different Roll Damping Components on the Roll Response 490
A4-1 Comparison of Theoretical Roll Motion Predictions with Model Experiment Results 491

A4-1 Comparison of Theoretical Roll Motion Predictions with Model Experiment Results

In this appendix results from the TRISKP code using a range of components to represent the roll damping are compared with model experiment results. The roll damping components included are those developed in Section 4.4.1 of Chapter 4. The results are compared to the complete set of model experiment results obtained for trimaran DVZ in regular waves. The model was tested at three speeds, with six incoming wave frequencies per speed. Further details of the model experimental setup are given in Section 4.3 of Chapter 4.

The results are presented as roll RAOs in Figure A4-1- 1 to Figure A4-1- 6. The key to the legend text in these figures is given in Table A4-1- 1. The roll RAOs are calculated assuming the total roll damping comprises the contribution of the components listed in the legend text. It can be seen clearly that the most significant components are roll damping induced by side hull heave and the contribution of the twin rudders fitted to the model (the appendage damping). Results are only shown for trimaran DVZ without roll damping appendages fitted. The effect of adding purpose designed roll damping appendages is discussed in Section 4.4.4 of Chapter 4.

Figure Legend Text	*Damping Component:*	
Bw	B_W	Wave radiation damping calculated using TRISKP
Bfn	B_F	Friction Damping
Be	B_E	Eddy Damping (Centre Hull Only)
Bl	B_L	Lift Damping (Centre Hull Only)
Bsh	B_{SHH}	Roll Damping Induced by Side Hull Heave
Ba	B_A	Appendage Damping

Table A4-1- 1: Key to legend text in figures showing the breakdown of the damping components calculated theoretically

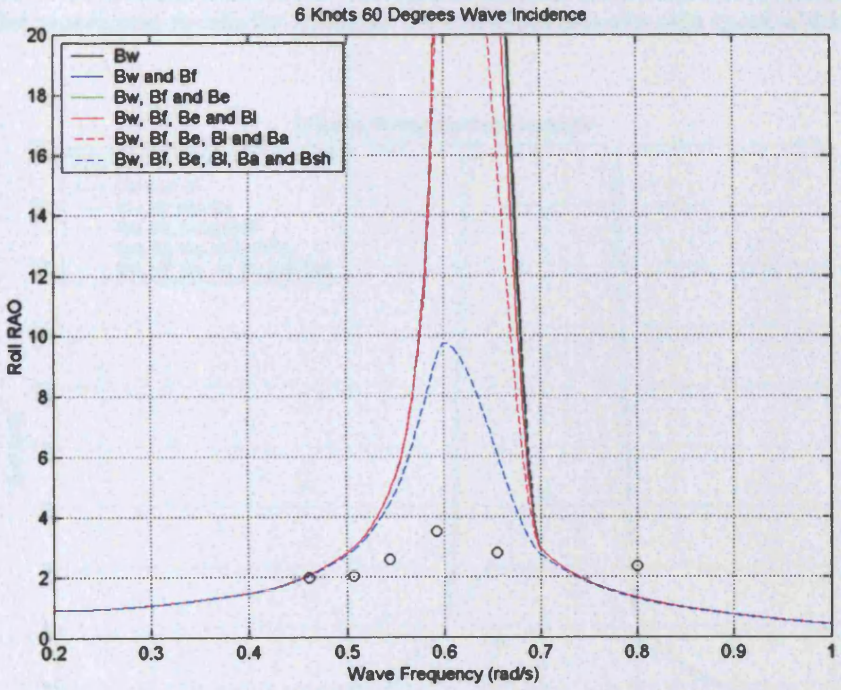

Figure A4-1- 1: Comparison of roll RAO calculated from components (theoretically) with model experiment results for trimaran DVZ in stern quartering seas at a ship speed of 6 knots

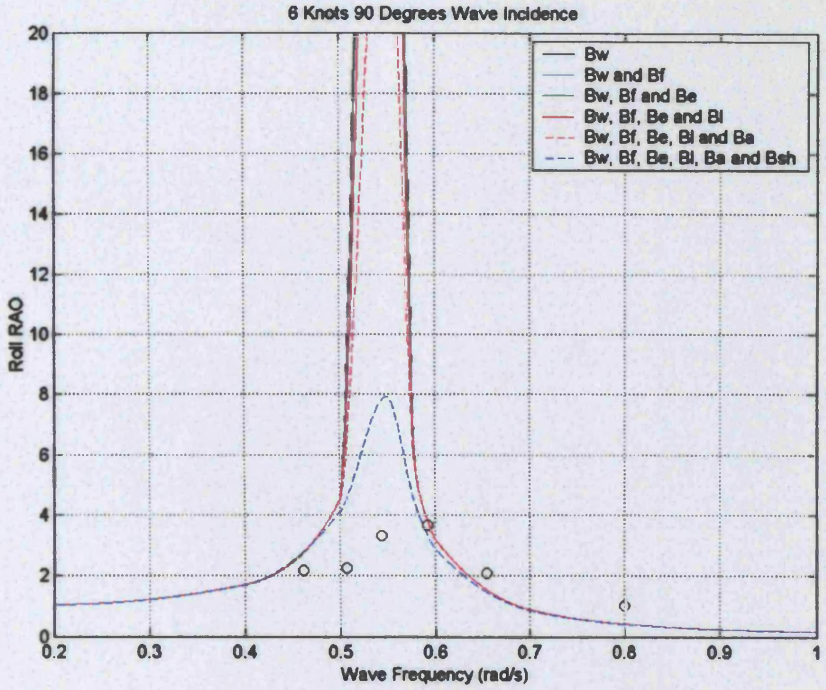

Figure A4-1- 2: Comparison of roll RAO calculated from components (theoretically) with model experiment results for trimaran DVZ in beam seas at a ship speed of 6 knots

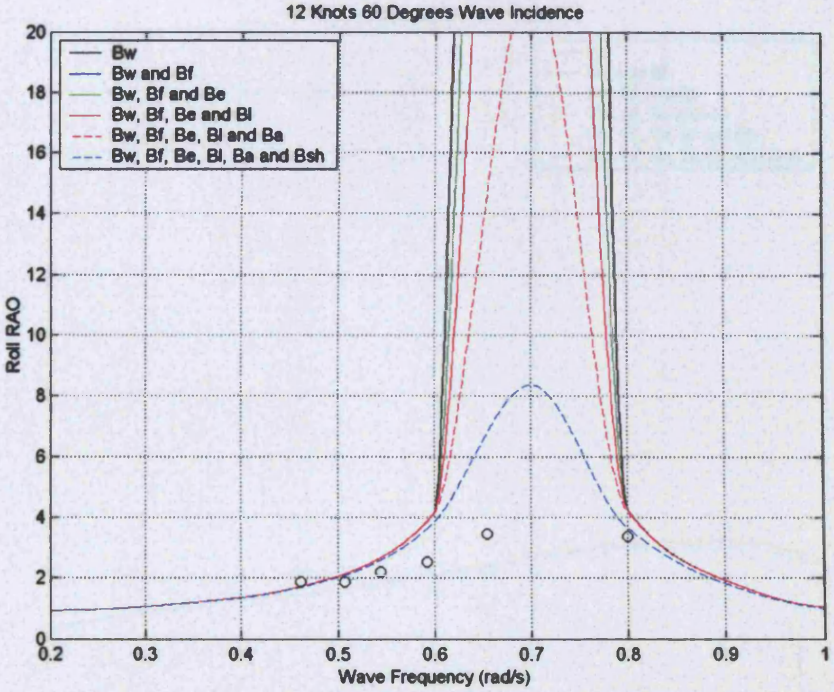

Figure A4-1- 3: Comparison of roll RAO calculated from components (theoretically) with model experiment results for trimaran DVZ in stern quartering seas at a ship speed of 12 knots

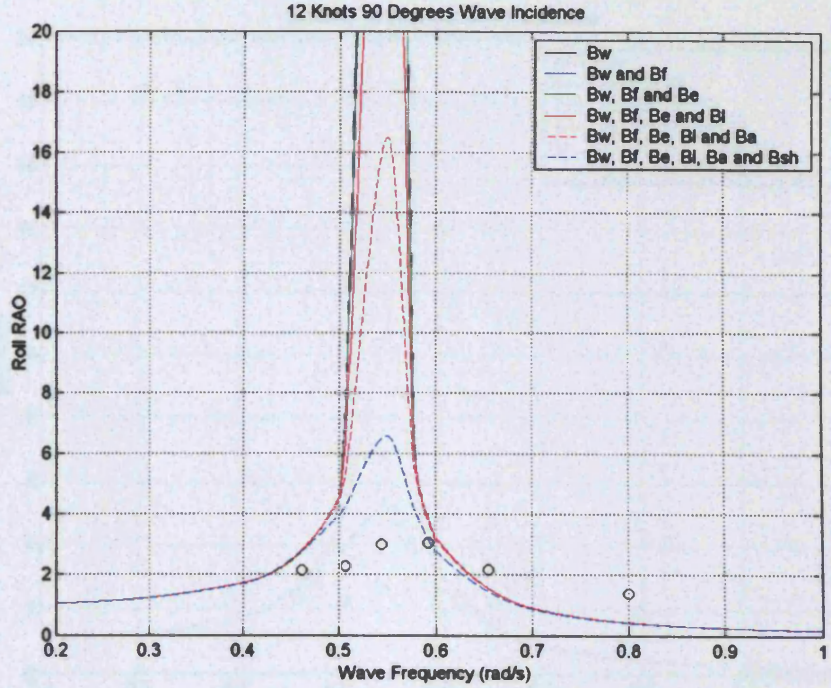

Figure A4-1- 4: Comparison of roll RAO calculated from components (theoretically) with model experiment results for trimaran DVZ in beam seas at a ship speed of 12 knots

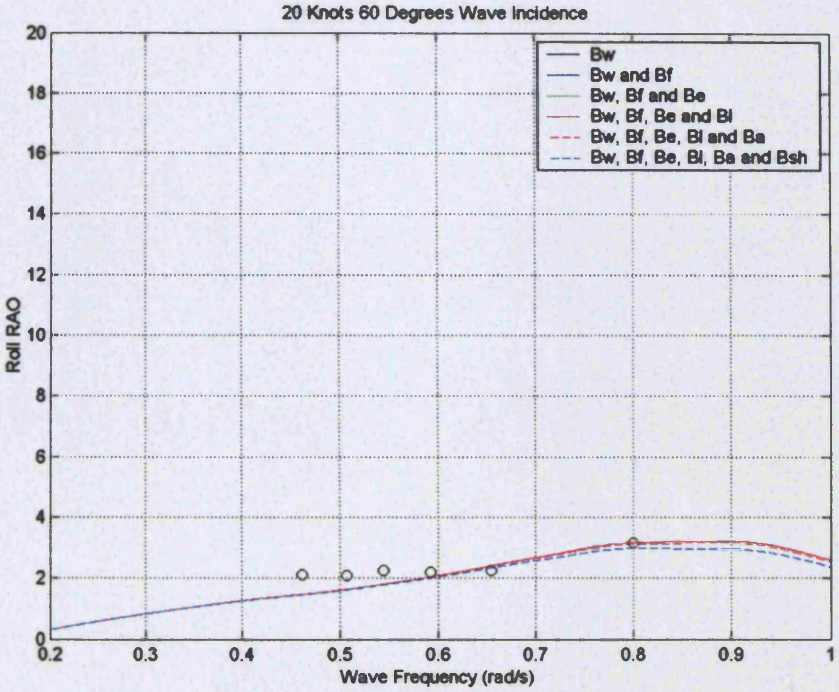

Figure A4-1- 5: Comparison of roll RAO calculated from components (theoretically) with model experiment results for trimaran DVZ in stern quartering seas at a ship speed of 20 knots

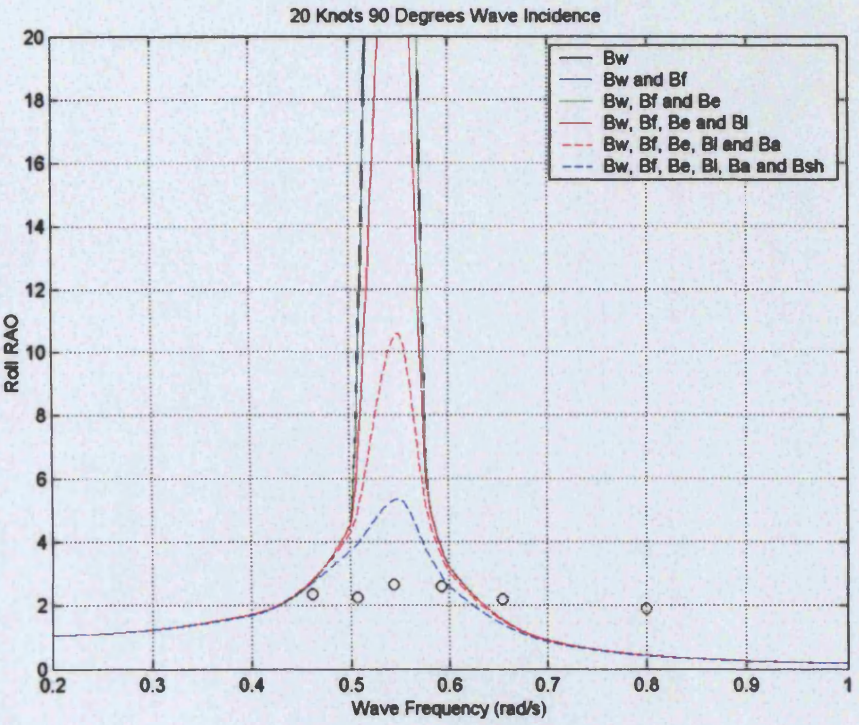

Figure A4-1- 6: Comparison of roll RAO calculated from components (theoretically) with model experiment results for trimaran DVZ in beam seas at a ship speed of 20 knots